Chapter 6

Ligand K-edge X-ray Absorption Spectroscopic Studies of the Electronic Structure of Models for the Fe-S Active Sites in Rubredoxin and Ferredoxins

6.1. Introduction

Metalloproteins containing iron-sulfur active sites are present in all forms of life and are most commonly involved in electron transfer. The 1Fe, 2Fe, and 4Fe active site structures of these proteins are shown schematically in Figure 6.1 and a brief description of each site is included here. For more extensive reviews of the reactivity and spectroscopy of these proteins, see references 1-6.

The 1Fe site (Figure 6.1a), found in rubredoxins, contains a single iron ion bound by four cysteine thiolate residues in a nearly T_d geometry. The biologically relevant redox process in rubredoxins involves a one-electron couple between Fe(II) and Fe(III). The 2Fe ferredoxin active site (Figure 6.1b) contains two ~T_d iron atoms di-μ-bridged by inorganic sulfides, with each iron bound to the protein through two cysteine thiolate residues. The biologically relevant redox process involves a one-electron couple between Fe(III)Fe(III) and Fe(III)Fe(II). The iron atoms in the dimer are antiferromagnetically coupled through a super-exchange pathway *via* the sulfides.[7-9] The oxidized state has an S=0 ground state and the reduced state, which is Class II localized,[10] has an S=1/2 ground state. The 4Fe active site (Figure 6.1c) is a tetramer of ~T_d iron atoms, each bound by a cysteine thiolate residue and three tri-bridged sulfides. The sulfide and iron atoms form the corners of a cube. The tetrameric unit exists in proteins in three stable oxidation states: $Fe(III)_3Fe(II)$, $Fe(III)_2Fe(II)_2$, and $Fe(III)Fe(II)_3$. In any given protein, however, only one of the two redox couples is functional. The $Fe(III)_3Fe(II)$/ $Fe(III)_2Fe(II)_2$ is active in the HiPIPs (high potential iron protein) and the $Fe(III)_2Fe(II)_2$/ $Fe(III)Fe(II)_3$ is active in the lower potential process characteristic of the classical 4Fe ferredoxins. In each redox state, the 4Fe cluster is Class III delocalized, so that each iron is electronically equivalent and displays an average oxidation state. The 4Fe site is described experimentally[11-13] and theoretically[14] as two high spin, mixed-valent, Class III, ferromagnetically-coupled Fe_2S_2 dimers which are antiferromagnetically coupled to each other. The ferromagnetic coupling of the dimers within the tetramer has been correlated to the delocalization of the site using a double exchange model.[15] However, the electronic structural basis for the observed delocalization, especially in contrast to the localized 2Fe sites, has not been established.

The nature of the electronic structure of these iron-sulfur active sites and its relationship to electron transfer reactivity is not yet fully understood. However, the ligand-metal interactions clearly play an important role in determining the reactivity of these sites. With the exception of the HiPIP proteins, the reduction potentials of iron-sulfur proteins are typically quite negative *vs.* NHE,[1] and this is at least in part

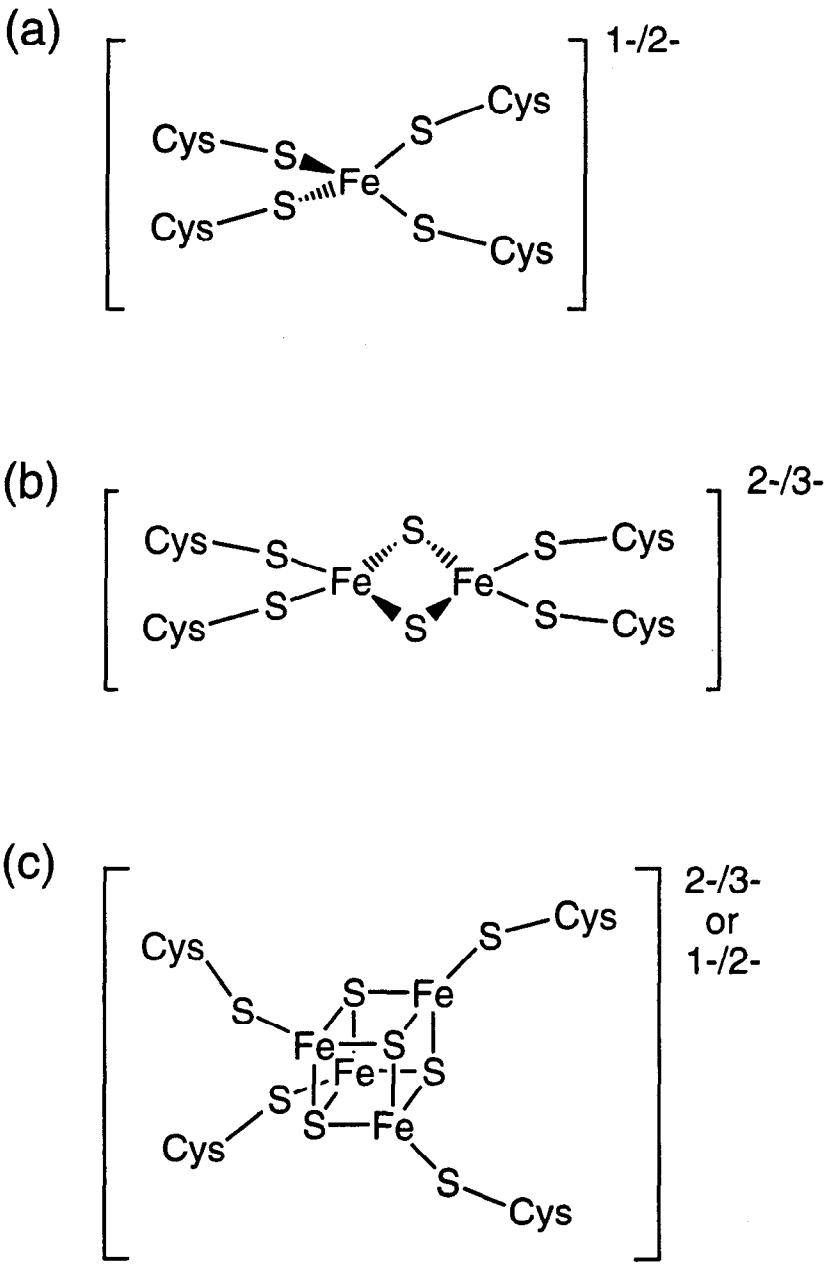

Figure 6.1. Schematic structures of iron-sulfur active sites (a) the one-iron site (b) the dimeric iron site and (c) the tetrameric iron site. The charges around each structure indicate the biologically relevant oxidations states found for these active sites.

determined by electrostatic interactions and exchange effects with the sulfur ligands. Calculations show that upon reduction, the additional electron density is strongly delocalized onto the ligands.[16,17] It has further been suggested that electron transfer in the Fe_2S_2 sites occurs *via* a ligand-to-metal charge transfer pathway.[16,17] Thus, a quantitative description of the ligand character in the redox active orbitals of these active sites is necessary to define the contribution of ligand-metal bonding to the reduction potentials and electron transfer pathways of the sites. Further, identification of the nature of possible superexchange pathways in the dimers as compared to the tetrameric clusters would help to define the source of delocalization in the tetramer.

As an experimental probe of the ligand-metal bonding in iron-sulfur sites, ligand K-edge X-ray absorption spectroscopic (XAS) studies have been conducted at the Cl and S K-edges for a series of Fe-S model complexes. Ligand K-edge XAS has been demonstrated to be a valuable tool in the investigation of ligand-metal bonding in open-shell metal ions. As demonstrated in Chapter 5 for the Cl K-edges of T_d $FeCl_4^{2-/1-}$, the K-edge absorption of a ligand bound to a ferrous or ferric iron exhibits a pre-edge feature which arises from transitions from the ligand 1s core orbital to the partially occupied antibonding metal d-derived orbitals of the site. These are a t_2 and e-set for a T_d metal center. Because of the localized nature of the Cl 1s orbital, the pre-edge transitions can have absorption intensity only if the metal d-derived orbitals contain a significant component of ligand 3p character as a result of covalency. Thus, pre-edge intensity serves as a probe of ligand-metal covalency. For metal centers with more than one d-manifold hole, a number of factors contribute to pre-edge intensity: transitions to several many-electron excited states (and to more than one metal d-derived orbital), multiplet effects in the d^{n+1} excited states, *and* the covalent contribution of the ligand to the metal d-derived orbitals. Expressions have been derived for T_d metal centers which take these contributions into account and allow the ligand covalency in the metal d-derived orbitals to be quantitatively related to ligand pre-edge intensity.[18] These expressions are given in equations 6.1 and 6.2 for ferrous and ferric complexes, respectively.

$$D_o(\text{Fe(II)}) = (c_1^2 + c_2^2 + \tfrac{1}{3} c_3^2)\, R^2 \langle s \mid \mathbf{r} \mid p \rangle^2 \qquad (6.1)$$

$$D_o(\text{Fe(III)}) = (c_1^2 + c_2^2 + \tfrac{2}{3} c_3^2)\, R^2 \langle s \mid \mathbf{r} \mid p \rangle^2 \qquad (6.2)$$

D_o is the total experimental intensity,[19] c_1^2 and c_2^2 are coefficients which reflect the ligand 3p σ and π covalency in the t_2-set of orbitals, respectively, c_3^2 is the coefficient which reflects π covalency in the e-set of orbitals, R is the ligand-metal bond distance, and $< s \mid \mathbf{r} \mid p >^2$ is the intensity of a pure ligand 1s —> 3p transition. Thus, ligand K-edge XAS can provide a direct probe of the ligand character in the redox active orbitals (the metal d-derived orbitals) in Fe-S systems.

In addition to pre-edge intensity, pre-edge and edge energies of ligand K-edge spectra can also be used to probe ligand-metal bonding. Both the ligand core energy and the energy of the metal d-derived orbitals affect the energy of a pre-edge transition (See Chapter 5, Figure 5.2). The ligand 1s core energy is related to the relative charge on the ligand. More charge donation to the metal results in a less negatively charged ligand and a consequent shift of the ligand 1s core to deeper binding energy. The energy of the metal d-derived orbitals has two contributions. First, the geometry of the ligand field (LF) of the complex determines the d-orbital energy splitting pattern and thus contributes to the metal d-derived orbital energy. Second, the overall d-manifold can shift in energy. This shift is related to both the coordination number of the metal (the total antibonding and repulsive interactions with the ligands) and the effective charge on the metal, which affects the energy of all the metal orbitals. The relative ligand 1s core energy is quantitated from the position of the rising edge. LF contributions to metal d-derived orbital energy shifts are determined from optical spectra. For T_d ferric tetrachlorides, the LF contribution to pre-edge energy has been shown to be negligible (see Chapter 5, Section 5.4.1). The observed pre-edge energy can be corrected for the ligand core and LF metal d-derived orbital energy shifts, allowing the contribution to the pre-edge energy from energy shifts of the d-manifold to be determined. For Cl K-edges, the charge on the ligand can also be determined from the rising edge energy.[20]

Here the Cl and S K-edge XAS data are presented for a series of iron-sulfur model complexes which serve as analogs for some of the above-described Fe-S active sites. A summary of the complexes included in this study, the iron oxidation states, coordination, and structural details are presented in Table 6.1. These model complexes, which exhibit structural and spectroscopic characteristics very similar to the proteins,[21] allow a detailed examination of the electronic structure of the Fe-S active sites.

Cl K-edges were measured for ~T_d $Fe(III)Cl_4^-$, diferric $[Fe_2S_2Cl_4]^{2-}$, and tetrameric $[Fe_4S_4Cl_4]^{2-}$, which though formally $Fe(III)_2Fe(II)_2$, contains four $Fe^{2.5+}$ due to the delocalized nature of the tetramer. This series allows us to compare the nature of the Fe-Cl bonding in each of these complexes.

Table 6.1. Summary of Fe-S Model Complex Structures[a]

Sample	Iron Coordination	Ave. Fe-S* BL (Å)	Ave. Fe-SR BL (Å)	X-Fe-X Angles	Ref.
Monomers					
$(Ph_4As)Fe(III)Cl_4$[b]	$FeCl_4$	-	2.182[b]	106.0 - 114.6	*g*
$(Et_4N)[Fe(III)(S_2\text{-o-xyl})_2]$	$Fe(SR)_4$	-	2.268	105.8 - 112.6	*h*
$(Et_4N)[Fe(III)(S\text{-durene})_4]$[c]	$Fe(SR)_4$	-	2.284	114.4 - 107.1	*i*
$(Et_4N)[Ga(III)(SPh)_4]$[b]	$Ga(SR)_4$	-	2.257	100.2 - 115.0	*j*
$Na(Ph_4As)[Fe(II)(S_2\text{-o-xyl})_2]$[b]	$Fe(SR)_4$	-	2.356	103.5 - 113.8	*h*
$(Ph_4P)_2[Fe(II)(SPh)_4]$	$Fe(SR)_4$	-	2.353	97.9 - 119.0	*k*
$(Et_4N)_2[Fe(II)(S\text{-2-Ph-}C_6H_4)_4]$	$Fe(SR)_4$	-	2.338	107.5 - 113.4	*l*
Dimers ($2Fe^{3+}$)					
$(Et_4N)_2[Fe_2S_2(S\text{-o-xyl})_2]$	$FeS^*_2(SR)_2$	2.208	2.304	104.7 - 112.3	*m*
$(Me_3NCH_2Ph)_2[Fe_2S_2(SEt)_4]$	$FeS^*_2(SR)_2$	ND			
$(Et_4N)_2[Fe_2S_2Cl_4]$	$FeS^*_2Cl_2$	2.200	2.251[e]	105.4 - 112.7	*n*
$CsFe(III)S_2$	FeS^*_4			infinite lattice of edge-sharing T_d-Fe	*o*
Tetramers ($4Fe^{2.5+}$)					
$(Et_4N)_2[Fe_4S_4(Smes)_4]$[d]	$FeS^*_3(SR)$	2.287	2.274	111.8 - 119.8	*p*
$(Et_4N)_2[Fe_4S_4(SBz)_4]$	$FeS^*_3(SR)$	2.310	2.239	103.7 - 117.3	*q*
$(Ph_4P)_2[Fe_4S_4(SEt)_4]$	$FeS^*_3(SR)$	ND			
$(Et_4N)_2[Fe_4S_4Cl_4]$[b]	FeS^*_3Cl	2.283	2.216[e]	102.3 - 120.2	*n*
$(Me_4N)_2[Fe_4Se_4(SPh)_4]$	$FeSe^*_3(SR)$	2.385[f]	2.273	97.4 - 120.2	*r*

[a] ND = crystal structure not determined; S* indicates bridging sulfide
[b] Data measured for related complex, see Table 6.2.
[c] S-durene = 2,3,5,6-tetramethylbenzenethiolate
[d] Smes = 2,4,6-trimethylbenzenethiolate
[e] Fe-Cl distance
[f] Fe-Se distance

[g] Zaslow, B.; Rundle, R. E. *J. Phys. Chem.* **1957**, *61*, 490-494.
[h] Lane, R. W.; Ibers, J. A.; Frankel, R. B.; Papaefthymiou, G. C.; Holm, R. H. *J. Am. Chem. Soc.* **1977**, *99*, 84-98.
[i] Millar, M.; Lee, J. F.; Koch, S. A.; Fikar, R. *Inorg. Chem.* **1982**, *21*, 4105-4106.
[j] Maelia, L. E.; Koch, S. A. *Inorg. Chem.* **1986**, *25*, 1896-1904.
[k] Coucovanis, D.; Swenson, D.; Baenziger, N. C.; Murphy, C.; Holah, D. G.; Sfarnas, N.; Simopoulos, A.; Kostikas, A. *J. Am. Chem. Soc.* **1981**, *103*, 3350-3362.
[l] Silver, A.; Koch, S. A.; Millar, M. *Inorg. Chim. Acta* **1993**, *205*, 9-14.
[m] Mayerle, J. J.; Denmark, S. E.; DePamphilis, B. V.; Ibers, J. A.; Holm, R. H. *J. Am. Chem. Soc.* **1975**, *97*, 1032-1045.
[n] Bobrik, M. A.; Hodgson, K. O.; Holm, R. H. *Inorg. Chem.* **1977**, *16*, 1851-1858.
[o] Nishi, M.; Ito, Y.; Ito, A. *J. Phys. Soc. Japan* **1983**, *52*, 3602-3610.
[p] Ueyama, N.; Sugawara, T.; Fuji, M.; Nakamura, A.; Yasuoka, N. *Chem. Lett.* **1985**, 175-178.
[q] Averill, B. A.; Herskovitz, T.; Holm, R. H.; Ibers, J. A. *J. Am. Chem. Soc.* **1973**, *95*, 3523-3534.
[r] Bobrik, M. A.; Laskowski, E. J.; Johnson, R. W.; Gillum, W. O.; Berg, J. M.; Hodgson, K. O.; Holm, R. H. *Inorg. Chem.* **1978**, *17*, 1402-1410.

S K-edges of a series of $Fe(II)(SR)_4^{2-}$ and $Fe(III)(SR)_4^-$ monomers provide a comparison of ferric and ferrous tetrathiolate sites. The S K-edge XAS of $Ga(III)(SR)_4^-$, which has a fully-occupied d-manifold and thus cannot exhibit pre-edge transitions, allows us to determine which features in the iron monomers may be assigned as pre-edge transitions.

The S K-edges of a series of diferric $[Fe_2S_2(SR)_4]^{2-}$ are here compared to the S K-edge of $[Fe_2S_2Cl_4]^{2-}$ and $CsFeS_2$ (an infinite lattice of edge-sharing FeS_4 tetrahedra). Because the latter two complexes have spectroscopic contributions only from sulfide ligands, the contributions from sulfide and thiolate in the $[Fe_2S_2(SR)_4]^{2-}$ dimer spectra can be determined.

A series of S K-edges for delocalized $[Fe_4S_4(SR)_4]^{2-}$ complexes (containing $Fe^{2.5+}$ ions) are compared herein to the spectra of $[Fe_4S_4Cl_4]^{2-}$ and $[Fe_4Se_4(SR)_4]^{2-}$. Because these latter compounds have contributions from only sulfide and thiolate, respectively, the contributions from sulfide and thiolate in the $[Fe_4S_4(SR)_4]^{2-}$ spectra can be assigned.

Preliminary analysis of pre-edge energies and intensities are presented and qualitative conclusions about Fe-S bonding in these complexes are discussed.

6.2. Experimental

6.2.1. Sample Preparation

The sulfur calibration sample $Na_2S_2O_3 \cdot 5H_2O$ was purchased from J.T. Baker and used without further purification. The chlorine calibration sample Cs_2CuCl_4 was synthesized according to published procedures.[22]

All Fe-S model compounds were prepared according to published methods. Compounds for which XAS data were measured and references for their syntheses are summarized in Table 6.2. $(Et_4N)FeCl_4$ was prepared as described in Chapter 5, Section 5.2.1.

For the XAS experiments, samples were ground into a fine powder under anaerobic conditions (at least several minutes of grinding with mortar and pestle). The powder was dispersed as thinly as possible (to minimize the possibility of self-absorption) on mylar tape containing an acrylic adhesive determined to be free of chlorine and sulfur contaminants. This procedure has been verified to minimize self-absorption effects in the data by systematically testing progressively thinner samples until

Table 6.2. Summary of Fe-S Model Systems

Sample	Synthesis
Monomers	
$(Et_4N)[Fe(III)(S_2\text{-o-xyl})_2]$	*d*
$(Et_4N)[Fe(III)(S\text{-durene})_4]^a$	*e*
$(Et_4N)[Ga(III)(S\text{-durene})_4]^a$	*f*
$(Et_4N)_2[Fe(II)(S_2\text{-o-xyl})_2]$	*f*
$(Ph_4P)_2[Fe(II)(SPh)_4]$	*g*
$(Et_4N)_2[Fe(II)(S\text{-2-Ph-}C_6H_4)_4]$	*h*
Dimers	
$(Et_4N)_2[Fe_2S_2(S\text{-o-xyl})_2]$	*i*
$(Me_3NCH_2Ph)_2[Fe_2S_2(SEt)_2]$	*j*
$(Et_4N)_2[Fe_2S_2Cl_4]$	*k*
$CsFe(III)S_2^b$	*l*
Tetramers	
$(Et_4N)_2[Fe_4S_4(Smes)_4]^c$	*m*
$(Et_4N)_2[Fe_4S_4(SBz)_4]$	*n*
$(Ph_4P)_2[Fe_4S_4(SEt)_4]$	*n*
$(n\text{-}Bu_4N)_2[Fe_4S_4Cl_4]$	*o*
$(Me_4N)_2[Fe_4Se_4(SPh)_4]$	*p*

a S-durene = 2,3,5,6-tetramethylbenzenethiolate

b This complex is an infinite lattice of tetrahedra with bridging sulfides

c Smes = 2,4,6-trimethylbenzenethiolate

d Lane, R. W.; Ibers, J. A.; Frankel, R. B.; Papaefthymiou, G. C.; Holm, R. H. *J. Am. Chem. Soc.* **1977**, *99*, 84-98.

e Millar, M.; Lee, J. F.; Koch, S. A.; Fikar, R. *Inorg. Chem.* **1982**, *21*, 4105-4106.

f Maelia, L. E.; Koch, S. A. *Inorg. Chem.* **1986**, *25*, 1896-1904.

g Coucovanis, D.; Swenson, D.; Baenziger, N. C.; Murphy, C.; Holah, D. G.; Sfarnas, N.; Simopoulos, A.; Kostikas, A. *J. Am. Chem. Soc.* **1981**, *103*, 3350-3362.

h Silver, A.; Koch, S. A.; Millar, M. *Inorg. Chim. Acta* **1993**, *205*, 9-14.

i Reynolds, J. G.; Holm, R. H. *Inorg. Chem.* **1980**, *19*, 3257-3260.

j Hagen, K. S.; Watson, A. D.; Holm, R. H. *J. Am. Chem. Soc.* **1983**, *105*, 3905-3913.

k Do, Y.; Simhon, E. D.; Holm, R. H. *Inorg. Chem.* **1983**, *22*, 3809-3812.

l Nishi, M.; Ito, Y.; Ito, A. *J. Phys. Soc. Japan* **1983**, *52*, 3602-3610.

m Zhou, J.; Scott, M. J.; Hu, Z.; Peng, G.; Münck, E.; Holm, R. H. *J. Am. Chem. Soc.* **1992**, *114*, 10843-10854.

n Averill, B. A.; Herskovitz, T.; Holm, R. H.; Ibers, J. A. *J. Am. Chem. Soc.* **1973**, *95*, 3523-3534.

o Rutchik, S.; Kim, S.; Walters, M. A. *Inorg. Chem.* **1988**, *27*, 1515-1516.

p Bobrik, M. A.; Laskowski, E. J.; Johnson, R. W.; Gillum, W. O.; Berg, J. M.; Hodgson, K. O.; Holm, R. H. *Inorg. Chem.* **1978**, *17*, 1402-1410.

the observed intensity no longer varies with the thickness of the sample. The tape was mounted across the window of an aluminum plate. Each sample was covered with a 6.35 μm polypropylene film window to protect the sample from exposure to air.

6.2.2. X-ray Absorption Measurements and Data Acquisition Parameters

X-ray absorption data were measured at the Stanford Synchrotron Radiation Laboratory using the 54-pole wiggler beamline 6-2 in low magnetic field mode (5 kG) with a Pt-coated focusing mirror and a Si(111) double crystal monochromator, under dedicated conditions (3.0 GeV, ~50 mA). Some data were measured on beamline X10C at the National Synchrotron Light Source (2.5 GeV, 200 mA). The monochromator was in both cases detuned ~30% to eliminate higher harmonic components in the X-ray beam. Details of the optimization of this set-up for low energy studies have been given in Chapter 1 (Section 1.2.5) as well as in an earlier publication.[23]

All S and Cl K-edge measurements were made at room temperature. The data were collected as fluorescence excitation spectra utilizing an ionization chamber as a fluorescence detector.[24,25] Several (2-3) scans were measured for each sample. The Cl K-edge spectral energy was calibrated from the Cl K-edge spectra of Cs_2CuCl_4, run at intervals between the samples. The maximum of the first edge-region feature in the spectrum was assigned to 2820.20 eV. Cl K-edge scans ranged from 2740 to 3100 eV, with a step size of 0.08 eV in the edge region. The S K-edge spectral energy was calibrated from the S K-edge spectra of $Na_2S_2O_3 \cdot 5H_2O$, run at intervals between the samples. The maximum of the first edge-region feature in the spectrum was assigned to 2472.02 eV. S K-edge scans ranged from 2420 to 2740 eV, with a step size of 0.08 eV in the edge region. Several samples [$CsFeS_2$, $(Et_4N)[Ga(S\text{-durene})]_4$, $(Et_4N)[Fe(S\text{-durene})]_4$, $(Et_4N)_2[Fe(S_2\text{-o-xyl})]_2$ and $(Et_4N)[Fe(S_2\text{-o-xyl})_2]$ had a larger pre-edge step size of 0.2 eV. The spectrometer resolution was ~0.5 eV.[23] Calculating and comparing first and second derivatives for model compounds measured during different experimental sessions results in a reproducibility in edge position of about ~0.1 eV for these experiments.

6.2.3. Data Reduction

Data were averaged and a smooth background was removed from all spectra by fitting a polynomial to the pre-edge region and subtracting this polynomial from the entire spectrum. Normalization of the data was accomplished by fitting a flat polynomial

or straight line to the post-edge region and normalizing the edge jump to 1.0 at 2840 eV for Cl K-edge data and 2490 eV for S K-edge data.

6.2.4. Fitting Procedures

The intensities and energies of Cl K-edge pre-edge features and the energies of S K-edge pre-edge features were determined by preliminary fits to the data. The fitting program EDG_FIT, which utilizes the double precision version of the public domain MINPAK fitting library[26] was used. EDG_FIT was written by Dr. Graham N. George of the Stanford Synchrotron Radiation Laboratory. Pre-edge features were modeled by pseudo-Voigt line shapes (simple sums of Lorentzian and Gaussian functions). This line shape is appropriate as the experimental features are expected to be a convolution of the Lorentzian transition envelope[27] and the Gaussian lineshape imposed by the spectrometer optics.[24,28,29] Spectral features were successfully reproduced using a fixed Lorentzian:Gaussian contribution of 50:50 for the pre-edge features in Cl K-edge spectra and of 35:65 for the pre-edge features in S K-edge spectra.

The number of functions employed to fit the rising edge background was chosen on the basis of features clearly indicated by the second derivative of the data. These rising edge functions were pseudo-Voight line shapes for which the Gaussian:Lorentzian mixture was allowed to vary to give the best empirical fit. In all cases the minimum number of functions required to successfully reproduce the data were utilized.

Fits were required to reproduce both the data and the second derivative of the data. For each spectrum, a number of fits which met these criteria were obtained. The value reported for the intensity of a Cl K-edge pre-edge feature (where peak area was approximated by the height x full-width-at-half-maximum (FWHM)) is the preliminary average of all the pseudo-Voigts which successfully fit the feature. Because the fits are preliminary, error in the intensity has not been calculated.

The overlapping nature of pre-edge features in the S K-edge spectra make determination of pre-edge intensities more complicated. However, preliminary fitting analysis has provided energies of pre-edge features.

6.2.5. Determination of Rising Edge Positions

The energies reported for the rising edge position were determined from the maximum in the first derivative of the data corresponding the rising edge inflection point.

These measurements were performed independently of the above described fitting procedures.

6.3. Results

6.3.1. Cl K-edges

Figure 6.2 shows the Cl K-edge spectra of $Fe(III)Cl_4^-$, $[Fe_2S_2Cl_4]^{2-}$, and $[Fe_4S_4Cl_4]^{2-}$. Each spectrum exhibits an intense, well-resolved pre-edge feature. The pre-edge energy is lowest for $Fe(III)Cl_4^-$ at 2820.8 eV, and highest for $[Fe_4S_4Cl_4]^{2-}$ at 2821.8 eV, with the pre-edge of $[Fe_2S_2Cl_4]^{2-}$ at 2821.6 eV. The pre-edge intensities are 1.50, 0.94, and 0.89 for $Fe(III)Cl_4^-$, $[Fe_2S_2Cl_4]^{2-}$, and $[Fe_4S_4Cl_4]^{2-}$, respectively. The rising edge inflection points are 2826.0 and 2825.6 eV for $Fe(III)Cl_4^-$ and $[Fe_2S_2Cl_4]^{2-}$, respectively; the rising edge inflection point for $[Fe_4S_4Cl_4]^{2-}$ is approximately ~2825.4 eV; however, the first derivative of this spectrum is less well-resolved. These data are tabulated in Table 6.3.

6.3.2. S K-edges of Monomeric Complexes

The S K-edge spectra of the monomeric complexes $[Fe(III)(S_2\text{-o-xyl})_2]^-$, $[Fe(III)(S\text{-durene})_4]^-$, and $[Ga(III)(S\text{-durene})_4]^-$ are shown in Figure 6.3. Each spectrum exhibits a maximum at the rising edge, which is sharpest for $[Ga(III)(S\text{-durene})_4]^-$. The energy of these maxima are at 2472.2, 2473.5, and 2473.0 eV for $[Fe(III)(S_2\text{-o-xyl})_2]^-$, $[Fe(III)(S\text{-durene})_4]^-$, and $[Ga(III)(S\text{-durene})_4]^-$, respectively. The spectra of both iron complexes also exhibit a pre-edge feature at lower energy which is absent in the gallium complex. The energy of this feature is centered at 2470.4 and 2470.3 eV for $[Fe(III)(S_2\text{-o-xyl})_2]^-$ and $[Fe(III)(S\text{-durene})_4]^-$, respectively. For these thiolate-based spectra the pre-edge feature and the maximum at the edge are referred to as transitions #3 and #4, respectively, for correlation with transitions in other spectra (*vide infra*). These transitions are indicated in Figure 6.3 and tabulated in Table 6.4.

Figure 6.4 shows the S K-edge spectra of the ferrous monomeric complexes $[Fe(II)(S_2\text{-o-xyl})_2]^{2-}$, $[Fe(II)(SPh)_4]^{2-}$, $[Fe(II)(S\text{-2-Ph-}C_6H_4)_4]^{2-}$. As in Figure 6.3, each spectrum exhibits a maximum at the rising edge. This feature is most well-resolved in $[Fe(II)(S_2\text{-o-xyl})_2]^{2-}$, appearing at 2471.7 eV, while the corresponding maxima in $[Fe(II)(SPh)_4]^{2-}$ and $[Fe(II)(S\text{-2-Ph-}C_6H_4)_4]^{2-}$ are observed at 2473.1 and 2473.2 eV. In analogy to the ferric monomers, these features are referred to as transition #4, as indicated

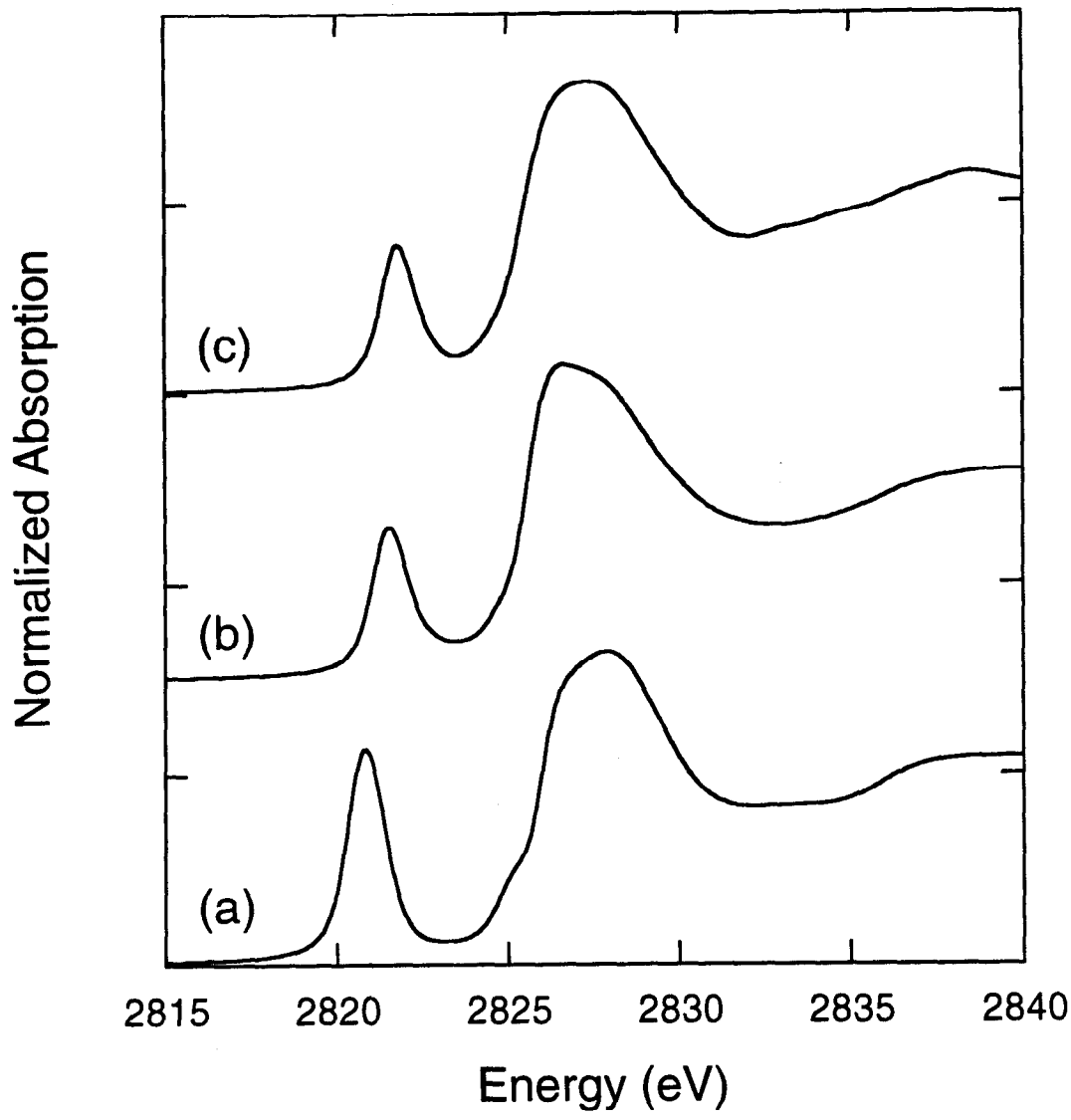

Figure 6.2. Cl K-edge spectra of (a) $Fe(III)Cl_4^-$, (b) $[Fe_2S_2Cl_4]^{2-}$ and (c) $[Fe_4S_4Cl_4]^{2-}$. Each spectrum exhibits an intense, well-resolved pre-edge feature. The energy of the feature is lowest and the intensity is highest in the spectrum of $Fe(III)Cl_4^-$.

Table 6.3. Cl K-edge Pre-edge Features: Energies and Intensities from Preliminary Fitting

Sample	Pre-edge Energy	Rising Edge Inflection Point	Pre-edge Intensity
$[Fe(III)Cl_4]^-$	2820.8	2826.0	1.50
$[Fe_2S_2Cl_4]^{2-}$	2821.6	2825.6	0.94
$[Fe_4S_4Cl_4]^{2-}$	2821.8	~2825.4†	0.89

† This energy is not well determined (see text).

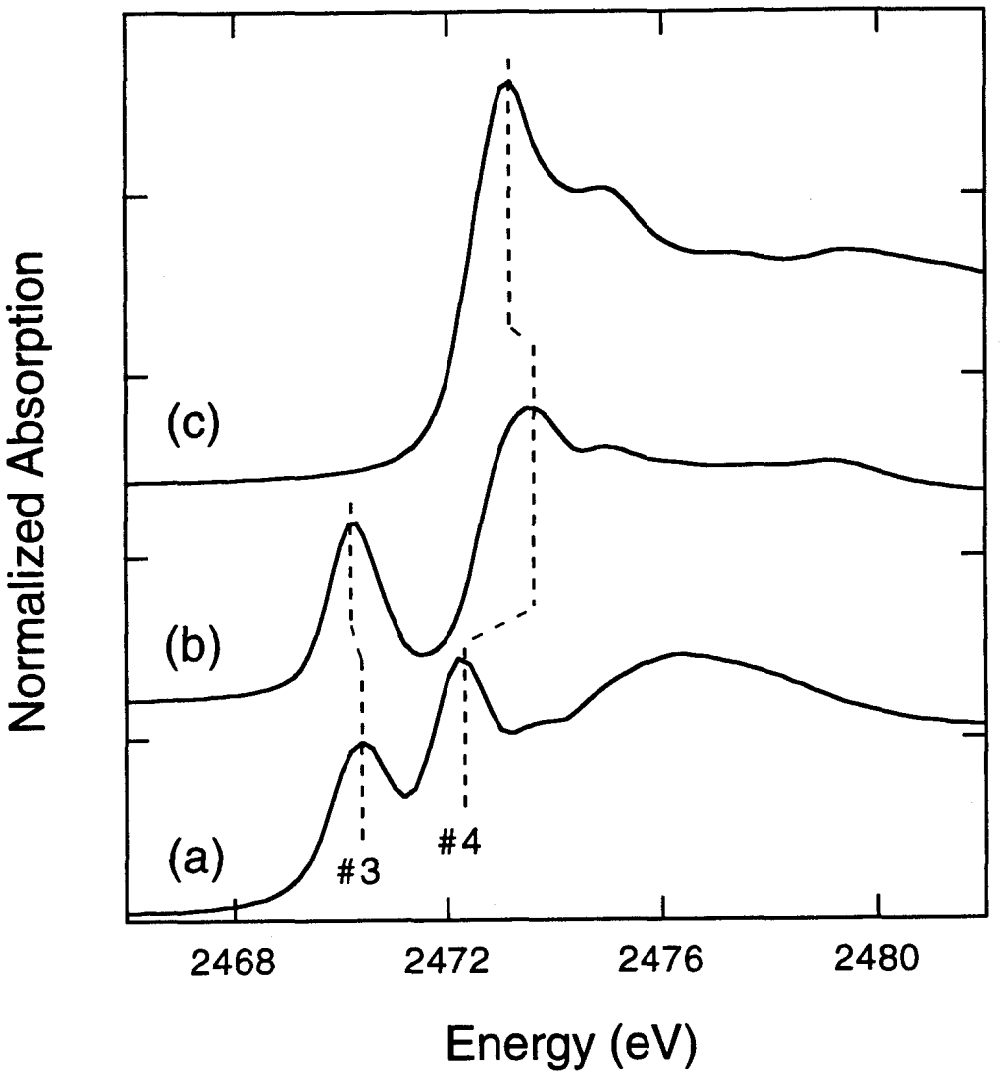

Figure 6.3. S K-edge spectra of (a) $[Fe(III)(S_2\text{-o-xyl})_2]^-$, (b) $[Fe(III)(S\text{-durene})_4]^-$, and (c) $[Ga(III)(S\text{-durene})_4]^-$. Each spectrum exhibits an intense transition at the rising edge onset, labeled here as transition #4 (see text). The ferric complex spectra each exhibit an intense pre-edge feature at similar energy (transition #3).

Table 6.4. S K-edge Pre-edge Energies from Preliminary Fitting

Sample	#S type	Transition #1 (eV)	Transition #2 (eV)	Transition #3 (eV)	Transition #4 (eV)	Transition #5 (eV)
Monomers						
$[Fe(III)(S_2\text{-o-xyl})_2]^-$	1			~ 2470.4	~ 2472.2	
$[Fe(III)(S\text{-durene})_4]^-$	1			~ 2470.3	~ 2473.5	
$[Ga(III)(S\text{-durene})_4]^-$	1			no pre-edge	~ 2473.0	
$[Fe(II)(S_2\text{-o-xyl})_2]^{2-}$	1			no pre-edge	~ 2471.7	
$[Fe(II)(SPh)_4]^{2-}$	1			no pre-edge	~ 2473.1	
$[Fe(II)(S\text{-2-Ph-}C_6H_4)_4]^{2-}$	1			no pre-edge	~ 2473.2	
Dimers						
$[Fe_2S_2(S\text{-o-xyl})_2]^{2-}$	2	~ 2469.3	~ 2469.9	~ 2470.7	~ 2472.0	
$[Fe_2S_2(SEt)_4]^{2-}$	2	~ 2469.3	~ 2469.9	~ 2470.6	~ 2472.7	
$[Fe_2S_2Cl_4]^{2-}$	1	~ 2469.2	~ 2469.6			~ 2474.4 (sh)
$CsFe(III)S_2$	1	~ 2469.6	~ 2470.0			~ 2474.1 (sh)
Tetramers						
$[Fe_4S_4(SBz)_4]^{2-}$	2	~ 2469.9	~ 2470.4		~ 2472.1	
$[Fe_4S_4(SEt)_4]^{2-}$	2	~ 2470.0	~ 2470.5		~ 2472.8	
$[Fe_4S_4(Smes)_4]^{2-}$	2	~ 2469.8	~ 2470.3		~ 2472.8	
$[Fe_4S_4Cl_4]^{2-}$	1	~ 2469.8	~ 2470.3			~ 2474.7 (sh)
$[Fe_4Se_4(SPh)_4]^{2-}$	1			~ 2470.8	~ 2473.1	

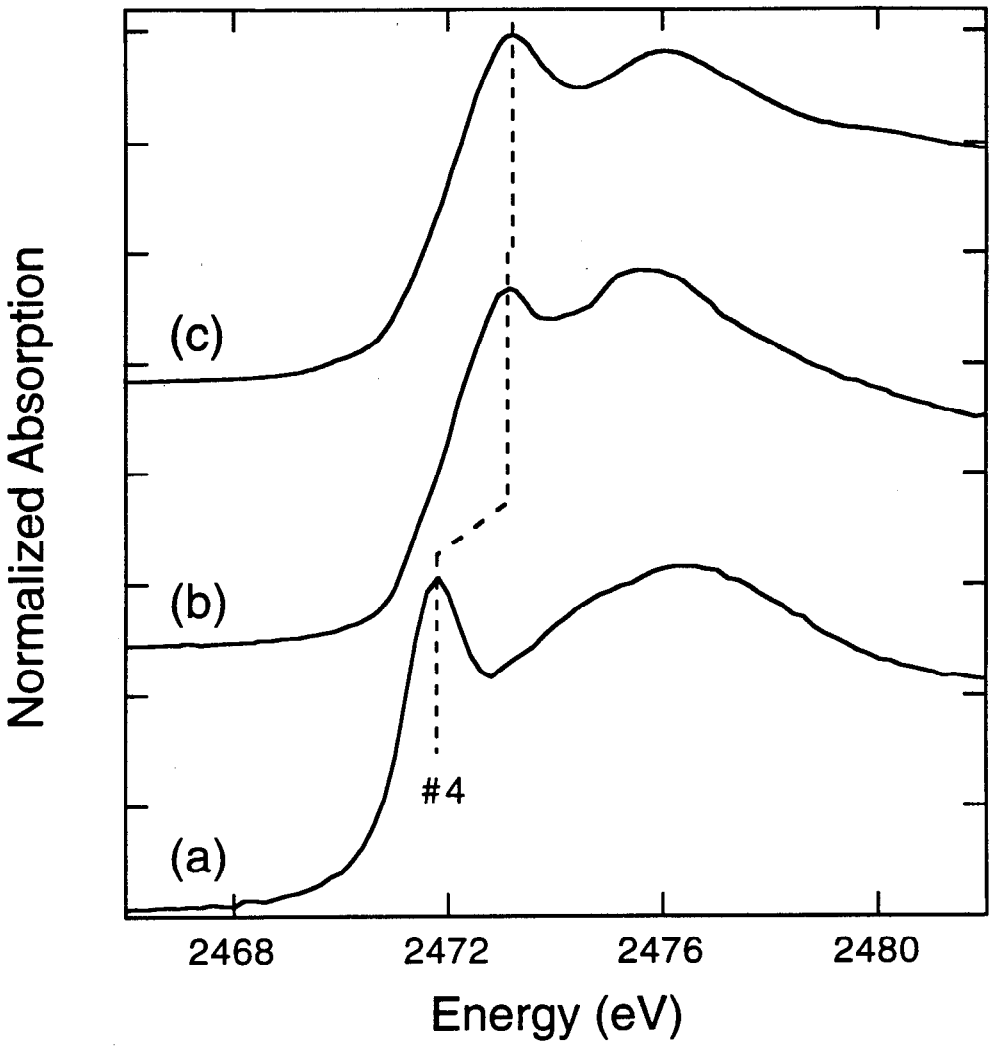

Figure 6.4. S K-edge spectra of (a) $[Fe(II)(S_2\text{-o-xyl})_2]^{2-}$, (b) $[Fe(II)(SPh)_4]^{2-}$, and (c) $[Fe(II)(S\text{-2-Ph-}C_6H_4)_4]^{2-}$. Each spectrum exhibits an intense transition at the rising edge which is at lower energy in the $[Fe(II)(S_2\text{-o-xyl})_2]^{2-}$ spectrum. It is labeled here as transition #4 (see text). There are no resolved pre-edge features in these spectra.

in Figure 6.4. Their energies are summarized in Table 6.4. Unlike for the ferric complexes, there is no clear evidence for any pre-edge features in these spectra. Note that the overall shape of the $[Fe(II)(S_2\text{-o-xyl})_2]^{2-}$ spectrum is similar to that of $[Fe(III)(S_2\text{-o-xyl})_2]^{-}$, but without the pre-edge feature and with a small shift in the energy of transition #4.

6.3.3. S K-edges of Dimeric Complexes

The S K-edge spectra of $[Fe_2S_2(S_2\text{-o-xyl})_2]^{2-}$ and $[Fe_2S_2(SEt)_4]^{2-}$ are shown in Figure 6.5 along with the second derivatives of the data. The spectra are considerably more complicated than those of monomeric complexes. There is a transition at the rising edge in each spectrum as well as a pre-edge band which, based on the second derivatives, has contributions from *at least* 3 transitions between 2469-2471 eV. Preliminary fitting of the $[Fe_2S_2(S_2\text{-o-xyl})_2]^{2-}$ data indicates pre-edge transitions at 2469.3, 2469.9 and 2470.7 eV, with a higher energy transition at 2472.0 eV. The pre-edge transitions in the spectrum of $[Fe_2S_2(SEt)_4]^{2-}$ have been fit with features at 2469.3, 2469.9, and 2470.6 eV. A fourth transition, which is sharper than in $[Fe_2S_2(S_2\text{-o-xyl})_2]^{2-}$ is observed at 2472.7 eV. These transitions are numbered #1-4, in order of increasing energy, so that the fourth transition corresponds to the maximum observed at the rising edge in the Fe-thiolate monomers. Transitions #1-4 are labeled in Figure 6.5 and their energies are tabulated in Table 6.4. Note that the energy of transition #4 in $[Fe_2S_2(S_2\text{-o-xyl})_2]^{2-}$ (2472.0 eV) is similar to that observed in the monomer $[Fe(III)(S_2\text{-o-xyl})_2]^{-}$ spectrum (2472.2 eV).

Figure 6.6 shows the S K-edge spectra and the second derivatives of the data for $[Fe_2S_2Cl_4]^{2-}$ and $CsFeS_2$. The spectra are very similar to each other, exhibiting an intense pre-edge feature and a rising edge shoulder. The pre-edge feature is best fit using two functions at 2469.2 and 2469.6 eV for $[Fe_2S_2Cl_4]^{2-}$ and 2469.6 and 2470.0 eV for $CsFeS_2$. The rising edge shoulder is at 2474.4 and 2474.1 eV for $[Fe_2S_2Cl_4]^{2-}$ and $CsFeS_2$, respectively. These transitions, tabulated in Table 6.4, are referred to as functions #1 and 2, due to the similarity in energy to transitions in the dimer spectra of Figure 6.5. The shoulder is designated transition #5. The approximate positions of these transitions are indicated in Figure 6.6. The inflection point of the rising edge (above the shoulder) is measured to be ~2475.6 and ~2475.7 eV in $[Fe_2S_2Cl_4]^{2-}$ and $CsFeS_2$, respectively. However, these values are not well-determined because the first derivatives are poorly resolved in this energy region.

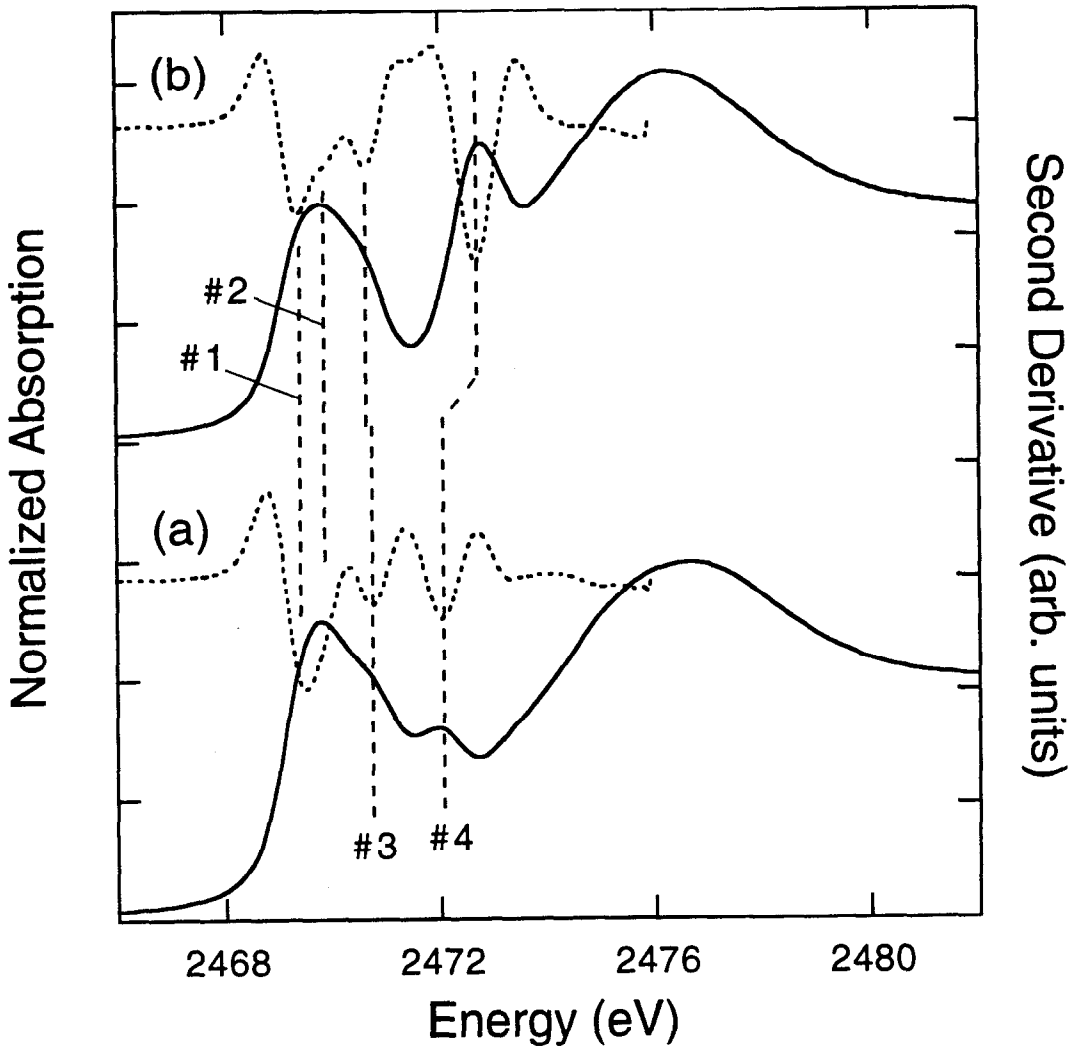

Figure 6.5. S K-edge spectra of the dimeric complexes (a) $[Fe_2S_2(S_2\text{-o-xyl})_2]^{2-}$ and (b) $[Fe_2S_2(SEt)_4]^{2-}$. The solid line is the data and the dotted line is the second derivative of the data in the pre-edge and edge region. Each spectrum exhibits a broad band of overlapping pre-edge transitions (at least three) at similar energies, as well as a transition to somewhat higher energy which varies depending on the nature of the thiolate ligand. The transition energies are designated with dashed lines and are labeled transitions #1-4 (see text).

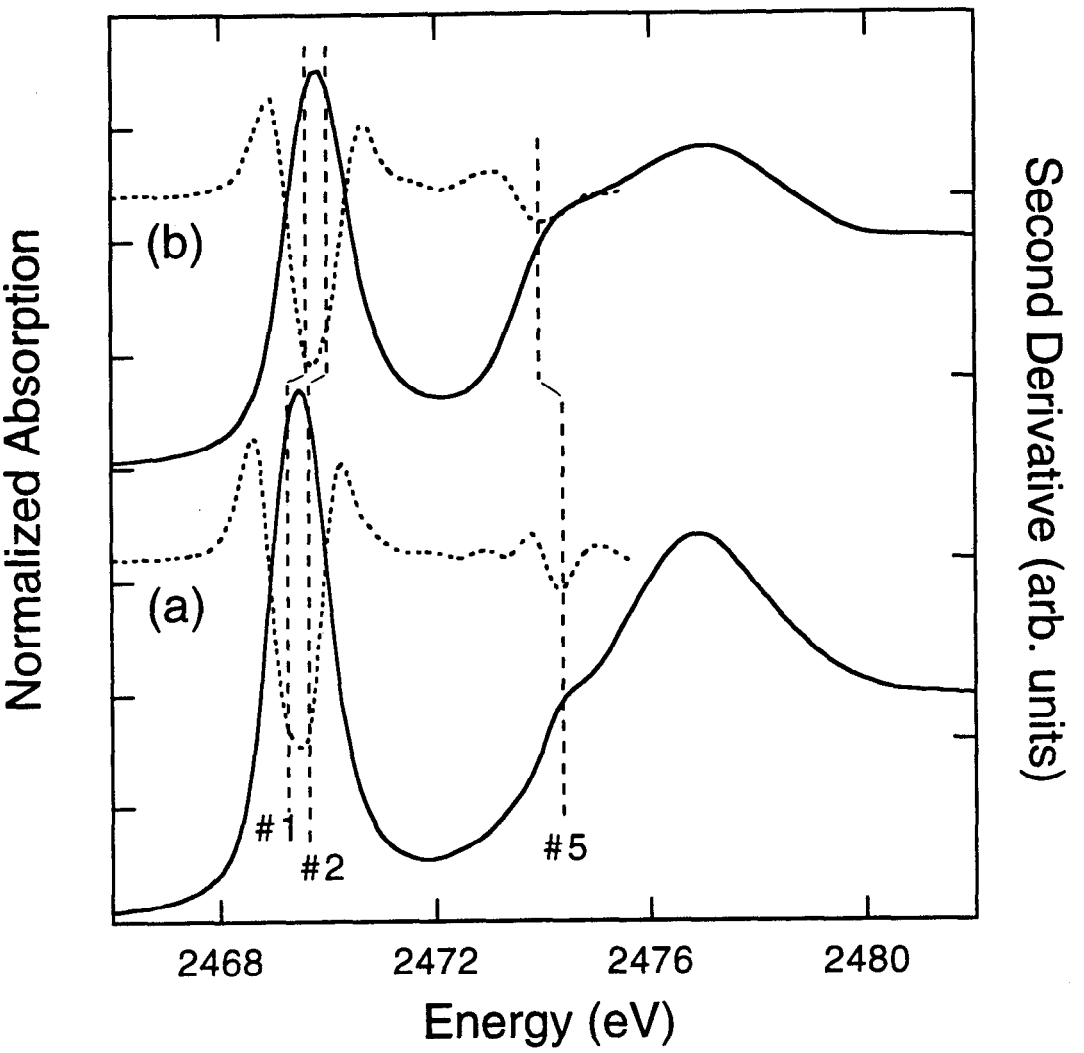

Figure 6.6. S K-edge spectra of (a) $[Fe_2S_2Cl_4]^{2-}$ and (b) $CsFeS_2$. Both complexes have only bridging sulfides. The solid line is the data and the dotted line is the second derivative of the data in the pre-edge and edge region. Each spectrum exhibits an intense pre-edge feature as well as a shoulder on the rising edge. The pre-edge transition energies, designated with dashed lines, are labeled transitions #1 and 2. The shoulder is designated transition #5 (see text).

6.3.4. S K-edges of Tetrameric Complexes

The S K-edge spectra and second derivatives of $[Fe_4S_4(SR)_4]^{2-}$ (R = Bz, Et, mes) are shown in Figure 6.7. The spectra are qualitatively similar to the dimer spectra (Figure 6.5). There is a pre-edge band which clearly has contributions from more than one transition as well as a transition in each spectrum at the rising edge. The pre-edge band and its second derivative for each complex exhibit less obvious structure than in the dimer spectra. Preliminary fitting of $[Fe_4S_4(SBz)_4]^{2-}$ (Figure 6.7a) indicates transitions at 2469.9 and 2470.4 eV and a higher energy transition at 2472.1 eV. The S K-edge of $[Fe_4S_4(SEt)_4]^{2-}$ (Figure 6.7b) is fit with transitions at 2470.0 and 2470.5 eV as well as a higher energy feature at 2472.8 eV. For $[Fe_4S_4(Smes)_4]^{2-}$ (Figure 6.7c), features at 2469.8 eV and 2470.3 eV were used to fit the pre-edge band, with a higher energy feature at 2472.8 eV. These transitions are numbered #1, 2, and 4, due to the similarity in the energies as compared to transitions in the dimer spectra. Their approximate energies are indicated in Figure 6.7. Note that the highest energy transition (#4) in the -SBz and -SEt thiolate tetramer spectra (2472.1 and 2472.8 eV, respectively) occur at nearly the same energy as transition #4 for the dimeric complexes with the same thiolate: 2472.0 eV for $[Fe_2S_2(S\text{-}o\text{-}xyl)_2]^{2-}$ and 2472.7 eV for $[Fe_2S_2(SEt)_4]^{2-}$.

Figure 6.8 shows the S K-edge spectra of $[Fe_4S_4Cl_4]^{2-}$ and $[Fe_4Se_4(SPh)_4]^{2-}$. The spectrum of $[Fe_4S_4Cl_4]^{2-}$ exhibits an intense pre-edge feature which is best fit with two transitions at 2469.8 and 2470.3 eV. A shoulder on the rising edge occurs at 2474.7 eV. These transitions are referred to as #1, 2, and 5 (Table 6.4), in analogy to those in the spectrum of $[Fe_2S_2Cl_4]^{2-}$. The spectrum of $[Fe_4Se_4(SPh)_4]^{2-}$ has a pre-edge feature at 2470.8, which is less intense than that for $[Fe_4S_4Cl_4]^{2-}$, and an intense transition at the rising edge at 2473.1 eV. These transitions are referred to as #3 and 4 (Table 6.4). All transitions are labeled in Figure 6.8. The inflection point of the rising edge (above the shoulder) for $[Fe_4S_4Cl_4]^{2-}$ is measured to be ~2475.7 eV. However, this value is not well-determined because the first derivative is poorly resolved in this energy region. The rising edge inflection point for $[Fe_4Se_4(SPh)_4]^{2-}$ can not be measured because it is obscured by the sharp transition at the rising edge.

6.4. Analysis

The analysis of these ligand K-edge data is organized into several sections. First, analysis of the Cl K-edge data explores Cl-Fe bonding interactions in a monomer *vs.* dimer *vs.* tetramer. Then, S-Fe bonding is examined separately in monomers, dimers and

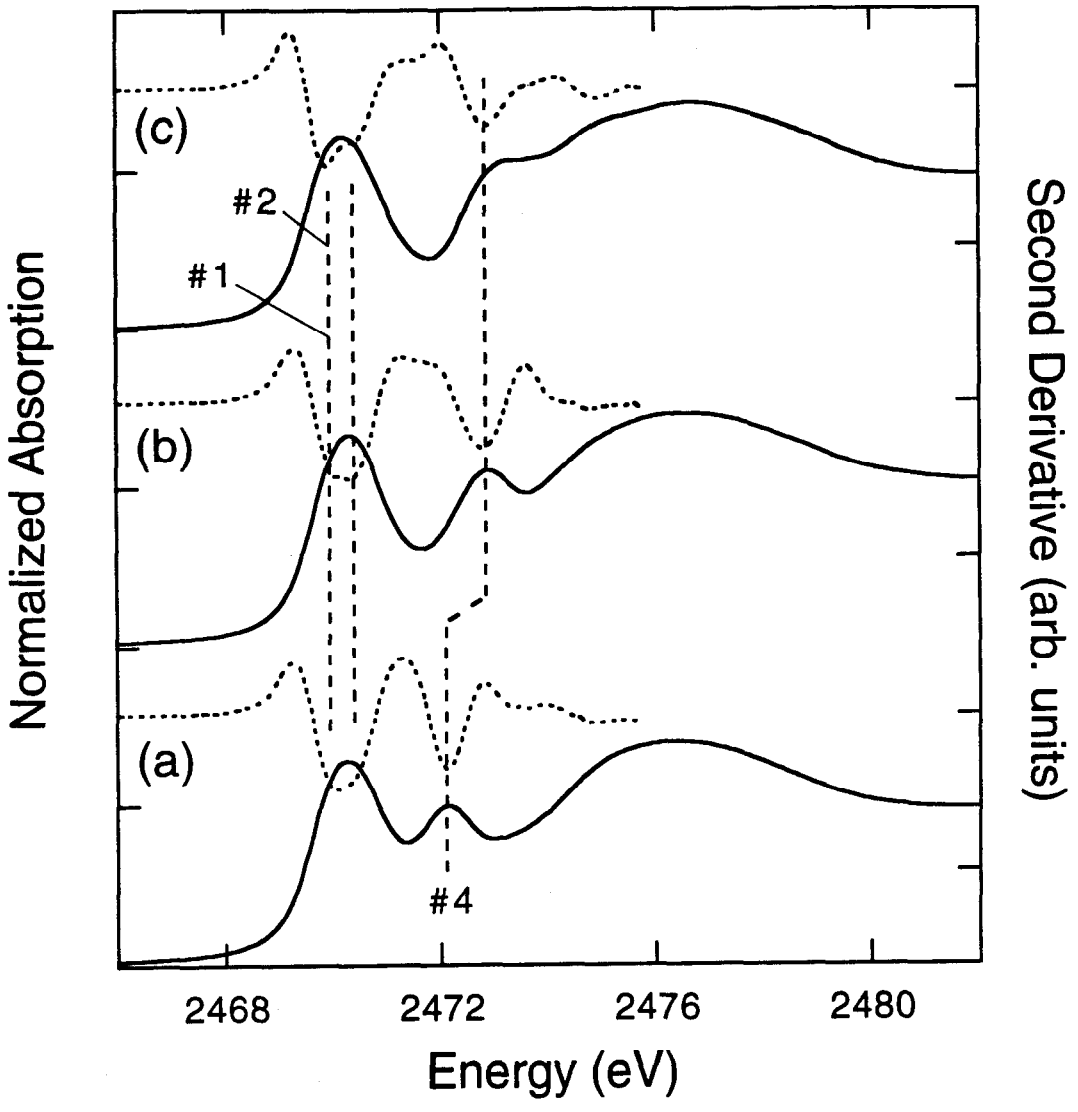

Figure 6.7. S K-edge spectra of $[Fe_4S_4(SR)_4]^{2-}$ (a) R = Bz, (b) R = Et, and (c) R = mes. The solid line is the data and the dotted line is the second derivative of the data in the pre-edge and edge region. Each spectrum exhibits a broad band of overlapping pre-edge transitions at similar energies, as well as a transition to somewhat higher energy which varies depending on the nature of the thiolate ligand. The transition energies are designated with dashed lines and are labeled transitions #1, 2 and 4 (see text).

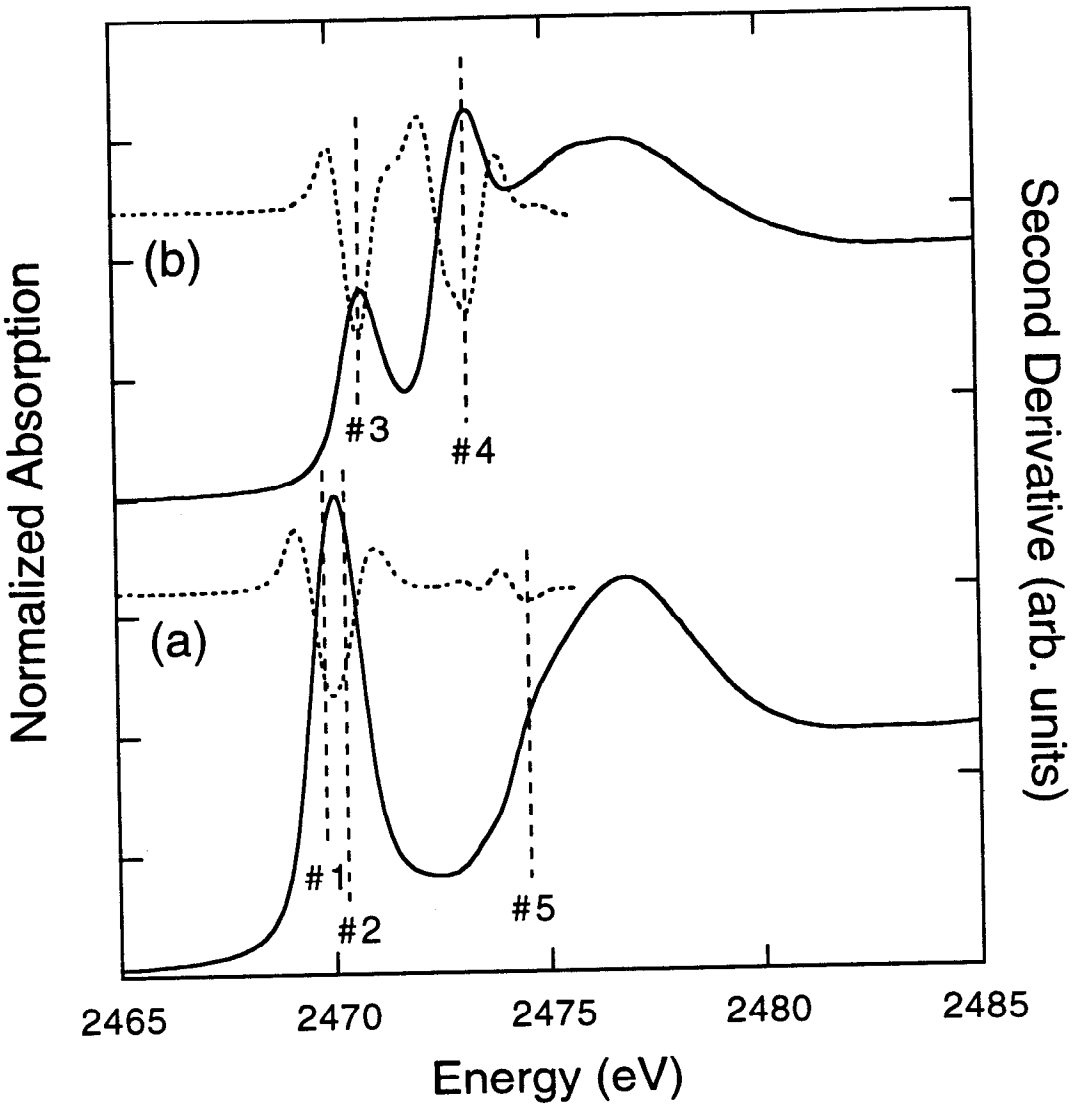

Figure 6.8. S K-edge spectra of (a) $[Fe_4S_4Cl_4]^{2-}$ and (b) $[Fe_4Se_4(SPh)_4]^{2-}$. The solid line is the data and the dotted line is the second derivative of the data in the pre-edge and edge region. The spectrum of $[Fe_4S_4Cl_4]^{2-}$ exhibits a more intense pre-edge feature at lower energy than that observed for $[Fe_4Se_4(SPh)_4]^{2-}$. The spectrum of $[Fe_4Se_4(SPh)_4]^{2-}$ also exhibits an intense transition at the onset of the rising edge while for $[Fe_4S_4Cl_4]^{2-}$ there is a rising edge shoulder. The energies of the transitions in each spectrum are designated with dashed lines and are labeled as described in the text.

tetramers. Finally, comparisons of S-Fe bonding in monomers *vs.* dimers *vs.* tetramers are made.

6.4.1. Cl K-edges

6.4.1.1. Pre-edge Transition Assignments. The intense pre-edge feature observed in the Cl K-edge spectrum of ~T_d Fe(III)Cl_4^- contains contributions from two transitions (see Chapter 5, Figure 5.4e and Table 5.4; note that the nomenclature used herein is defined in Chapter 5). The lower energy transition ($^6A_1$ —> ^{5}E-parent) is to the partially occupied e-set of T_d orbitals and the higher energy transition ($^6A_1$ —> $^5T_2$-parent) is to the partially occupied t_2-set of T_d orbitals. The total intensity (from both transitions) in the pre-edge feature was shown to reflect the sum of two-thirds of the e-set (π) covalency plus the total (π+σ) t_2-set covalency (see equation 6.2).

The assignment of pre-edge transitions in the Cl K-edge of $[Fe_2S_2Cl_4]^{2-}$ is made in analogy to that of Fe(III)Cl_4^-, because it has the same T_d ferric ground ($e^2t_2^3$) configuration and thus will have the same excited states. The assignment of pre-edge transitions in $[Fe_4S_4Cl_4]^{2-}$ is somewhat more complicated because the iron is in a +2.5 oxidation state. However, it is likely that the pre-edge feature also contains contributions from transitions to both the e- and t_2-sets of orbitals.

6.4.1.2. Pre-edge Intensities. The Cl K-edge pre-edge spectral intensity of $[Fe_2S_2Cl_4]^{2-}$ is lower than for Fe(III)Cl_4^- (see Table 6.3). Thus, the Fe-Cl covalency which is reflected in the pre-edge intensity (two-thirds of the e-set (π) covalency plus the total (π+σ) t_2-set covalency) is lower in the dimer. For Fe(III)Cl_4^-, this covalency was determined to be ~30% (see Chapter 5, Table 5.13). Application of equation 6.2 to the Cl pre-edge intensity of $[Fe_2S_2Cl_4]^{2-}$ then gives the Fe-Cl covalency ($c_1^2 + c_2^2 + \frac{2}{3}c_3^2$) to be ~18%. In the dimer, each iron is coordinated by two bridging sulfides and two terminal chlorides, rather than by four chlorides. The reduction in Fe-Cl covalency indicates that the bridging sulfides are better ligands than chloride, causing the Fe-Cl interaction to be less covalent in the mixed ligand system. The difference is also reflected in the Fe-Cl bond length, which is ~0.1 Å longer in the Fe-S dimer than in Fe(III)Cl_4^- (Table 6.1).

The pre-edge intensity is somewhat lower in the spectrum of $[Fe_4S_4Cl_4]^{2-}$ than for $[Fe_2S_2Cl_4]^{2-}$. This may indicate a small decrease in Fe-Cl covalency in the tetramer. However, each iron center in the tetramer has an additional 0.5 electrons in its d-manifold relative to the dimer. As was seen in Chapter 5 (see Section 5.4.2), pre-edge intensity is related both to covalency as well as to the number of vacancies in the d-manifold of a

complex, which determines the probability of an allowed transition. Thus, the pre-edge intensity of a ligand bound to $Fe^{2.5+}$ may be decreased relative to a Fe^{3+} interaction for the same covalency. Expressions analogous to those for a ligand bound to a T_d Fe(III) ion in Chapter 5, must be derived for the $Fe^{2.5+}$ center in order to determine the effect this might have on intensity.

6.4.1.3. Edge and Pre-edge Energies. The rising edge inflection point of Fe(III)Cl_4^- is at higher energy (2426.0 eV) than that of $[Fe_2S_2Cl_4]^{2-}$ (2425.6 eV) which indicates that the Cl 1s core in the monomer is at deeper binding energy. This is consistent with the relative pre-edge intensities, which demonstrate that the Fe-Cl interaction in the monomer is more covalent. Larger covalency in the monomer allows the Cl to donate more electron density to the iron and causes its core to shift to deeper binding energy. The relationship between the Cl K-edge position and chloride charge has been derived[30] and can be applied to these data to obtain an estimate of the charge on the chloride ligand in each complex. The charge calculated for the chloride in Fe(III)Cl_4^- is -0.33 and that in $[Fe_2S_2Cl_4]^{2-}$ is -0.46.

The rising edge position is lower for $[Fe_4S_4Cl_4]^{2-}$ than for $[Fe_2S_2Cl_4]^{2-}$ (Table 6.3). The charge calculated for the Cl in $[Fe_4S_4Cl_4]^{2-}$ from the rising edge inflection point is ~-0.52. Thus, the Cl in the tetramer donates less charge to iron than in the dimer. This decrease in charge donation may indicate that the decrease in pre-edge intensity in the tetramer reflects a decrease in covalency.

The energy of the pre-edge feature in the spectrum of Fe(III)Cl_4^- is at much lower energy than in the spectrum of $[Fe_2S_2Cl_4]^{2-}$. The contribution of the Cl 1s core energy to the pre-edge energy is determined from the rising edge inflection point, which indicates the Cl 1s core is deeper in Fe(III)Cl_4^-. If the energies of the metal d-derived orbitals (the T_d t_2 and e-set) are the same in both complexes, the pre-edge transition in the monomer would occur at higher energy. However, since the dimer pre-edge is higher in energy, the metal d-derived orbitals in the dimer must be significantly higher in energy than in Fe(III)Cl_4^-. The effect of LF splittings on the pre-edge energy is negligible for T_d Fe(III) complexes. Thus, the difference in energy of the metal d-derived orbitals must be related to the overall d-manifold energy. Since the oxidation state of iron in both complexes is the same, this difference likely arises from increased electrostatic repulsive interactions with 2 S^{2-} and 2 Cl^- ligands in the dimer relative to four chlorides in the monomer.

The pre-edge energy in $[Fe_2S_2Cl_4]^{2-}$ is somewhat lower than in $[Fe_4S_4Cl_4]^{2-}$ and the rising edge inflection indicates the dimer 1s core is at deeper binding energy. If the metal d-derived orbitals were at the same energy in both complexes, the dimer pre-edge would occur at higher energy. Thus, the pre-edge energies indicate that the tetramer

metal d-derived orbitals are at higher energy than in the dimer. In analogy to T_d Fe(III) systems, the LF is not likely to significantly affect the energy of the pre-edge feature. Thus, the d-manifold in the tetramer must be higher in energy, consistent with a somewhat less positive iron center ($Fe^{2.5+}$ *vs.* Fe^{3+}).

6.4.2. S K-edges of Monomeric Complexes

6.4.2.1. Transition Assignments. The pre-edge feature in the S K-edge spectra of $[Fe(III)(SR)_4]^-$ complexes (Figure 6.3) is assigned in analogy to the Cl K-edge pre-edge feature in $Fe(III)Cl_4^-$ (see Chapter 5, Figure 5.4e) and thus contains contributions from transitions from the thiolate sulfur 1s orbital to both the e- and t_2-sets of T_d orbitals. This assignment is supported by the fact that the feature is absent in the spectrum of $[Ga(III)(S\text{-durene})_4]^-$ which has no d-manifold vacancies and thus cannot exhibit pre-edge transitions. Based on the MCl_4^{n-} results presented in Chapter 5, one would expect the ferrous pre-edge to be observed as a weak shoulder on the rising edge. Since no such feature is observed in the spectra of $Fe(II)(SR)_4^{2-}$ complexes, it is assumed that the pre-edge transitions are overlapping with the rising edge in energy.

Because the intense transition at the rising edge (transition #4) is present in each spectrum, including $[Ga(III)(S\text{-durene})_4]^-$, it is attributed to an electric dipole-allowed transition localized on the thiolate ligand. Further evidence for this assignment comes from the fact that the energy of the transition is dependent on the nature of the thiolate (*vide infra*).

6.4.2.2. Ferric Pre-edge Energies. The energies of the pre-edge features in $[Fe(III)(S_2\text{-o-xyl})_2]^-$ and $[Fe(III)S\text{-durene}_4]^-$ are nearly identical (2470.4 and 2470.3 eV, respectively). Because the rising edge region is complicated by the intense thiolate-based transition, it is not straightforward to estimate thiolate 1s core energy shifts experimentally. The similarity in pre-edge energies, then, may indicate that the thiolate 1s core orbital energies and the metal d-derived orbital energies of these complexes are the same, or it may simply indicate that the difference between the S 1s and the metal d-derived orbitals energies are similar.

6.4.3. S K-edges of Dimeric Complexes

6.4.3.1. Transition Assignments. The S K-edge spectra of dimeric Fe-S complexes are more complicated than the monomeric complexes due to contributions to the spectrum from more than one kind of sulfur. The energy of the transition observed at

the rising edge (#4) is very similar in $[Fe_2S_2(S_2\text{-o-xyl})_2]^{2-}$ and $[Fe(S_2\text{-o-xyl})_2]^{-}$ (See Figure 6.5) and is assigned in analogy to the monomers as a thiolate-based transition. Further evidence for this assignment comes from the fact that it is absent in $[Fe_2S_2Cl_4]^{2-}$ and $CsFeS_2$, which contain no thiolate.

Transitions in the pre-edge region are assigned by first examining the sulfide spectra of $[Fe_2S_2Cl_4]^{2-}$ and $CsFeS_2$ (Figure 6.6). The pre-edge feature in these spectra is attributed to two transitions assigned, in analogy to those in $Fe(III)Cl_4^-$ and $Fe(III)(SR)_4^-$, as transitions from the sulfide 1s orbital to both the e- and t_2-sets of T_d metal d-derived orbitals. Both $[Fe_2S_2Cl_4]^{2-}$ and $CsFeS_2$ display a shoulder on the rising edge which is likely due to a transition to a molecular orbital with both S 3p and metal (*e.g.* 4s) character. This transition is not observed in the $[Fe_2S_2(SR)_4]^{2-}$ complexes because it is obscured by the thiolate-based transition at the rising edge. The pre-edge transitions in $CsFeS_2$ occur at slightly higher energy than in $[Fe_2S_2Cl_4]^{2-}$. The similarity in rising edge inflection points in the spectra would indicate, then, that the pre-edge energy difference comes from higher energy metal d-derived orbitals in $CsFeS_2$. This probably reflects an electrostatic effect from the all-sulfide ligation in $CsFeS_2$.

The energies of the sulfide transitions in the $[Fe_2S_2Cl_4]^{2-}$ spectrum are nearly identical to those of the two lowest energy transitions from the $[Fe_2S_2(SR)_4]^{2-}$ dimers (Figure 6.5). Thus, transitions #1-2 in the $[Fe_2S_2(SR)_4]^{2-}$ dimer spectra are assigned as sulfide-based pre-edge transitions. The higher energy pre-edge transition (#3), which is similar in energy to that of the pre-edge features in $Fe(III)(SR)_4^-$ spectra, is assigned as a thiolate-based pre-edge transition. Theoretically, the thiolate and sulfide ligands will each give rise to two pre-edge transitions (one to each the e- and t_2-sets of metal d-derived orbitals). Thus, the pre-edge band must contain four overlapping pre-edge transitions.

6.4.3.2. Pre-edge Transition Energies. Based on the above assignments, the sulfide-based transitions occur at lower energy than the thiolate-based transitions. Since the transitions within each dimer are to the same metal d-derived orbitals, pre-edge transition energy differences directly reflect differences in sulfur core 1s energies. Thus, the sulfide 1s core is at less deep binding energy than the thiolate 1s core.

The energies of the sulfide-based and thiolate-based pre-edge features from different $[Fe_2S_2(SR)_4]^{2-}$ dimers are nearly identical. This may indicate that the respective sulfur 1s core orbital energies and the metal d-derived orbital energies of these complexes are the same, or it may indicate that the difference between the sulfur 1s and the metal d-derived orbital energies are similar.

6.4.3.3. Pre-edge Transition Intensities. Sulfide and thiolate are not present in the sample in equal amounts and thus to do not contribute to the spectrum equally. To compare the intensities of their pre-edge transitions, the respective pre-edge intensities must be re-normalized based on the fraction of the given type of sulfur contributing to the spectrum. Sulfide-based transition intensity will be re-normalized by a factor of 3 and thiolate-based transition intensity will be re-normalized by a factor of 3/2. Before re-normalization, the lower energy sulfide-based pre-edge transitions (#1 and #2) in the Fe-S dimer spectra appear qualitatively more intense than the thiolate-based pre-edge transition (#3) (see Figure 6.5). Thus the re-normalization process will clearly result in sulfide-based transitions with larger intensity than thiolate-based transitions. This qualitative result indicates that the amount of sulfide character in the metal d-derived orbitals is greater than the thiolate character, consistent with the bridging nature of the sulfide.

Increased covalency is likely related to greater charge donation by each sulfide (relative to thiolate) which would shift the sulfide 1s core to relatively deeper binding energy. However, as has been shown in the above energy analysis, this charge donation is not enough to shift the sulfide core energy deeper than the thiolate core energy.

6.4.4. S K-edges of Tetrameric Complexes

6.4.4.1. Transition Assignments. The transition observed at the rising edge (#4) for $[Fe_4S_4(SR)_4]^{2-}$ spectra (Figure 6.7) is assigned as in the monomers and dimers as a thiolate-based transition. Support for this assignment comes from the fact that it is absent in the spectrum of $[Fe_4S_4Cl_4]^{2-}$, which has no thiolates. Further, the energy of this feature is very similar for systems with the same thiolate: ($[Fe_4S_4(SEt)_4]^{2-}$ and $[Fe_2S_2(SEt)_4]^{2-}$), ($[Fe_4S_4(SBz)_4]^{2-}$ and $[Fe_2S_2(S_2\text{-o-xyl})_2]^{2-}$) and, ($[Fe_4Se_4(SPh)_4]^{2-}$ and $[Fe(II)(SPh)_4]^{2-}$).

Transitions in the pre-edge region are assigned by first examining the spectra of $[Fe_4S_4Cl_4]^{2-}$ and $[Fe_4Se_4(SPh)_4]^{2-}$ (Figure 6.8). The sulfide-based pre-edge feature in $[Fe_4S_4Cl_4]^{2-}$ is assigned, in analogy to the transitions in the S K-edge spectrum of $[Fe_2S_2Cl_4]^{2-}$, as transitions (#1-2) from the sulfide 1s orbital to both the e- and t_2-sets of T_d orbitals. The thiolate-based pre-edge transition in $[Fe_4Se_4(SPh)_4]^{2-}$ occurs at slightly higher energy than the sulfide-based transitions in $[Fe_4S_4Cl_4]^{2-}$. Theoretically, the thiolate and sulfide ligands in these systems should each give rise to two pre-edge transitions (to both the e- and t_2-sets of metal d-derived orbitals) and it is thus assumed that the $[Fe_4Se_4(SPh)_4]^{2-}$ pre-edge feature also contains two transitions. In analogy to the

$[Fe_2S_2Cl_4]^{2-}$ spectrum, the rising edge shoulder in the $[Fe_4S_4Cl_4]^{2-}$ spectrum is attributed to a transition to a molecular orbital with both S 3p and metal (*e.g.* 4s) character.

The pre-edge region of the $[Fe_4S_4(SR)_4]^{2-}$ spectra were fit using only two transitions, the energies of which are very similar to the transitions in $[Fe_4S_4Cl_4]^{2-}$. However, because both $[Fe_4S_4Cl_4]^{2-}$ and $[Fe_4Se_4(SPh)_4]^{2-}$ exhibit pre-edge features, the pre-edge band in the $[Fe_4S_4(SR)_4]^{2-}$ spectra is attributed (in analogy to the dimeric systems) to both sulfide and thiolate transitions. Figure 6.9 shows a composite S K-edge spectrum which is the sum of the $[Fe_4S_4Cl_4]^{2-}$ and $[Fe_4Se_4(SPh)_4]^{2-}$ spectra, plotted with the experimental spectrum of $[Fe_4S_4(SEt)_4]^{2-}$. The spectra are very similar, indicating that both sulfide and thiolate transitions are likely to occur under the pre-edge band in the $[Fe_4S_4(SR)_4]^{2-}$ spectra. Based on the spectra of $[Fe_4S_4Cl_4]^{2-}$ and $[Fe_4Se_4(SPh)_4]^{2-}$, the sulfide transitions in the tetramer pre-edge band are assumed to be at lower energy. As in the dimers, each ligand is expected to give rise to two pre-edge transitions (to the e- and t_2-sets of T_d orbitals) for a total of four pre-edge transitions.

6.4.4.2. Pre-edge Transition Energies. Based on the above assignments, the sulfide-based transitions occur at lower energy than the thiolate-based transitions. Since the transitions within each complex are to the same metal d-derived orbitals, the energy splittings indicate that the sulfide 1s core is at less deep binding energy than the thiolate 1s core.

The energies of the pre-edge features in the $[Fe_4S_4(SR)_4]^{2-}$ tetramer spectra are nearly identical, indicating that the energies of the sulfide and thiolate transitions are similar across the series. As in the dimers, this may indicate that the respective sulfur 1s core orbital energies and the metal d-derived orbital energies of these complexes are the same, or it may indicate simply that the difference between the sulfur 1s and the metal d-derived orbital energies are similar.

6.4.4.3. Pre-edge Transitions Intensities. Because the pre-edge transitions are less well-resolved for the tetramers than for the dimers, it is difficult to analyze even qualitative differences in transition intensity. However, the composite spectrum in Figure 6.9 (of $[Fe_4S_4Cl_4]^{2-}$ plus $[Fe_4Se_4(SPh)_4]^{2-}$) is similar to the experimental tetramer spectrum. This indicates that the experimental tetramer pre-edge intensities are at least qualitatively similar to the intensities in the spectra of each $[Fe_4S_4Cl_4]^{2-}$ and $[Fe_4Se_4(SPh)_4]^{2-}$. These data indicate that the sulfide pre-edge intensity is significantly greater than the thiolate intensity (see Figure 6.8). This qualitative result indicates that the sulfide-Fe interaction is more covalent than the thiolate-Fe interaction, consistent with the bridging nature of the sulfide.

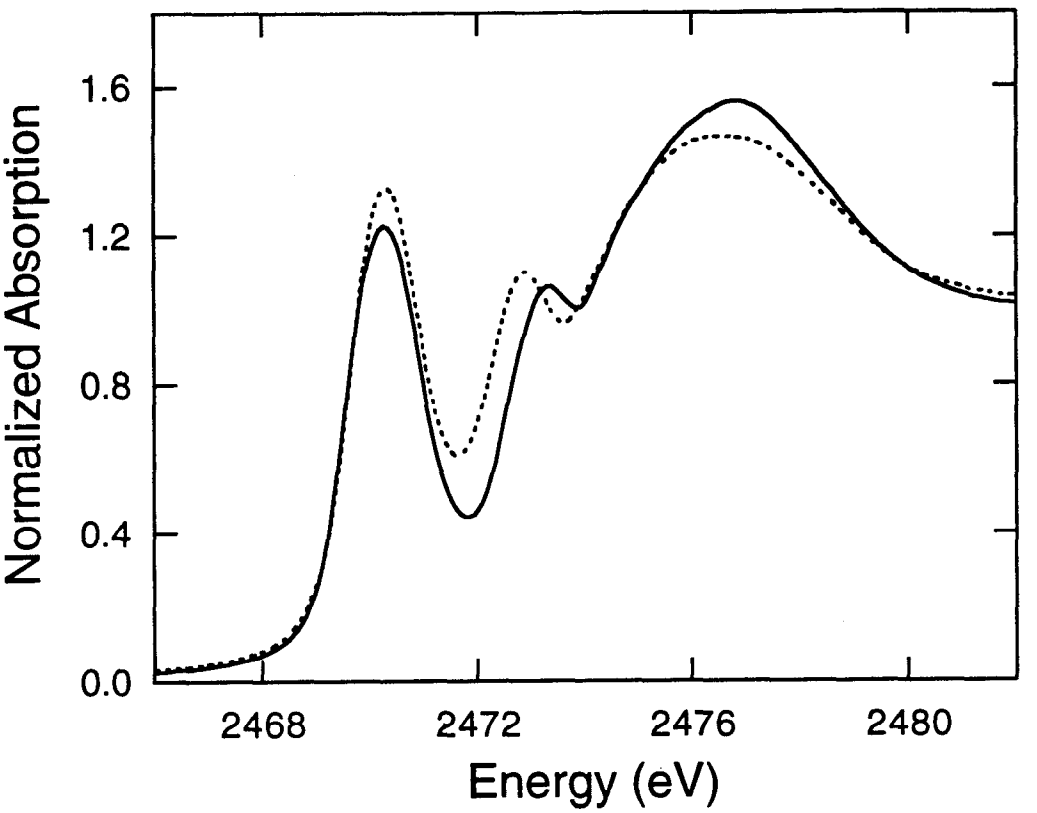

Figure 6.9. Composite S K-edge spectrum (—) constructed from a normalized 1:1 summation of the $[Fe_4S_4Cl_4]^{2-}$ and $[Fe_4Se_4(SPh)_4]^{2-}$ spectra. The S K-edge spectrum of $[Fe_4S_4(SEt)_4]^{2-}$ (·····) is plotted for comparison. The features in the composite spectrum are very similar to those in the true experimental spectrum.

Increased covalency is likely related to greater charge donation by sulfide (relative to thiolate) which would shift the sulfide 1s core to relatively deeper binding energy. However, as has been shown in the above energy analysis, this charge donation is not enough to shift the sulfide core energy to deeper energy than the thiolate core.

6.4.5. Fe-S Bonding in 1Fe, 2Fe and 4Fe Complexes

6.4.5.1. Iron oxidation state: $[Fe(II)(S_2\text{-o-xyl})_2]^{2-}$ *vs.* $[Fe(III)(S_2\text{-o-xyl})_2]^{-}$. Because $[Fe(II)(S_2\text{-o-xyl})_2]^{2-}$ does not exhibit a pre-edge feature, the thiolate-Fe bonding can not be compared for ferrous *vs.* ferric iron centers. However, the thiolate-based transition (#4) observed at the onset of each rising edge can be compared (Figure 6.3a and 6.4a). That this transition is somewhat lower in energy in the ferrous complex might indicate that the thiolate 1s core energy is less deep for thiolate bound to Fe(II). Thus, the thiolate bound to Fe(II) would donate less charge (is more negatively charged) than that bound to Fe(III). This is consistent with results observed in Cl K-edges for $FeCl_4^{2-/1-}$ (see Chapter 5) and with the longer bond lengths observed in the ferrous complex (see Table 6.1). Because the energy of the thiolate-based transition varies with the nature of the thiolate, it is unclear whether energies of this transition can be used generally (*e.g.*, between different thiolates) to measure S 1s core shifts.

6.4.5.2. Bridging Sulfide Bonding: $[Fe_2S_2Cl_4]^{2-}$ *vs.* $[Fe_4S_4Cl_4]^{2-}$. Figure 6.10 shows the S K-edge spectra of $[Fe_2S_2Cl_4]^{2-}$ and $[Fe_4S_4Cl_4]^{2-}$. The rising edge inflection points are very nearly the same (~2475.6 and ~2475.7 eV for $[Fe_2S_2Cl_4]^{2-}$ and $[Fe_4S_4Cl_4]^{2-}$, respectively). Despite the fact that the energies are not well-defined, the similarity indicates that the sulfide 1s cores are at similar energy. Thus, the total charge donated by a doubly-bridging sulfide is similar to that of a triply-bridging sulfide; and the charge donated per iron by a given sulfide is greater in the dimer than in the tetramer. This would also indicate that the total charge donation from sulfide ligands is the same for an iron in a dimer and in a tetramer. Since the oxidation states of the irons are different, however, this difference in charge donation may not reflect intrinsic properties of a doubly bridged vs. triply bridged sulfide, but may reflect differences in the oxidation state of the metal (the $Fe^{2.5+}$ in the tetramer is less able to accept charge from the coordinating ligands).

The pre-edge transitions occur at lower energy in the S K-edge spectrum of $[Fe_2S_2Cl_4]^{2-}$ than $[Fe_4S_4Cl_4]^{2-}$. Because the core energies are similar, this must arise from differences in the metal d-derived orbital energies, which reflect differences in

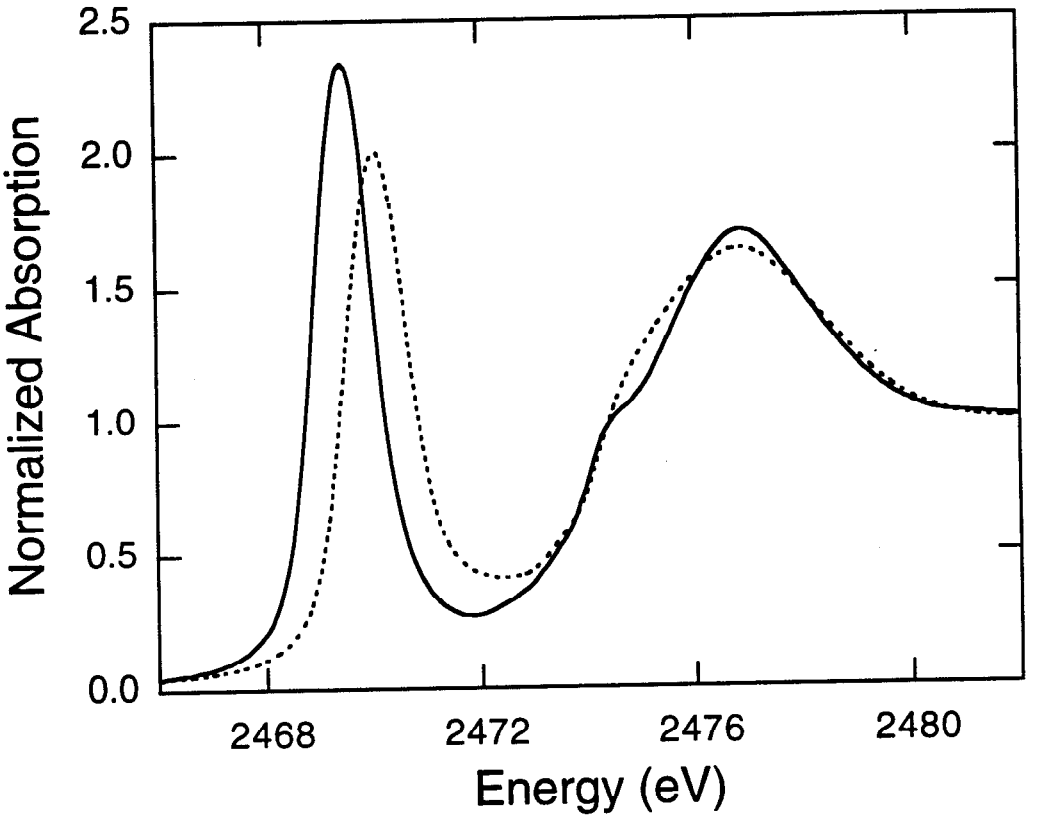

Figure 6.10. Sulfide S K-edge spectra of $[Fe_2S_2Cl_4]^{2-}$ (—) and $[Fe_4S_4Cl_4]^{2-}$ (·····). The pre-edge transition is lower in energy and more intense for the dimer and the rising edge inflection is at higher energy for the dimer than for the tetramer.

d-manifold energy. The result is consistent with the deeper energy of the iron d-manifold in the dimer due to the increased charge on the metal relative to the tetramer. The same result was observed in the Cl K-edge spectra of the terminal chlorides of these complexes (see Section 6.4.1).

The pre-edge transition is more intense in the dimer spectrum, possibly indicating that the sulfide character is greater in the metal d-derived orbitals of the dimer than in the tetramer. This would be consistent with the rising edge energy analysis, which suggests that each sulfide-iron interaction is stronger in the dimer. Note that the decrease in intensity in the tetramer may also be related to the change in d-orbital occupancy in the $Fe^{2.5+}$ ion. Expressions analogous to those for a ligand bound to a T_d Fe(III) ion in Chapter 5, must be derived for the $Fe^{2.5+}$ center in order to determine the effect this might have on intensity.

6.4.5.3. Terminal Thiolate Bonding: $[Fe_2S_2(SEt)_4]^{2-}$ *vs.* $[Fe_4S_4(SEt)_4]^{2-}$

Figure 6.11 shows the S K-edge spectra of $[Fe_2S_2(SEt)_4]^{2-}$ and $[Fe_4S_4(SEt)_4]^{2-}$ comparing systems with the same terminal thiolate ligand. The energy of the pre-edge band is lower in the dimer than in the tetramer, which is consistent with the d-manifold shift described above for $[Fe_2S_2Cl_4]^{2-}$ *vs.* $[Fe_4S_4Cl_4]^{2-}$.

The pre-edge transitions are better resolved in the dimer than in the tetramer. (There is less of an energy spread in the transitions of the tetramer). Since the transitions within each complex are to the same set of metal d-derived orbitals, the thiolate and sulfide 1s core orbitals must be closer in energy in the tetramer than in the dimer. The sulfide core energies are observed to be similar in the dimers and tetramers (based on the spectra of $[Fe_2S_2Cl_4]^{2-}$ and $[Fe_4S_4Cl_4]^{2-}$). Thus, transition energy differences must come from variations in thiolate core energy between dimer and tetramer. The thiolate must be more negative (closer to the charge of sulfide) in the tetramer, indicating the thiolate donates less charge in the tetramer than in the dimer. A similar result was obtained for the terminal chlorides in $[Fe_2S_2Cl_4]^{2-}$ and $[Fe_4S_4Cl_4]^{2-}$ from the rising edge inflection points of the Cl K-edge spectra.

6.5. Discussion

Features in the Cl and S K-edge spectra of Fe-S systems have been assigned qualitatively and preliminary results have been presented. Spectra of complexes containing terminal thiolate ligands display an intense thiolate-based feature at the rising edge. The energy of this feature varies significantly with the type of thiolate ligand. In

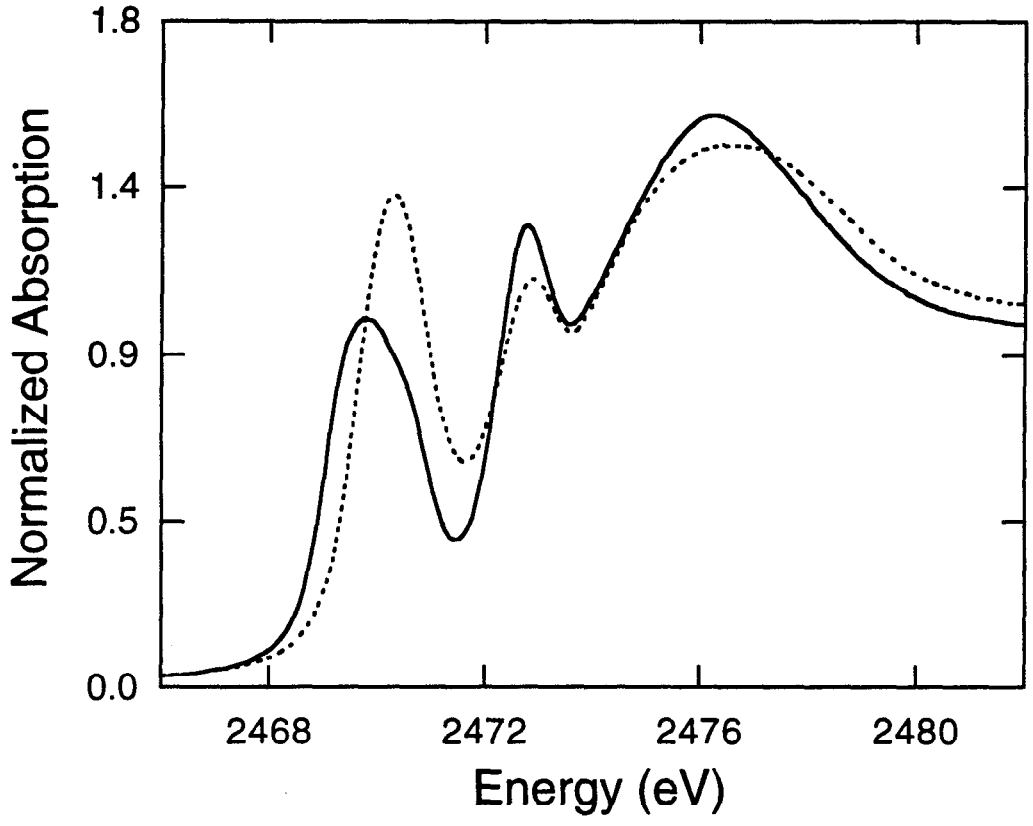

Figure 6.11. S K-edge spectra of $[Fe_2S_2(SEt)_4]^{2-}$ (—) and $[Fe_4S_4(SEt)_4]^{2-}$ (·····). The transitions which contribute to the pre-edge band in the dimer are much better resolved than in the tetramer spectrum. The sharp transition which occurs at the rising edge is at the same energy in both spectra.

order to understand the source of these energy shifts, the nature of the orbitals involved in the thiolate transition must be defined.

The S K-edge spectra of ferrous tetrathiolates do not exhibit a resolved pre-edge feature and thus ferrous-thiolate bonding can not be probed using ligand XAS. This study did not, however, examine any ferrous-sulfide interactions. The pre-edge transitions of sulfide ligands have been shown to appear at lower energy than thiolate pre-edges in those systems with both ligand types. It is possible, then, that ferrous-sulfide systems would exhibit pre-edge feature intensity and that ligand XAS could successfully be applied, for instance, to the investigation of the one-electron reduced form of the 2Fe site which is a localized, Class II, Fe(II)Fe(III) dimer.

In the spectra of both dimeric and tetrameric Fe-S sites, both sulfide and thiolate pre-edge features are observed. The thiolate transitions occur at higher energy, reflecting the deeper 1s core of the less negative thiolate ligand. The sulfide covalency in the metal d-derived orbitals appears to be greater than the thiolate, due to the bridging nature of the sulfide ligands.

The bridging sulfide ligands in the tetramer donate the same total charge as in the dimer. Thus, charge donated per iron by a given sulfide is greater in the dimer than in the tetramer. Further, the sulfide pre-edge intensity is greater for the dimer, suggesting that the sulfide covalency in the metal d-derived orbitals of the dimer is greater than in the tetramer. However, to confirm this result, expressions analogous to those in Chapter 5 for a ligand bound to a T_d Fe(III) ion, must be derived for the $Fe^{2.5+}$ center, in order to determine the effect the oxidation state difference might have on intensity. Both terminal thiolates and terminal chlorides donate less charge in the tetramer than in the dimer. This may be related to the difference in oxidation state of the metal in each cluster. Finally, spectra indicate that the d-manifold energy in the tetramers is at less deep binding energy than the dimer, consistent with differences in iron oxidation state.

These qualitative results demonstrate that the sulfide and thiolate contributions to spectra of Fe-S complexes can be identified. The pre-edge transition energies and intensities must now be quantitated in order to gain a more thorough understanding of the relationship between electronic structure and electron transfer reactivity in these sites, as well as the differences which give rise to electron delocalization in the tetramers *vs.* localization in the dimers. This quantitative interpretation of these data can be accomplished using a combination of empirical fitting techniques and theoretical energy splittings and intensity ratios, like those presented in Chapter 5 and shown schematically for $Fe(III)Cl_4^-$ in Figure 5.4e.

6.6. Acknowledgments

This research was supported by grants from NSF (CHE-9217628, E.I.S.) (CHE91-21576, K.O.H.), and NIH (RR 01209, K.O.H.). SSRL operations are funded by the Department of Energy, Office of Basic Energy Sciences. The Biotechnology Program is supported by the NIH, Biomedical Research Technology Program, National Center for Research Resources. Further support is provided by the Department of Energy, Office of Health and Environmental Research. We would also like to thank Dr. Patrick Frank for helpful advice regarding the syntheses of many of the compounds included in this study and Kendra Williams for assistance with the preliminary fitting of the ligand K-edge data and in the assembly of information for this Chapter.

6.7. References and Notes

(1) Stiefel, E. I.; George, G. N. In *Bioinorganic Chemistry*; Bertini, I.; Gray, H. B.; Lippard, S. J.; Valentine, J. S., Ed.; University Science Books: Mill Valley, CA, 1994; pp 365-453.

(2) Gray, H. B.; Ellis, W. R., Jr. In *Bioinorganic Chemistry*; Bertini, I.; Gray, H. B.; Lippard, S. J.; Valentine, J. S., Ed.; University Science Books: Mill Valley, CA, 1994; pp 315-364.

(3) Thomson, A. J. In *Metalloproteins, Part 1: Metal Proteins with Redox Roles*; Harrison, P. M., Ed.; Verlag Chemie: Weinheim, 1985; pp 79-120.

(4) *Iron-Sulfur Proteins*; Spiro, T. G., Ed.; John Wiley & Sons, Inc.: New York, 1982.

(5) *Iron-Sulfur Proteins, Vol. I, Biological Properties*; Lovenberg, W., Ed.; Academic Press: New York, 1973.

(6) *Iron-Sulfur Proteins, Vol. II, Molecular Properties*; Lovenberg, W., Ed.; Academic Press: New York, 1973.

(7) Anderson, P. W. *Solid State Phys.* **1963**, *14*, 99.

(8) Hay, P. J.; Thibeault, J. C.; Hoffman, R. *J. Am. Chem. Soc.* **1975**, *97*, 4884-4899.

(9) de Loth, P.; Cassioux, P.; Daudey, J. P.; Malrieu, J. P. *J. Am. Chem. Soc.* **1981**, *103*, 4007-4016.

(10) Johnson, C. E. *J. Appl. Phys.* **1971**, *42*, 1325-1331.

(11) Middleton, P.; Dickson, D. P. E.; Johnson, C. E.; Rush, J. D. *Eur. J. Biochem.* **1980**, *104*, 289-296.

(12) Münck, E.; Papaefthymiou, V.; Surerus, K. K.; Girerd, J.-J. *ACS Symp. Ser.* **1988**, *372*, 302-325.

(13) Bertini, I.; Briganti, F.; Luchinat, C.; Scozzafava, A.; Sola, M. *J. Am. Chem. Soc.* **1991**, *113*, 1237-1245.

(14) Aizman, A.; Case, D. A. *J. Am. Chem. Soc.* **1982**, *104*, 3269-3279.

(15) Papaefthymiou, V.; Girerd, J.-J.; Moura, I.; Moura, J. J. G.; Münck, E. *J. Am. Chem. Soc.* **1987**, *109*, 4703-4710.

(16) Noodleman, L.; Baerends, E. J. *J. Am. Chem. Soc.* **1984**, *106*, 2316-2327.

(17) Noodleman, L.; Norman, J. G.; Osborne, J. H.; Aizman, A.; Case, D. A. *J. Am. Chem. Soc.* **1985**, *107*, 3418-3426.

(18) See Chapter 5, Section 5.4.2.2.

(19) Note that equations 6.1 and 6.2 describe total multiplet intensity. Experimental intensity can be reduced due to higher state mixing in intermediate ligand fields (see Chapter 5).

(20) See Chapter 2, Section 2.4.1.

(21) Holm, R. H.; Berg, J. In *Iron-Sulfur Proteins*; Spiro, T. G., Ed.; John Wiley & Sons, Inc.: New York, 1982; pp 1-66.

(22) McGinnety, J. A. *J. Am. Chem. Soc.* **1972**, *94*, 8406-8413.

(23) Hedman, B.; Frank, P.; Gheller, S. F.; Roe, A. L.; Newton, W. E.; Hodgson, K. O. *J. Am. Chem. Soc.* **1988**, *110*, 3798-3805.

(24) Lytle, F. W.; Greegor, R. B.; Sandstrom, D. R.; Marques, E. C.; Wong, J.; Spiro, C. L.; Huffman, G. P.; Huggins, F. E. *Nucl. Instr. Meth.* **1984**, *226*, 542-548.

(25) Stern, E. A.; Heald, S. M. *Rev. Sci. Instrum.* **1979**, *50*, 1579-1582.

(26) Argonne National Laboratory; B. S. Garbow, K. E. Hillstrom, J. J. More.

(27) Agarwal, B. K. *X-ray Spectroscopy*; Springer-Verlag: Berlin, 1979, pp 276ff.

(28) Tyson, T. A.; Roe, A. L.; Frank, P.; Hodgson, K. O.; Hedman, B. *Phys. Rev. B* **1989**, *39A*, 6305-6315.

(29) Lytle, F. W. In *Applications of Synchrotron Radiation*; Winick, H.; Xian, D.; Ye, M. H.; Huang, T., Ed.; Gordon & Breach: New York, 1989; pp 135.

(30) Shadle, S. E.; Hedman, B.; Hodgson, K.; Solomon, E. I. *Inorg. Chem.* **1994**, in press.

Chapter 7

Electrochemical and X-ray Absorption Studies of the 2Fe2S Active Site in Spinach Ferredoxin

7.1. Introduction

Spinach ferredoxin (Fd) is a small (~11,000 MW) protein which serves as an electron carrier in the photosynthetic pathway.[1] The 2Fe active site, pictured below, exists in two biologically relevant redox states: the oxidized diferric form and the one-electron reduced, trapped-valence Fe(III)Fe(II) site.

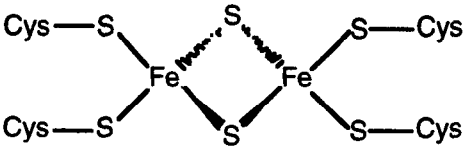

In order to understand the electronic structural basis for the facile electron transfer function of this protein, it is necessary to study the protein in both redox states. Despite the extensive work done to model the 2Fe ferredoxin active site, stable formation of a mixed-valent model complex has been elusive. Such a complex has been generated in solution, but not in high purity and with a lifetime of only ~10^{-3} sec at room temperature.[2] Because X-ray absorption spectroscopy (XAS) requires samples of high purity which are stable for many hours, model studies of the mixed-valent site, such as those described in Chapter 6, are not currently possible. Thus, in an effort to gain information about the one-electron reduced, mixed-valent active site, studies have been undertaken to electrochemically generate this redox state in the protein and then study the site using XAS.

Using electrochemical methods to produce and stabilize redox states of interest for XAS has been successfully applied to XAS studies of the iron-molybdenum cofactor (FeMoco) of nitrogenase at both the Mo K-edge and the S K-edge.[3,4] The methodology and apparatus developed for these studies has provided a basis for the studies described herein. The sample, contained in a sealed cell, is controlled electrochemically through its contact with a reticulated vitreous carbon (RVC) electrode. RVC has an open pore structure which allows efficient electrolysis without stirring. And, unlike metal electrodes, the RVC electrode has negligible absorption and scattering properties in the X-ray energy regions of interest. Electrochemical studies of FeMoco which utilized this apparatus were performed in NMF solution.[3,4] In order to successfully control the aqueous electrochemistry of Fd several adaptations were made to the apparatus and experimental strategy and are described in this chapter.

The reduction potential of Fd is -0.42 V (vs. SHE)[5] and the protein is highly negatively charged, carrying a charge of -17 at neutral pH (for the oxidized form of the

protein). The protein has been successfully reduced directly using modified gold electrodes,[6] metal oxide electrodes,[7] and pyrolytic graphite (PG) electrodes. Extensive studies utilizing PG electrodes to study the electrochemistry of Fd directly have specific relevance to this study. The PG electrode edge used as the active surface is characterized by negatively charged C-O groups,[8,9] similar to the modified surface of RVC used in this study. Armstrong and coworkers found that the addition of a positively charged, redox inert complex ($[Cr(NH_3)_6]^{3+}$) functioned electrostatically as a modulator of electrochemical behavior, presumably making the interaction between the negatively charged electrode and the negatively charged Fd more favorable.[8] Addition of $[Cr(NH_3)_6]^{3+}$ not only stimulated the initial electrochemical response, but also retarded the deterioration of response with time.[8]

This chapter first describes the tests which were performed to characterize the RVC electrode response and to determine the optimal conditions for electrochemical control of Fd. Then, the details of the X-ray spectroelectrochemical experiments are described. Because this was the first attempt to electrochemically stabilize a metalloprotein in aqueous solution for XAS measurements, a number of unanticipated problems were discovered during the experiments. These difficulties and steps which were taken to address them are presented. Due to the experimental problems, the reliability of the XAS results is limited. However, preliminary results are presented and discussed.

7.2. Experimental

7.2.1. Isolation and Preparation of Spinach Ferredoxin

Spinach ferredoxin (Fd) used in these experiments was prepared in one of two ways. A portion of the protein used was purified according to the method of Petering and Palmer[10] with modifications which have been previously described.[11] The second purification approach combined the method of Ellefson, *et al.*[12] for the isolation of spinach plastocyanin and that of Borchert and Wessels[13] for the combined isolation of plastocyanin and Fd. The latter procedure was followed through the step in which the dissolved acetone precipitate was loaded onto an anion exchange (DEAE-52) column. Plastocyanin was eluted with 0.2 M NaCl. Then the Fd was eluted with 0.35 M NaCl. The remaining steps in the purification followed the procedure of Borchert and Wessels.[13] For both procedures all purification steps were carried out in a cold room at 4°C. The purity of the Fd was measured by the A(422)/A(278) absorption ratio. Petering

and Palmer report this ratio to be 0.48 for pure Fd.[10] Final experimental ratios used here were 0.46 to 0.48. Protein not to be used immediately was stored as a dilute protein solution at -70°C in 0.15 M Tris-HCl or Tris-Trifluoroacetate (Tris-Tfa) buffer, pH=7.3, ~0.1% NaN_3 buffer with 1.0 M NaCl to stabilize the protein.

Preparation of the samples for electrochemical or XAS experiments was done in a cold room at 4°C. Dilute protein was concentrated in an Amicon ultrafiltration device with a YM5 filter and loaded onto G-25 column to reduce the salt concentration of the solution. Protein was eluted using 0.15 M Tris-Tfa, pH=7.3, 0.1 M NaCl buffer to exchange protein in Tris-HCl buffer for Tris-Tfa. These steps were taken to reduce the interference of chloride absorption at the S K-edge in XAS experiments. Protein was then concentrated to 1-3 mM using an Amicon ultrafiltrator with a YM5 filter, or Centricon-3 or -10 ultrafiltration devices. A UV/Vis absorption spectrum was taken to verify the purity of the sample. The A(422)/A(278) absorption ratio ranged from 0.44 to 0.48 for different sample preparations.

Protein was made anaerobic for the electrochemistry experiments by placing ~1 ml of concentrated protein solution and a flea stir bar in a crimp top vial with a septum. The top was crimped on and two syringe needles were placed through the septum. In a cold room (~4°C) the vial was placed in a small beaker and put in a sealed jar with gas inlet and outlet valves. The jar was clamped onto a stir plate and buffer-saturated Ar or He was blown through the jar. Figure 7.1 shows a schematic of this set up. Helium was used exclusively for XAS experiments because this reduced the formation of bubbles in previously run solution samples. After 20-30 minutes, the gas flow was turned off and the valves to the jar closed. Quickly, the cap to the jar was unscrewed and the syringe needles removed. The vial top was wrapped with 1-2 layers of Saran wrap and rubber-banded in place. The vial of anaerobic protein solution was then brought into an anaerobic glove box.

7.2.2. Preparation of Mediators and Electrochemistry Solutions

Methyl viologen dichloride hydrate and the ligand 1,4,7-triazacyclononane ([9]aneN_3) were used as purchased from Aldrich Chemical Co. $[Co^{III}([9]aneN_3)_2]Cl_3$ (hereafter, Co9ane) was synthesized according to published methods[14] with minor modifications. After addition of the ligand to the $CoCl_2$ solution, a precipitate formed which, while initially yellow, turned red-brown with increased exposure to air. The solid was filtered and redissolved in H_2O. The solution was very basic and, upon acidification with 12 M HCl, a yellow precipitate formed, which was filtered and washed with cold

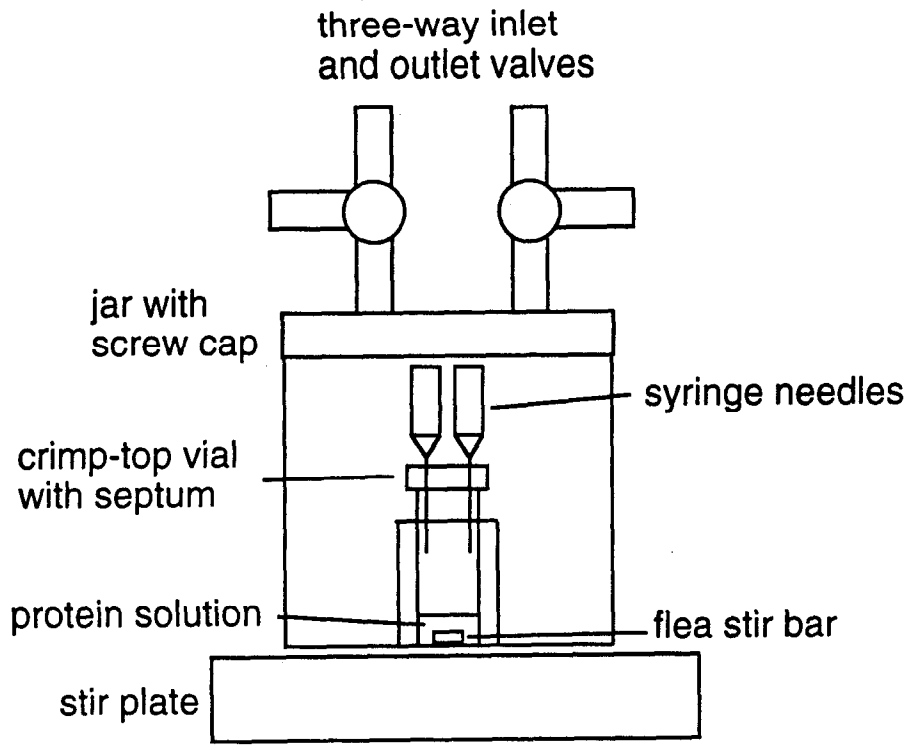

Figure 7.1. Apparatus for preparation of anaerobic protein solutions.

ethanol. The formation of desired product was verified using UV/Vis spectroscopy. The reduced form of the mediator $[Co^{II}([9]aneN_3)_2]Cl_2$ was synthesized anaerobically in an inert atmosphere box with an O_2 concentration of less than 3 ppm. $CoCl_2 \cdot 6H_2O$ was dissolved in dry DMSO in a Schlenk flask. The triazacyclononane ligand, dissolved in ethanol, was added to the DMSO solution with stirring. A precipitate formed which was filtered in a Schlenk filter inside the glove box using a pump and trap attached to the box atmosphere. The solid had a slightly yellowish tinge and was shown by UV/Vis spectroscopy to contain approximately 6.5% oxidized sample.

Buffers and solutions for Fd electrochemistry were prepared from 18 MΩ water which had been deoxygenated using the freeze-pump-thaw technique and was stored under an inert atmosphere.

7.2.3. Preparation of the Reticulated Vitreous Carbon Electrode

Reticulated vitreous carbon (RVC)[15] sponge (100 ppi) was obtained from ERG, Inc. (Oakland, CA). The RVC as purchased is not water-wettable. Chemical modification of the surface was necessary for aqueous work. The treatment, adapted from published procedures,[16] involved stirring 1" x 2" pieces of RVC in a solution of 0.2 M $KMnO_4$ in 2 M H_2SO_4 for ~35 minutes. After 35 minutes the treated RVC sank quickly in a beaker of water and no bubbles were observed in the RVC pores. Treated RVC was rinsed until the DI water wash ran visibly clear. Treated pieces were then stirred in fresh DI water, exchanging the bath at least three times, followed by an ethanol rinse. The RVC was allowed to air-dry thoroughly before use.

7.2.4. Electrochemistry

7.2.4.1. Instrumentation. All electrochemical experiments were performed using a BAS (West Lafayette, IN) CV-27 voltammograph, which was interfaced to a Hyundai 8088-based personal computer via a DAS-16 A/D board (Metrabyte, Taunton, MA). Software for cyclic voltammetry and coulometry was written by Dr. Benjamin J. Feldman.

The reference electrode was an Ag/AgCl (3 M KCl saturated with AgCl) microelectrode (Model MI-401, Microelectrodes Inc. Londonderry, NH).

7.2.4.2. Electrochemical Tests. Electrochemical tests were performed to characterize the electrochemistry of all components of the experiment before XAS experiments were performed. The cell used for this purpose is shown schematically in

Figure 7.2a. It consists of a teflon torus which screws onto a Kel-F rod, in which is embedded a concentric glassy carbon rod. The teflon torus surrounds the ~50 µl sample space into which a small piece of RVC is fit tightly. The teflon torus has a small hole through which a 24 gauge Pt wire is placed in contact with the RVC, providing an electrical contact with the working electrode. The sample space is filled slowly with solution using a Hamilton gas-tight syringe. The reference electrode and an agar/3M KCl solution salt bridge are put in contact with the top of the RVC surface, ensuring electrochemical connection. A Pt wire is held in contact with the far side of the salt bridge which constitutes the auxiliary half-cell. Once testing was underway, more than one cell became necessary and an "ad hoc" version of this cell was used (Figure 7.2b). The sample space consisted of the tip of a microcentrifuge tube embedded in modeling clay and held in a microcentrifuge tube. The "ad hoc" cell holds approximately the same volume as the original test cell.

Electrochemical tests were performed in an anaerobic "wet-box" with an O_2 concentration of 150 ppm. All tests were performed at room temperature. UV/Vis spectra of Fd samples, taken before and after testing, showed minimal degradation of protein, even after tests lasting many hours.

7.2.4.3. The XAS Electrochemical Cell and Set-up. The X-ray absorption spectroelectrochemical cell is pictured in Figure 7.3. The details of its assembly are described elsewhere.[3] The cell consists of an auxiliary compartment (back) and the sample compartment (front), separated by a Nafion 117 membrane (DuPont). Both spaces are filled with water-wettable RVC. A thin window covers the sample space and allows X-rays and fluorescent intensity to pass in and out of the sample cell. In experiments #2-5, 6.3 µm polypropylene was used as a window material. In experiments #6-7, 7.6 µm Kapton was used. Window materials were obtained from Chemplex (Eastchester, NY). Separate Pt wires provide contact with the auxiliary and sample electrodes; a port for a reference electrode provides contact with the sample space. In these experiments, the auxiliary compartment was filled (*via* syringe) with ~200 µl of a redox buffer. It was made in advance from anaerobic 0.15 M Tris-Tfa buffer, pH=7.3, with 0.1 M NaCl and contained the oxidized and reduced forms of the Co9ane complex in equal concentrations of ~2x the concentration of Fd used in the sample space. The sample compartment was filled with ~350-400 µl of a solution of 10:1 Fd:Co9ane mediator. This solution was prepared just before loading from anaerobic stock solutions of the protein and mediator each in 0.15 M Tris-Tfa buffer, pH=7.3, with 0.1M NaCl. The protein solution was pre-equilibrated with He, as described above, prior to the addition of mediator.

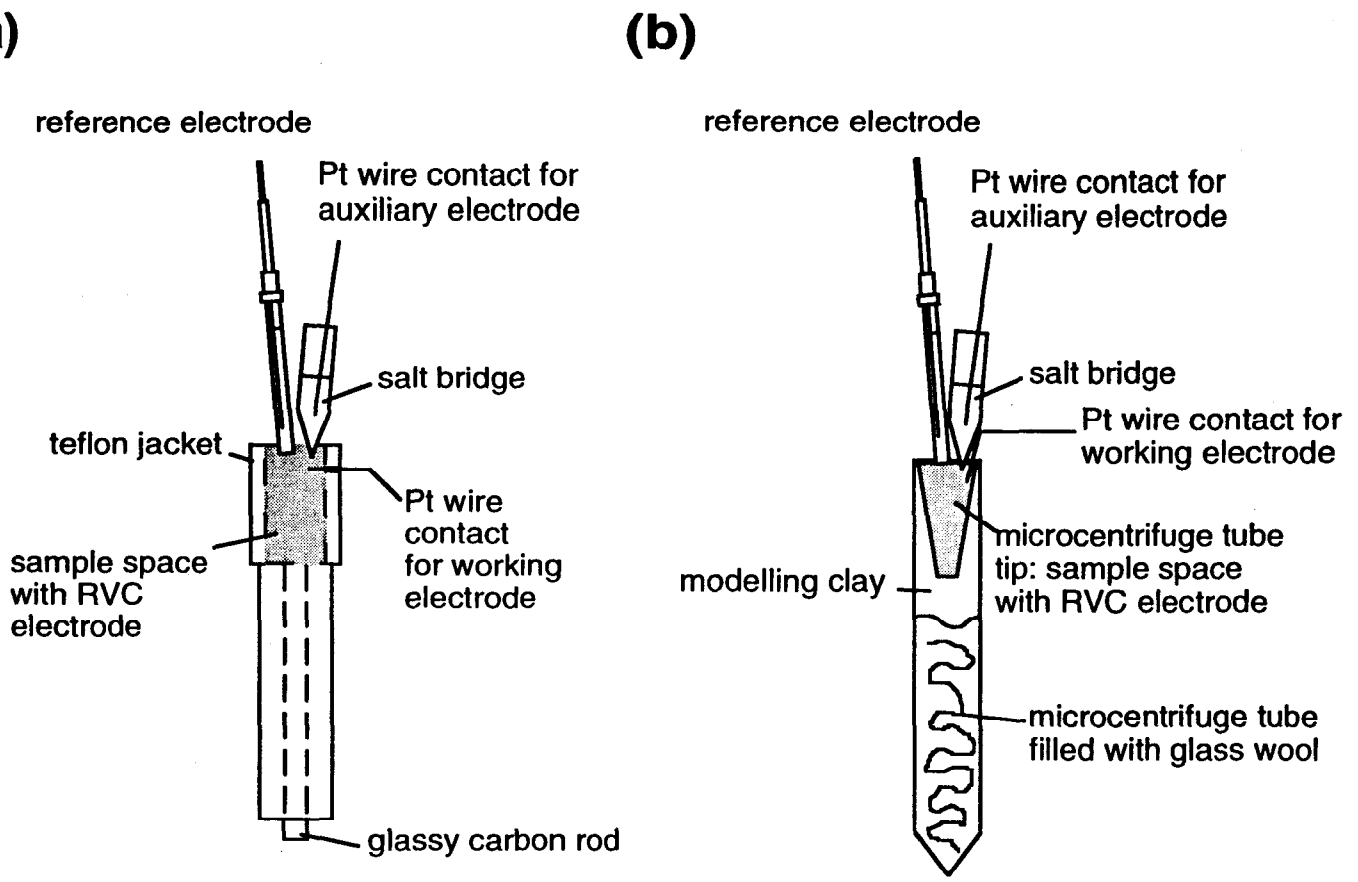

Figure 7.2. Electrochemical test cells. (a) the electrochemical test cell used for characterization of ferredoxin electrochemistry. (b) "ad hoc" electrochemical test cell. See text for detailed descriptions.

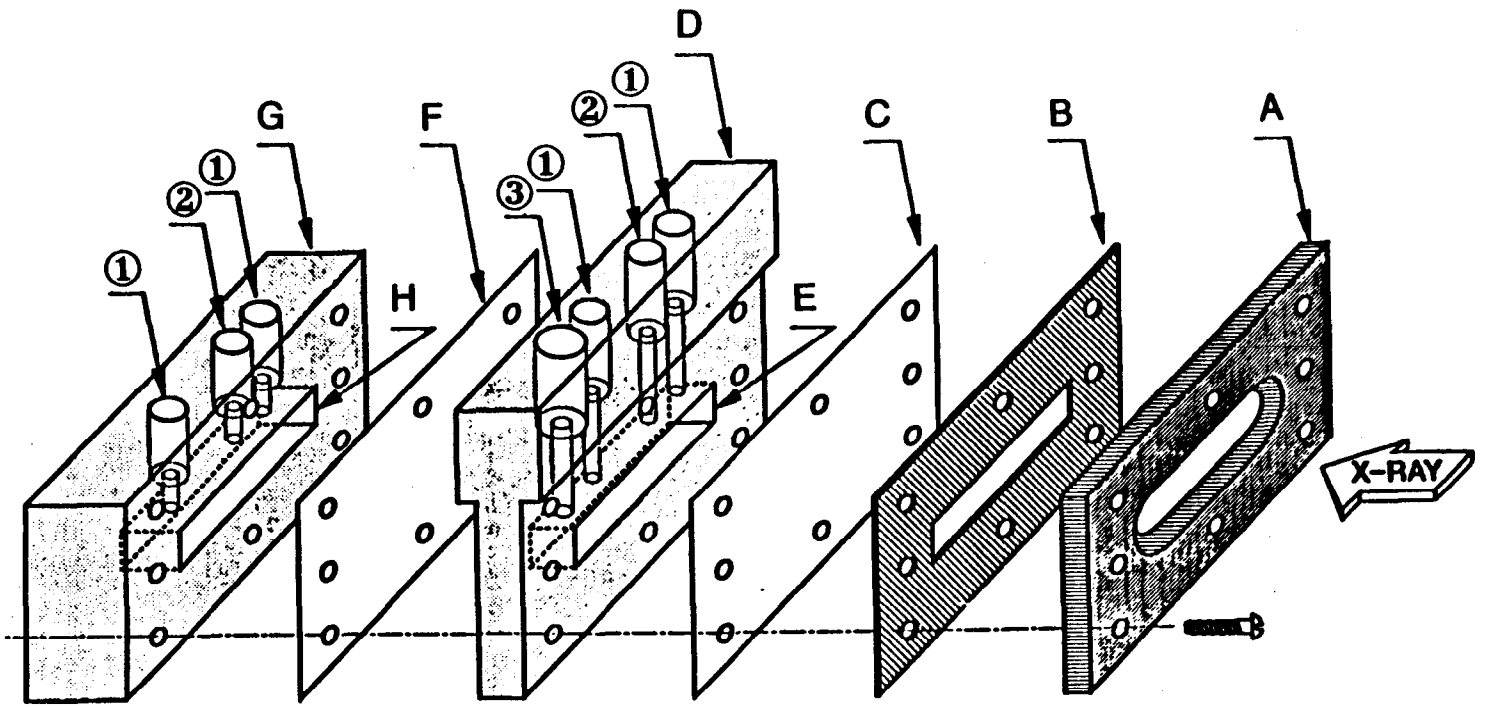

Figure 7.3. Diagram of the X-ray spectroelectrochemical cell used in this study. The labelled parts are: A. Aluminum front-plate; B. 1 mm butyl rubber gasket; C. Window; D. Sample section; E. Sample compartment; F. Nafion-117 conducting membrane; G. Rear section; H. Rear compartment for redox buffer. Spaces E and H are filled with water-wettable RVC. Holes designated with a ① are used to fill the respective compartments. Holes designated by a ② allow for connection to the RVC with Pt wire. The hole marked with a ③ allows reference electrode contact with the sample solution. During use, all the port holes contain silicone rubber septa. The seal is made by inserting and tightening stainless steel Allen screws bored to accommadate the electrode and Pt wires. Figure taken from reference 3.

7.2.4.4. Electrochemical Measurements. Cyclic voltammetry and coulometry were used in these studies to verify and modify, respectively, the redox state of the sample. In a cyclic voltammogram (CV), the applied voltage to the electrochemical cell is swept from an oxidizing voltage to a reducing voltage and back (or from a reducing voltage to an oxidizing voltage and back), monitoring the current generated in the sample. For Fd, CVs were performed between -0.2 V and -0.8 V.

Coulometric measurements involve the application of a constant oxidizing (-0.2 V) or reducing (-0.8 V) voltage for a fixed period of time during which the coulombs, Q, (the current passed per unit time) was monitored. Coulometry was used to convert an oxidized sample to the reduced state (and *vice versa*) and to quantitate the electrochemical conversion.

7.2.5. XAS Measurements and Data Acquisition.

All XAS experiments were carried out at the Stanford Synchrotron Radiation Laboratory under dedicated operations (3.0 GeV, ~50 mA) with radiation from the SPEAR storage ring.

Fe K-edge data were measured on beamline 4-1 with a Si(220) double-crystal monochromator. The monochomator was detuned ~50% to minimize higher harmonic components in the X-ray beam. Data were collected as fluorescence excitation spectra. Data were collected from 6830 to 7474 eV, with a step size of 0.15 eV in the edge region. The monochromator slits were set to a vertical height of 1 mm and the spectrometer resolution was ~1.0 eV.

S K-edge data were measured using the 54-pole wiggler beamline 6-2 in low magnetic field mode (5 kG) with a Si(111) double-crystal monochromator and a post-monochromator flat harmonic rejection mirror. Data shown in Figure 7.9, which were collected in 1991, were measured without the harmonic rejection mirror. For these experiments, the monochromator was detuned ~30% to minimize higher harmonic components in the
X-ray beam. All data were collected as fluorescence excitation spectra. Data were collected from 2440 to 2575 eV, with a step size of 0.08 eV in the edge region. The spectrometer resolution was ~0.5 eV.[17] A reproducibility in edge position determination of ~0.1 eV for these experiments was obtained by calculating and comparing first and second derivatives for model compounds measured during different experimental sessions. The sample box was purged with He or buffer-saturated He. All measurements were made at room temperature.

For spectra of oxidized protein samples (pre-equilibrated with He) not under electrochemical control, the protein solution was loaded *via* syringe into a 1 mm teflon spacer cell, sealed in back by a layer of Mylar tape and in front by a 6.3 μm polypropylene window.

The Fe K-edge energy was calibrated from the Fe K-edge spectra of an Fe foil, run at intervals between the sample scans. The first inflection point in the rising edge of this spectrum was assigned to 7111.2 eV. The S K-edge energy was calibrated from the S K-edge spectra of $Na_2S_2O_3 \cdot 5H_2O$, run at intervals between the sample scans. The maximum of the first pre-edge feature in this spectrum was assigned to 2472.02 eV. Due to the often long intervals between calibrations scans in these experiments, the energy calibration of some of these data may not be well determined.

7.2.6. Data Reduction

A smooth pre-edge background subtraction was removed from all spectra by fitting a polynomial to the pre-edge region and subtracting this polynomial from the entire spectrum. Normalization of the data was accomplished by fitting a flat polynomial or a straight line to the post-edge region and normalizing the edge jump to 1.0 at 7130 eV for the iron edges and at 2490 eV for the sulfur edges.

7.3. Characterization of the Electrochemistry of Spinach Ferredoxin

This section describes electrochemical tests which were conducted to characterize the RVC electrode response and to determine the optimal conditions for electrochemical control of Fd. A variety of tests were performed which were limited primarily by the availability of large quantities of Fd for tests. The following sections describe those results which have a bearing on the design of the XAS experiment.

Unless otherwise noted, all of the tests described in this section were conducted in the electrochemical test cell described in the Experimental Section 7.2.4.2 (Figure 7.2). This cell was used instead of the XAS electrochemical cell because of its relatively simple assembly and its smaller volume requirement.

7.3.1. Choice of Scan Rate and Electrolyte Concentration.

Tests were first performed to determine the electrochemical capability of the chemically modified RVC electrode. The Co9ane complex was chosen as the redox

agent for testing because its reduction potential (-0.41 V vs. SHE) is close to that of Fd, allowing characterization of the electrode response in the voltage region of interest.

The results of a series of CV experiments which tested different electrolyte concentrations and different CV scan rates on a ~1 M Co9ane solution are given in Table 7.1. The peak separation (the voltage between the anodic and cathodic peak maxima) will be 60 mV in the limit of purely diffusive electrochemistry.

Table 7.1. Comparison of Experimental Variables for Cyclic Voltammograms of Co9ane

Trial	Scan Rate (V/sec)	Concentration of Electrolyte (M)§	Peak Separation (mV)	Anodic Peak Current (mA)
1	0.01	0.1	72	0.11
2	0.02	0.1	70	0.13
3	0.05	0.1	91	0.18
4	0.07	0.1	100	0.20
5	0.01	0.2	72	0.10
6	0.02	0.2	67	0.13
7	0.05	0.2	80	0.18
8	0.10	0.2	109	0.25

§ electrolyte used was NaCl.

The results clearly show that at slower sweep rates the electrochemistry approached the diffusion-controlled limit. In addition, as the scan rate is reduced, so is the CV anodic peak current. The concentration of electrolyte in the solution does not make any detectable difference with respect to the variables tested in these experiments.

As a result of these data, a scan rate of 0.02 V/sec was used in all subsequent experiments. This allowed experiments to be reasonably close to diffusion limited and to still have clear anodic and cathodic peak currents. Also, this rate was used for Fd electrochemistry with a PG electrode.[8] Further, the concentration of supporting electrolyte used in all subsequent experiments was 0.1 M NaCl. The higher concentration did not appear to enhance the electrochemistry, and using the lower concentration allowed us to minimize the absorption by chloride ions at the S K-edge in XAS experiments.

7.3.2. Choice of Mediator and Protein-Mediator Ratio.

Initial attempts (not described in this chapter) to electrochemically reduce the spinach Fd protein directly with the RVC electrode were unsuccessful. It was thus decided to utilize a mediator in the redox process. The mediating substance was chosen on the basis that it have a reduction potential within 50 mV of that of Fd. Further, based on the results of Armstrong and coworkers,[8] who showed that the electrochemistry of spinach Fd was significantly enhanced and stabilized by the addition of the redox inert, positively charged species $Cr(NH_3)_6^{3+}$, the redox couple of the mediator was chosen to be as positively charged as possible. The species which most closely fit these criteria is that of Co9ane, which has a 2+/3+ redox couple and a reduction potential of -0.41 V.[14]

To characterize the behavior of Fd with a mediator as completely as possible, tests were also performed using methyl viologen (MV) as a mediator. (The redox couple for MV is 1+/2+ and so it was not as well suited to act as an electrostatic modulator of the electrochemistry.) Cyclic voltammograms of each mediating substance alone and in a solution which was ~ 2:1 protein:mediator are shown in Figure 7.4. The electrochemical parameters measured from these data are given in Table 7.2. The data clearly show that the CVs of the individual mediating species alone is significantly different from the protein-mediator solutions. The two protein-mediator solutions are, however, very similar.

Table 7.2. Literature and Experimentally-Determined Reduction Potentials

Redox Active Species	Reduction potential (vs. SHE)	Average of Anodic and Cathodic Peak Potentials (vs. Ag/AgCl)§
Co9ane	-0.41 V[14]	~ -0.56 V
MV	-0.45 V	~ -0.65 V
Fd	-0.42 V[5]	
Fd:Co9ane (~2:1)		~ -0.61 V
Fd:MV (~2:1)		~ -0.63 V

§ The reduction potential of a saturated Ag/AgCl electrode vs. SHE at 25°C is 0.199 V

These experimental results are in good agreement with published reduction potentials and indicate that the electrochemistry observed in the protein-mediator solution is that of Fd and not of the mediator. Based on these results, the Co9ane complex was used as a mediator in all subsequent electrochemistry of Fd.

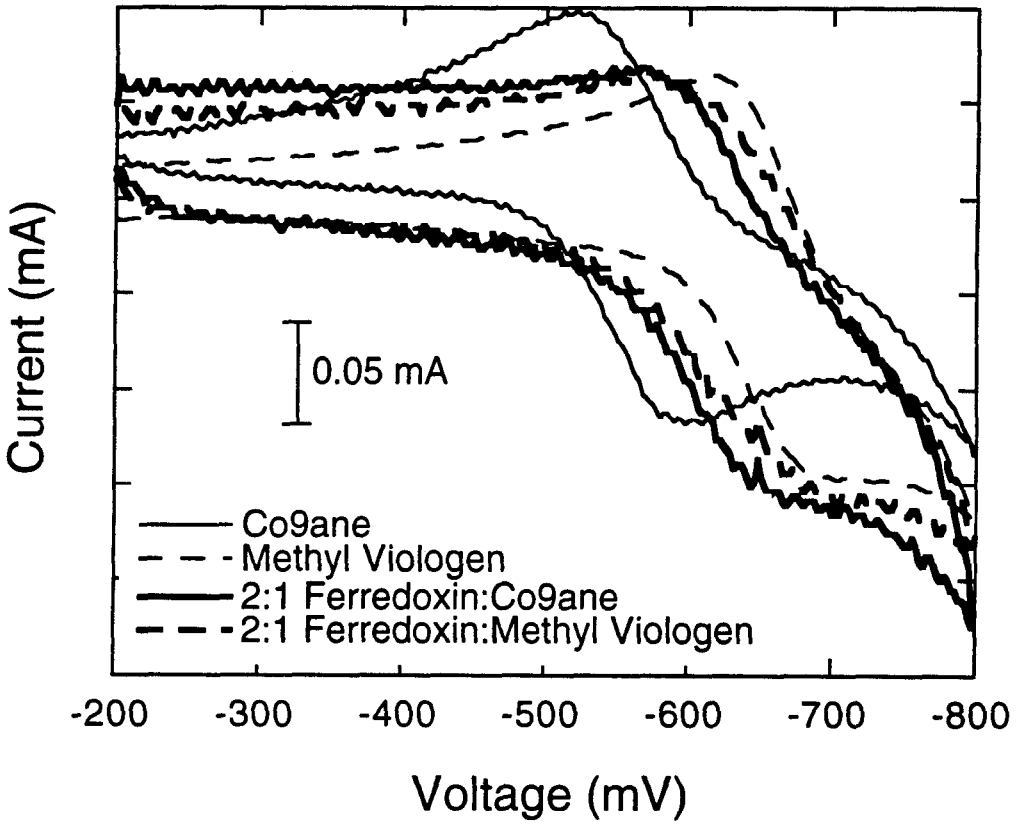

Figure 7.4. Cyclic voltammograms of Co9ane (—), methyl viologen (---), spinach ferredoxin in a 2:1 ratio with Co9ane (——), and spinach ferredoxin in a 2:1 ratio with methyl viologen (- - - -). Solutions were made from anaerobic buffer (0.15 M Tris-triflouroacetate, pH=7.3) with an electrolyte concentration of 0.1 M NaCl. Concentrations of the redox active species in each scan were 1 mM for the Co9ane and methyl viologen and ~0.3 mM ferredoxin for the protein solutions. The current for the ferredoxin solutions was multiplied by five (5) to put voltammograms on a convenient scale for comparison.

Further tests were performed to determine the optimal ratio of Fd:mediator. The experiments described above used a 2:1 ratio. Tests using 100:1 and 10:1 ratios were also performed. Figure 7.5 shows a comparison of the CVs under these three conditions. While the absolute current response is variable due to different solution concentrations, the electrochemical response is similar in each case. In addition, coulometric results (see below) and the longevity of electrochemical control (not described in detail) were also similar.

A 10:1 Fd:Co9ane ratio was used in subsequent electrochemical experiments. This balanced the need to maximize the concentration of positively charged species in solution with the need to minimize the concentration of chloride ions (the Co9ane complex has chloride counterions).

7.3.3. Choice of Conditions for Coulometry.

Another set of test experiments was conducted to determine the parameters required to fully reduce or oxidize the protein in solution in a coulometric experiment. Table 7.3 shows the results of coulometric experiments for Co9ane alone, and for Fd in ratios of 10:1 and 100:1 with Co9ane.

The values calculated for Q (the number of mC which should be required to fully reduce or oxidize the entire sample) do not agree quantitatively with the experimentally determined value of Q because only approximate volumes and concentrations were used in the calculation for these test experiments. These data are provided, however, to give an idea of the relative magnitude of Q expected for each experiment.

Results of coulometric experiments of the Co9ane moderator alone show that the coulometry in both the oxidation and reduction directions was equivalent. However, for the protein solution, as demonstrated most clearly by the results of the 100:1 Fd:Co9ane solution, which used a constant coulometric duration of five minutes, the coulometry of re-oxidation is much less efficient than that of reduction. For the 10:1 Fd:Co9ane solution, the duration of coulometry was varied. The results show that increasing the duration of the coulometric oxidation increases the quantitative oxidation of the sample. Based on these qualitative results, it was decided to use a 15 minute reduction and a 30 minute oxidation in the XAS electrochemical experiments.

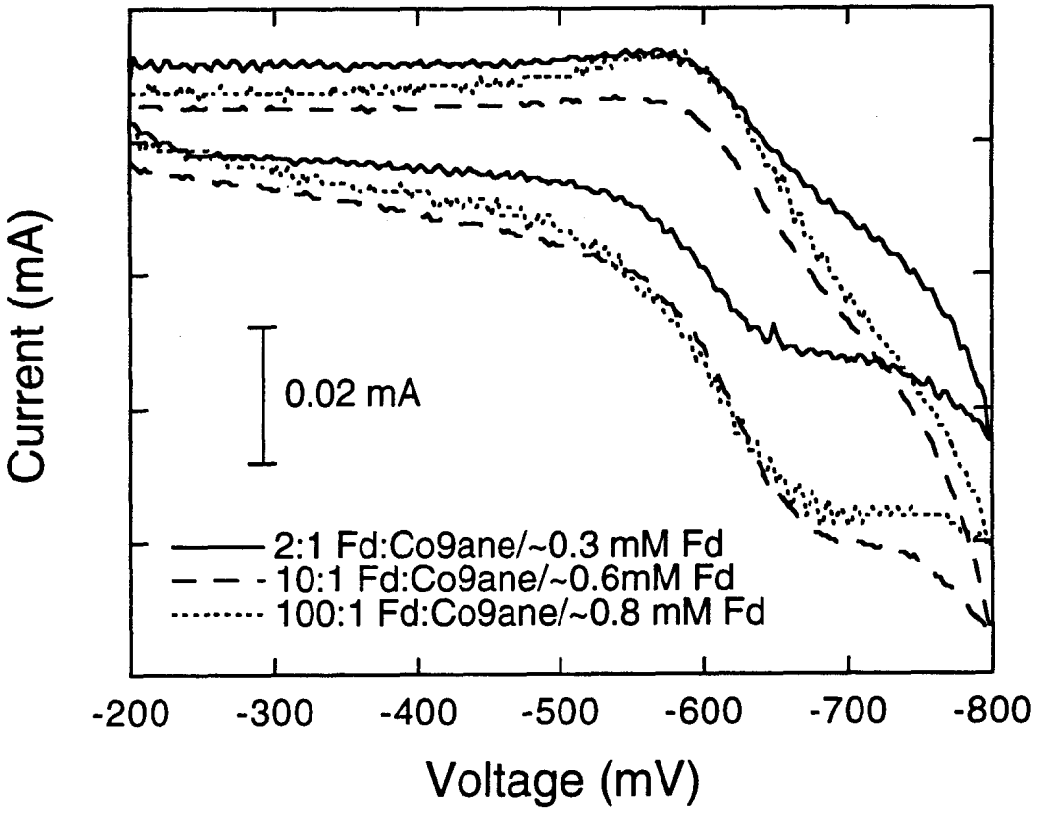

Figure 7.5. Cyclic voltammograms of spinach ferredoxin in a 2:1, 10:1, and 100:1 ratio with the Co9ane mediator. The ferredoxin concentration in each sample was ~0.3 mM, 0.6 mM, and 0.8 mM for the 2:1, 10:1, and 100:1 ratios respectively. Solutions were made from anaerobic buffer (0.15 M Tris-triflouroacetate, pH=7.3) with an electrolyte concentration of 0.1 M NaCl.

Table 7.3. Comparison of Coulometric Tests of Spinach Ferredoxin Electrochemistry.

Sample	Duration of Coulometry (minutes)	calculated Q (mC)	Q/reduction (mC)	Q/oxidation (mC)
Co9ane†	5	37		19
	5		19	
	10			18
	10		21	
100:1	5	3.9	3.0	
Fd:Co9ane	5			1.3
	5		2.4	
	5			1.5
	5		2.4	
	5			1.2
	5		2.0	
	5			1.3
10:1	5	2.2	2.4	
Fd:Co9ane	5			0.7
	15		3.1	
	15			1.6
	15		3.0	
	25			1.9
	10		3.0	
	42			2.3
	10		2.8	

† Conducted in the XAS electrochemical cell.

7.3.4. Characterization of Long-term Electrochemical Control.

Determination of the proper length for a coulometric experiment (*vide supra*) was complicated by the apparent lack of long-lasting, consistent electrochemistry in our apparatus. As XAS experiments often take many hours, understanding the nature of the loss of electrochemical control is of great importance and a number of tests were conducted to determine how long adequate electrochemical control could be maintained.

In all experiments, a consistent gradual loss of signal in the CVs as well as a loss of the measured value of Q in a coulometric experiment was observed. The rate of this loss was, however, not consistent. We strongly suspected that this loss of electrochemistry over time was, at least in part, due to dehydration of the solution in the test cell.

To test this hypothesis, an experiment was conducted in which Co9ane alone was reduced in the test cell, poised at -0.8 V and allowed to sit overnight. Figure 7.6 shows the CVs taken at the beginning of this experiment. After ~10 hours, no solution was visible at the top of the sample space and complete loss of electrochemistry resulted (Figure 7.6, inset). CVs taken after an addition of buffer to the sample space are shown in Figure 7.6 and exhibit only slightly less current amplitude than at the start of the experiment. These results confirm that at least part of the loss of electrochemistry over time was due to loss of solution from our unsealed test apparatus.

The loss of signal observed in the protein solutions may also be related to the denaturation of protein on the electrode surface. In several long-running Fd experiments, a gradual loss of signal was observed. Figure 7.7a shows CVs which are representative of this loss of signal. The magnitude and rate of this loss of electrochemical response was, however, similar to that of the mediator alone and it was assumed that the loss of response was primarily related to the dehydration of the solution in the testing apparatus.

With the protein solutions, another unexpected result was observed near the end of several experiments. Figure 7.7b shows several CVs taken more than three hours into an experiment, after 6 coulometric cycles. CV #K was taken immediately prior to a coulometric oxidation. CV #L was taken just after this coulometric oxidation and exhibits an unexplained peak in the CV ~ -0.4 V. CV #M was taken after a coulometric re-reduction of the sample and does not exhibit the unexplained peak. The exact nature of the contaminant giving rise to this signal was not determined, but it appears to be a slow-forming oxidized species, presumably resulting from the large number of coulometric cycles performed in these test experiments.

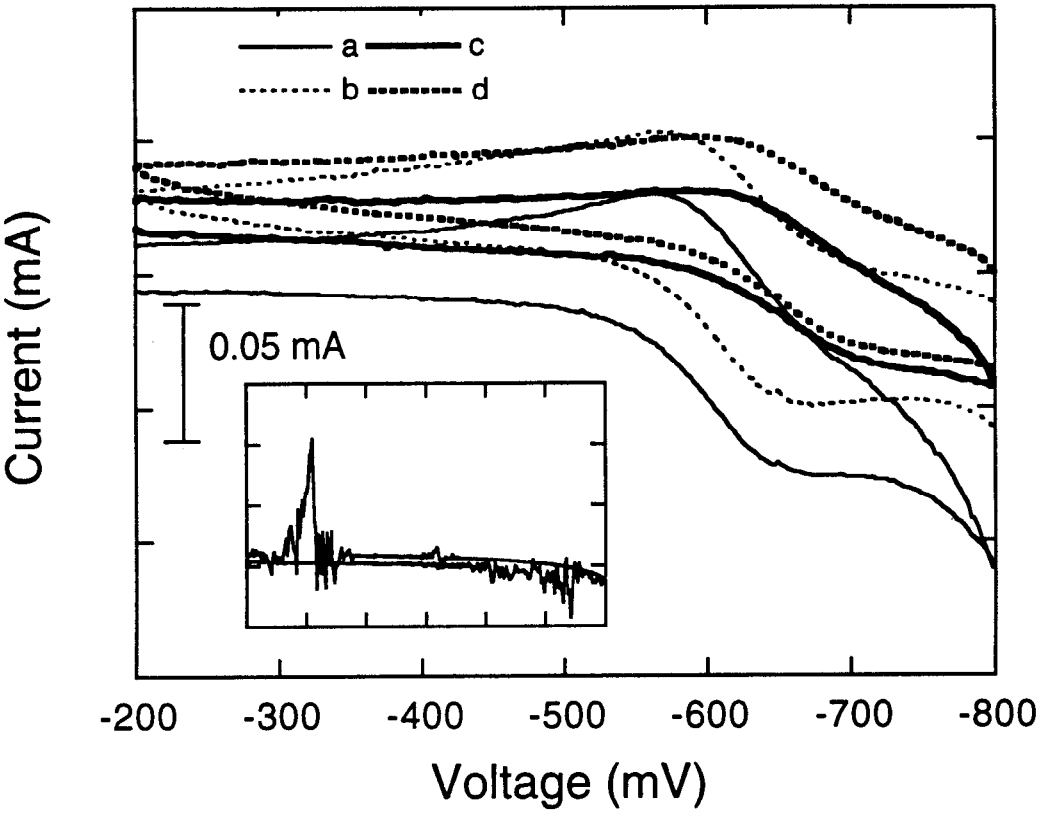

Figure 7.6. Cyclic voltammograms of a 1 mM solution of Co9ane in anaerobic buffer (0.15 M Tris-triflouroacetate, pH=7.3) with an electrolyte concentration of 0.1 M NaCl. CV's (a) [—] and (b) [▪▪▪▪] were taken at the start of the experiment starting from an oxidized and reduced voltage, respectively. The inset shows the electrochemical response of the cell after sitting for ~10 hours, poised at a potential of -0.8 V. CV's (c) [▬▬] and (d) [---] were taken from an oxidized and reduced voltage, respectively, after buffer was added to the cell.

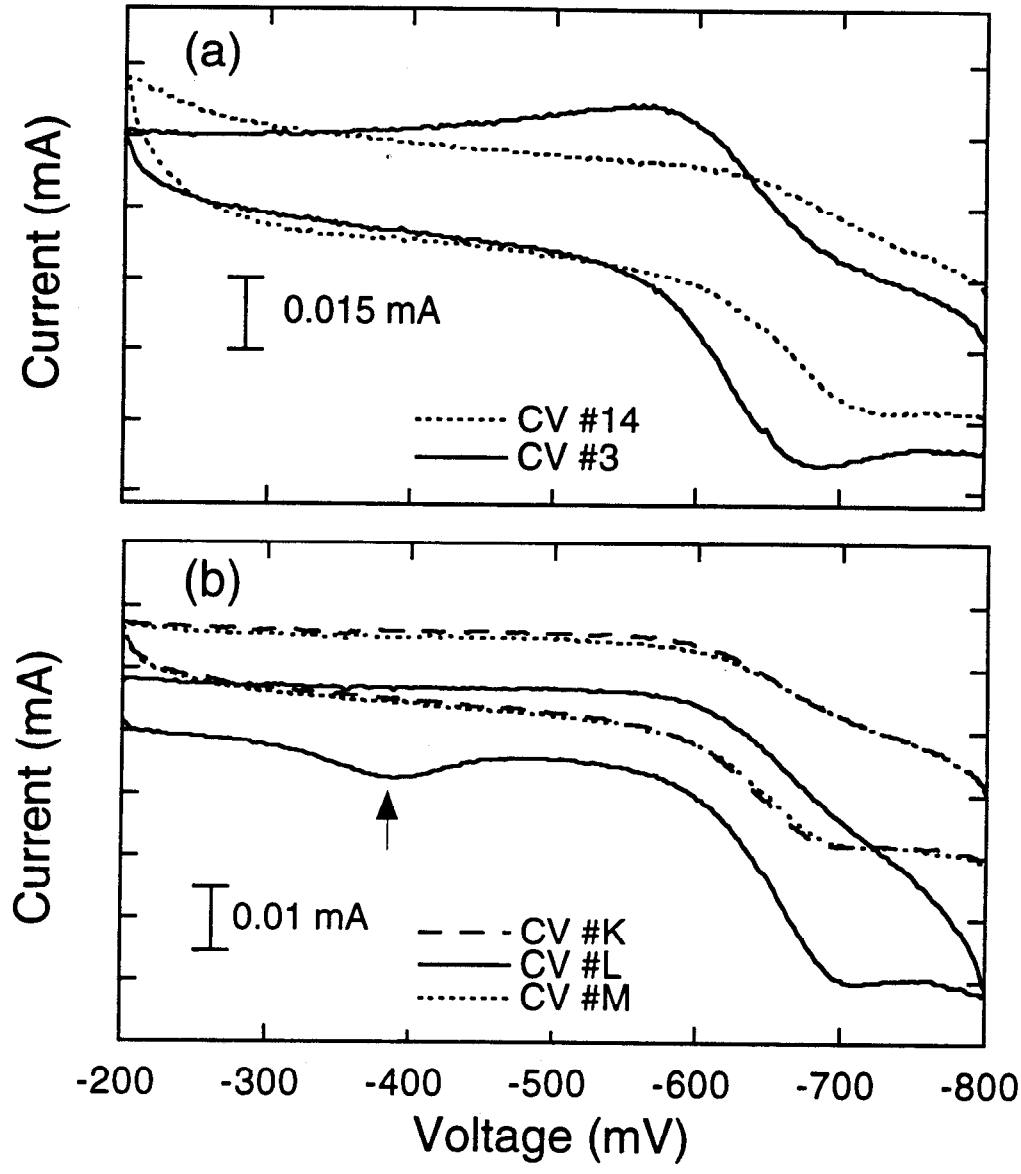

Figure 7.7 Cyclic voltammograms from two tests of a 10:1 Fd:Co9ane mediator solution in anaerobic buffer (0.15 M Tris-triflouroacetate, pH=7.3) with an electrolyte concentration of 0.1 M NaCl. Ferredoxin concentration was ~0.6 mM. (a) CV #3 (—) was taken in the first 25 minutes of the experiment, while CV #14 (••••) was taken after more than 10 hours. (b) CV #K was taken approximately 3.5 hours into the experiment after several coulometric cycles. Between K and L was a 40 minute coulometric oxidation and between L and M was a 10 minute coulometric reduction. CV #L exhibits an extra peak (designated with an arrow) not present in CV's #K and #M taken before and after, respectively.

Because dehydration of the solution clearly contributed to the loss of electrochemical response, an experiment was conducted in the sealed XAS electrochemical cell using the Co9ane mediator. Electrochemical response was maintained for over seven hours (at which time the cell was disassembled). Figure 7.8 shows selected CVs from this experiment. The data show a marked decrease in response over time. At the beginning of the experiment the window of the cell showed clearly that the sample space was filled with solution. However, after several hours, the sample space in contact with the window appeared dry. At the time, it was assumed that the loss of solution at the front of the sample space was due to hydration of the Nafion membrane.

Despite several problematic results, these tests showed that the electrochemistry of Fd mediated by Co9ane could be maintained over the time which would elapse during an XAS experiment. It remained to be determined whether the decrease in response over time would render problematic the production and stabilization of reduced Fd and thus, the collection of reliable XAS data.

7.4 Spectroelectrochemical Studies

7.4.1. Experimental Strategy

The planned experimental strategy for these experiments is as follows. S and Fe K-edge XAS data would be measured for the oxidized protein in a teflon sample cell (not under electrochemical control). These data would serve as reference spectra for the electrochemical studies.

Then, in the spectroelectrochemical cell, S K-edge data would be measured on the oxidized protein (poised at -0.2 V). After a coulometric reduction, S K-edge data would be measured on the reduced protein (poised at -0.8 V). The entire electrochemical apparatus would then be moved to a high energy XAS set-up and Fe K-edge data would be collected on the reduced protein (poised at -0.8 V). After a coulometric reoxidation, we would collect Fe K-edge data on the oxidized protein (poised at -0.2 V). Cyclic voltammograms (CVs) would be taken before and after each data set to verify the electrochemical control of the sample. Reproduction of the oxidized reference spectra taken as described above would serve as verification of the integrity of the sample. UV/Vis of the recovered sample after completion of the experiment would serve as a second control. This plan would allow us to collect S and Fe K-edge data on the *same* sample and would provide reliable correlation between the data sets.

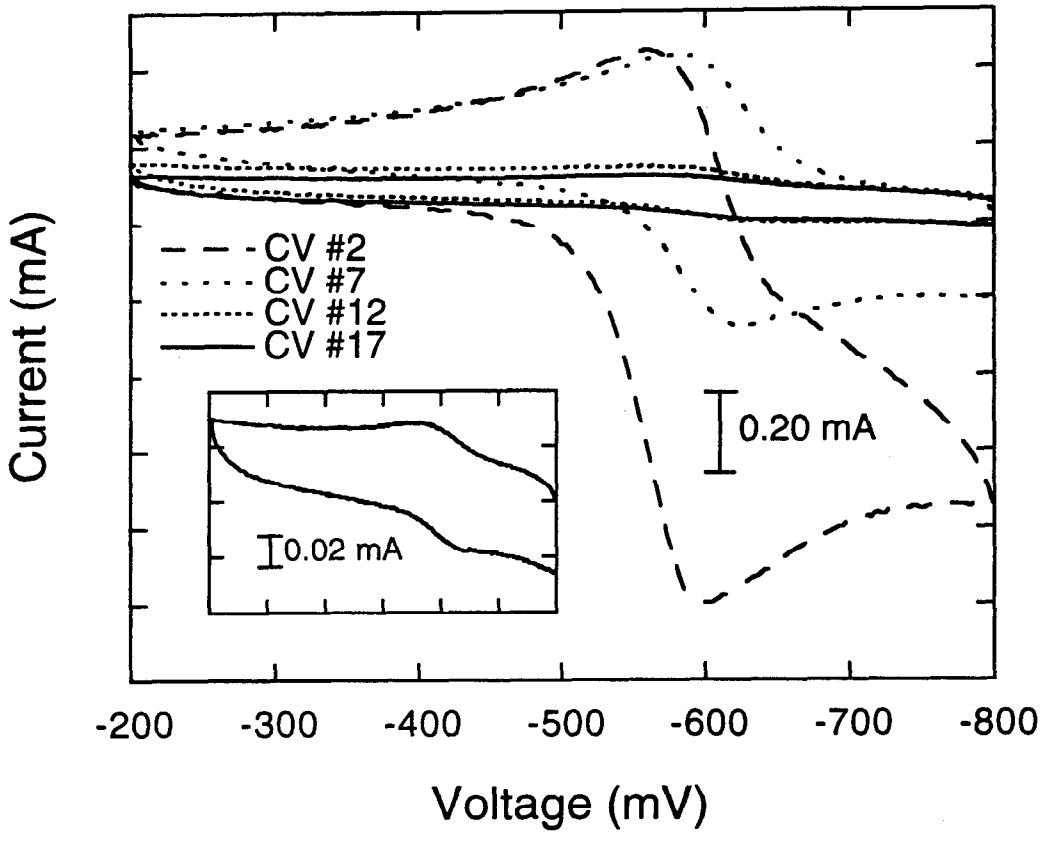

Figure 7.8. Cyclic voltammograms of a 1 mM solution of Co9ane in anaerobic buffer (0.15 M Tris-triflouroacetate, pH=7.3) with an electrolyte concentration of 0.1 M NaCl. This test was conducted in the electrochemical XAS cell. CV #2 was taken within 5 minutes of beginning the experiment. CV #7 was taken after 5 coulometric cycles, ~1 hour into the experiment. CV #12 was taken after an additional 5 hours poised at -0.8 V. CV #17 (shown also in inset) was taken after 4 additional coulometric cycles, nearly 8 hours into the experiment.

7.4.2. Experimental Results

7.4.2.1. Oxidized Ferredoxin. Shown in Figure 7.9 is the S K-edge XAS data for oxidized Fd. The solid line is the reference spectrum collected as described above at the time of the electrochemical experiments (1993). The dashed line is data collected two years prior (1991). While the same peaks are present in both spectra, the ratios between the intensities of the features vary. Both spectra are characterized by a broad pre-edge feature ~2470 eV. The rising edge comes to a sharp maximum ~2473 eV and exhibits a shoulder on the high energy side at ~2474 eV. The source of the different intensity ratios for these samples is unknown.

Figure 7.10 shows the Fe K-edge XAS spectrum for oxidized Fd. The spectrum is characterized by a sharp, well-resolved pre-edge feature ~7112 eV, corresponding to the Fe 1s —> 3d transition made allowed by 4p mixing in the T_d Fe site. There is a shoulder on the rising edge ~7120 eV and the rising edge maximum is broad.

7.4.2.2. Electrochemical Experiments. A total of seven attempts at the electrochemical XAS experiments were made. The first (exp. #1), performed with a solution of 3 mM Fd, resulted in precipitation of the sample, presumably caused by a misconnection of the electrochemical leads. However, the concentration of the sample was over three times that used in any of the preliminary tests. It is unknown what effect this high concentration would have on the experiment. All subsequent experiments were performed on samples which were diluted to 1.0 mM Fd to provide more possible attempts at the experiment. Of the other seven tests, three were performed only at the S K-edge due the unavailability of a second experimental station for the high-energy experiment.

Table 7.4 summarizes the problems encountered in the course of these experiments which limited the collection of reliable XAS data. The problems were neither isolated, nor consistent. Thus, some problems were discovered too late to attempt to remedy them, or to ascertain the origin of the problem.

Figure 7.11 shows the results of the coulometric reductions and oxidations for experiments #2-5. The plot shows the measured Q *vs.* the amount of time which had passed since the experiment began. The calculated value for Q was ~37 mC (shown as an open square in Figure 7.11). In general, the later in the experiment the coulometry was performed, the smaller the value of Q. The outlying data point, designated by an arrow, was measured during exp. #5 at a point in the experiment when electrochemical control had not been successfully established.

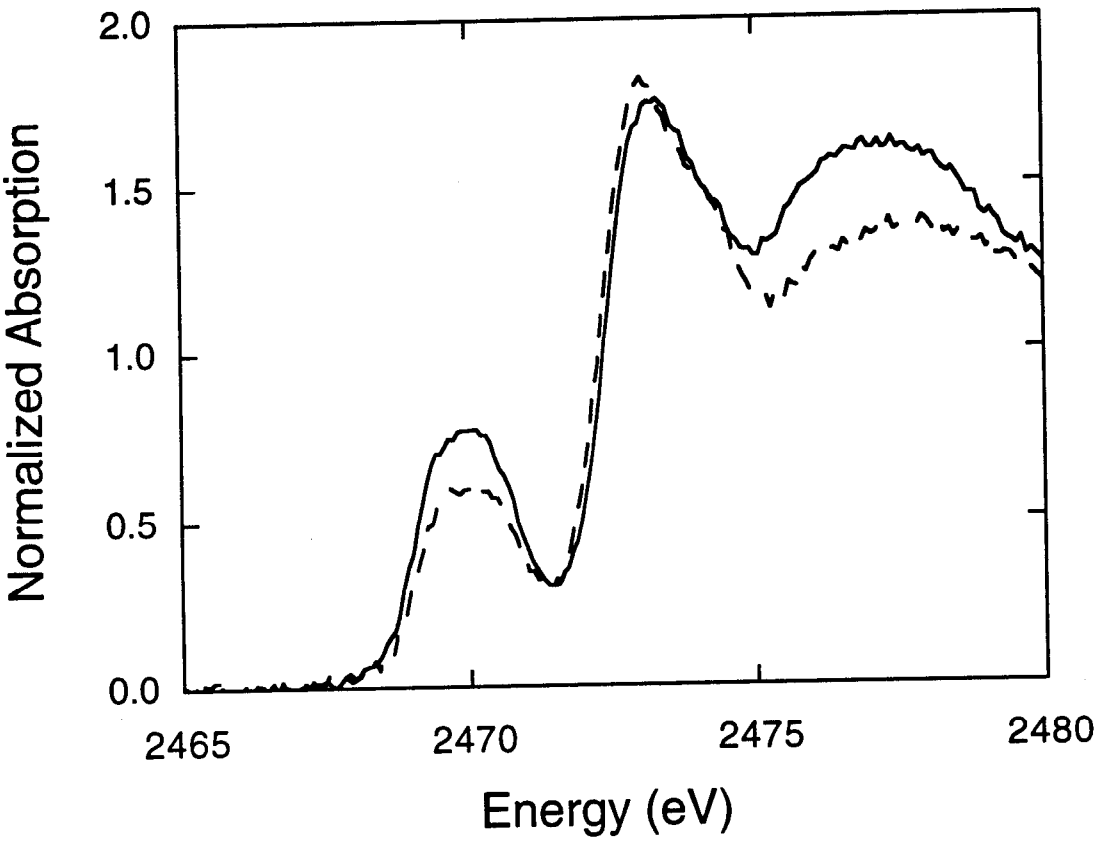

Figure 7.9. S K-edge X-ray absorption spectra of oxidized spinach ferredoxin using a teflon spacer sample cell. Shown are data measured in 1993 (—) and in 1991 (---). For data measured in 1993, only the first scan is shown.

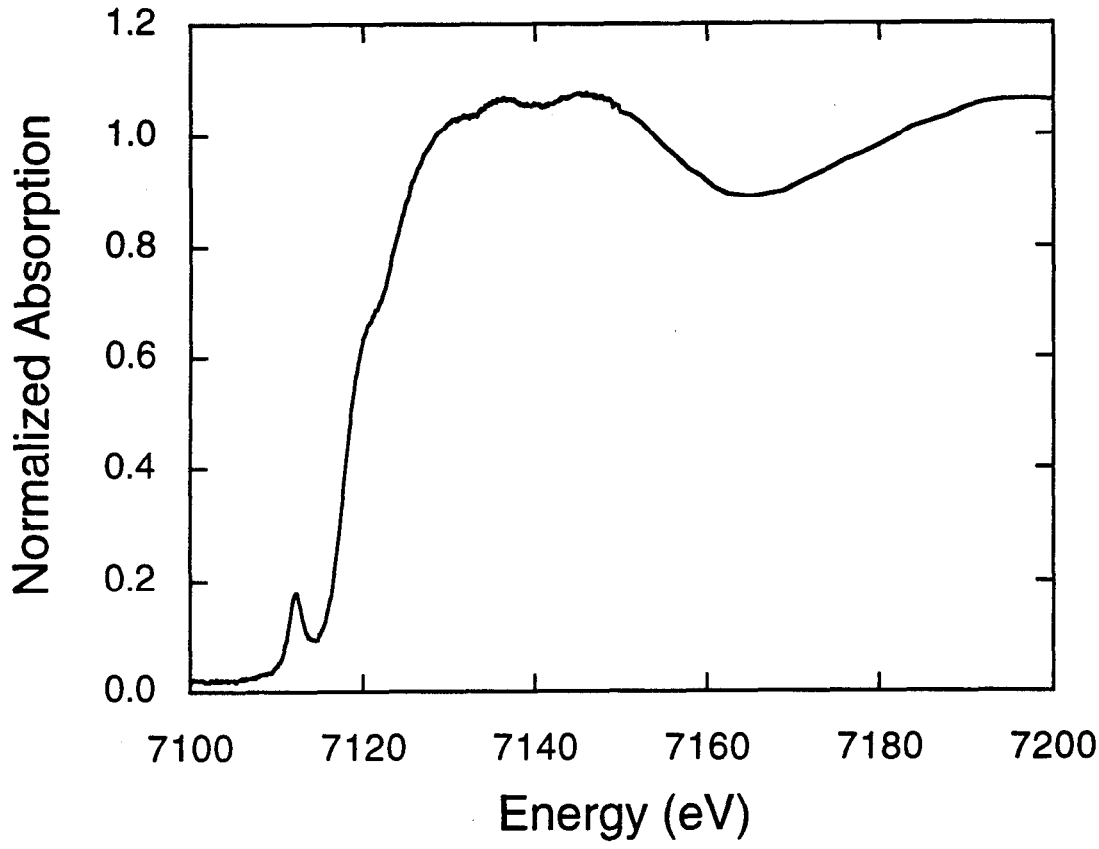

Figure 7.10. Fe K-edge X-ray absorption spectrum of oxidized spinach ferredoxin using a teflon spacer sample cell.

Table 7.4. Problems Encountered in X-ray Spectroelectrochemical Experiments of Spinach Ferredoxin

Problem	Related Figure	Suspected Cause/ Description Of The Problem	Implemented Remedy	Result	To Try in the Future
loss of electrochemical control	Figures 7.11, 7.12	loss of solution due to soaking of Nafion membrane	pre-soaked Nafion membrane by filling auxialiary compartment & waiting 2.5 hours to fill sample space	no change	
		dehydration due to rapid purging of the sample space atmosphere	saturated purge gas with buffer; placed petri dish of buffer in sample space	sample stayed hydrated longer; longer duration of electrochemical control	
			tested different window materials for ability to prevent evaporation	unclear[a]	repeat experiments using Kapton as a window material
		passivation of electrode			use a redox-inert, positively-charged modulator

Table 7.4. continued

Problem	Related Figure	Suspected Cause/ Description Of The Problem	Implemented Remedy	Result	To Try in the Future
set-up of experiment too long		purging of sample space at low energy took 30+ minutes	increased He flow to S K-edge set up	cut down on the time a little	machine a smaller sample box
			started at Fe K-edge	allowed successful coulometric reduction	
oxidized data could not be reproduced in the e-chem cell	Figure 7.13	the electrochemical cell OR background problem on the low energy beam line	more experiments need to be conducted to ascertain the cause(s)		
impurity in the sample	Figures 7.14, 7.15	spurious peaks seen in the data and in CVs but UV/Vis did not indicate any impurity	more experiments need to be conducted to ascertain the source of the impurities		

[a] experiments conducted with 7.6 μm Kapton had other problems

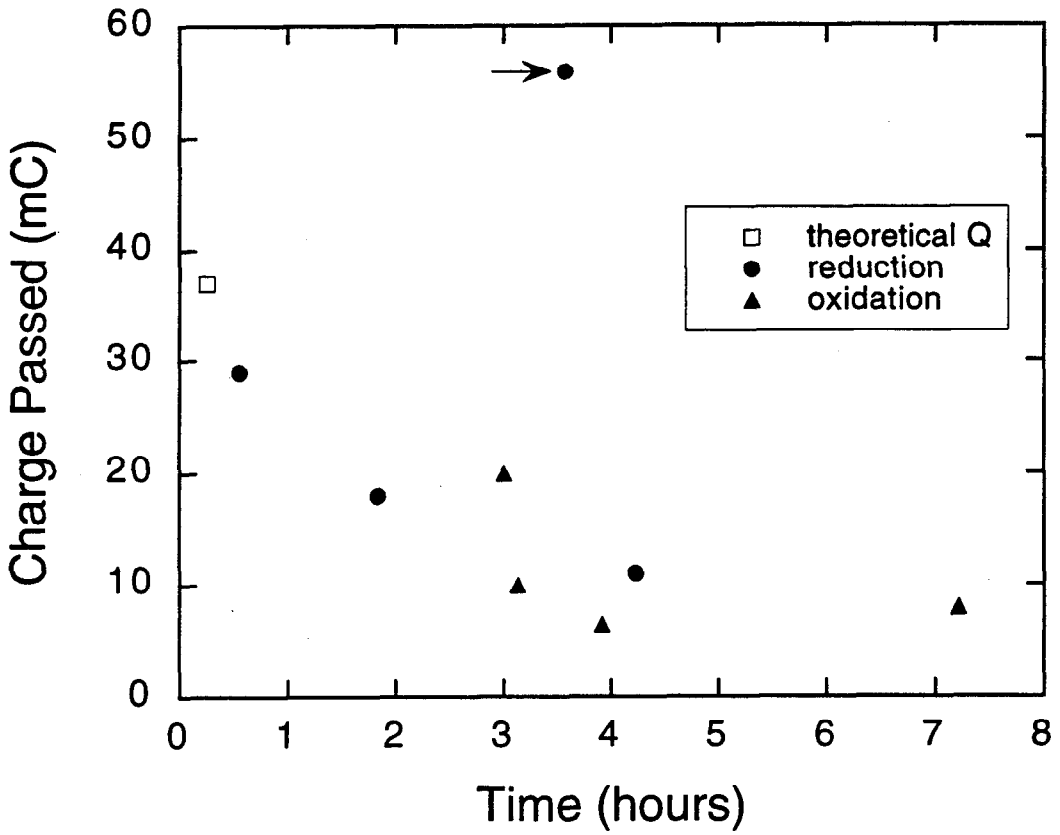

Figure 7.11. Plot of magnitude of Q (mC) passed *vs.* time since the start of the experiment for spectroelectrochemical experiments #2-5. The outlying point, designated with an arrow, was taken during exp. #5 when electrochemical control had not been established.

Figure 7.12 shows the manifestation of this loss of electrochemical response in the CVs taken in exp. #3. CVs are shown which were taken at intervals throughout the experiment and data indicate a gradual loss of electrochemical response with time.

There are several possible sources of this loss of electrochemical control, which was faster than that which had been observed in the tests conducted prior to the XAS experiments. After disassembling the cell from exp. #2, the sample space was characterized by varying degrees of dryness. Thus, it appeared that the problem, at least in part, was connected to dehydration of the sample. To test the possibility that hydration of the Nafion membrane was soaking up the sample solution, during exp. #3 the cell was allowed to sit for 2.5 hours after filling the auxiliary compartment, after which time the sample space was filled and the experiment performed. The result was the same as in exp. #2.

The only other possibility for such loss of solution was evaporation through the polypropylene window used in experiments #2-5 due to the rapid purge of the sample space with He. For exp. #4, a petri dish of buffer was placed in the bottom of the sample box and the sample space He was saturated with buffer by passing it through two bubblers. While evaporation still occurred to some extent, it was slowed significantly. In exp. #2 and #3, the front of the sample space (at the window) was completely dry upon disassembly. In exp. #4, however, the cell was still largely hydrated even after several hours. This significantly extended the duration of electrochemical control.

In another effort to remedy the sample evaporation problem, in the intervening weeks between exps. #2-5 and exps #6-7, tests in the spectroelectrochemical cell using the Co9ane mediator were performed using different window materials than the 6.3 μm polypropylene used in the initial attempts. Windows of 3.6 μm Mylar, 4.0 μm Prolene, and 7.6 μm Kapton were tested. All windows slowed evaporation relative to the polypropylene, the most successful being the 7.6 μm Kapton. However, the thicker window material also increases the attenuation of the beam and the fluorescence signal. Exps #6 and #7 were performed using 7.6 μm Kapton. Unfortunately, other problems with these experiments make it impossible to determine the effect of changing the window material.

It is also probable that some loss of electrochemical control is related to passivation of the RVC electrode. This may be due to coating of the electrode surface with denatured protein. While we did not have time to characterized this problem sufficiently (or attempt to remedy it), in the future it might be helpful to add a redox-inert, positively-charges species (in addition to the mediator) to act as an additional modulator of electrochemistry.

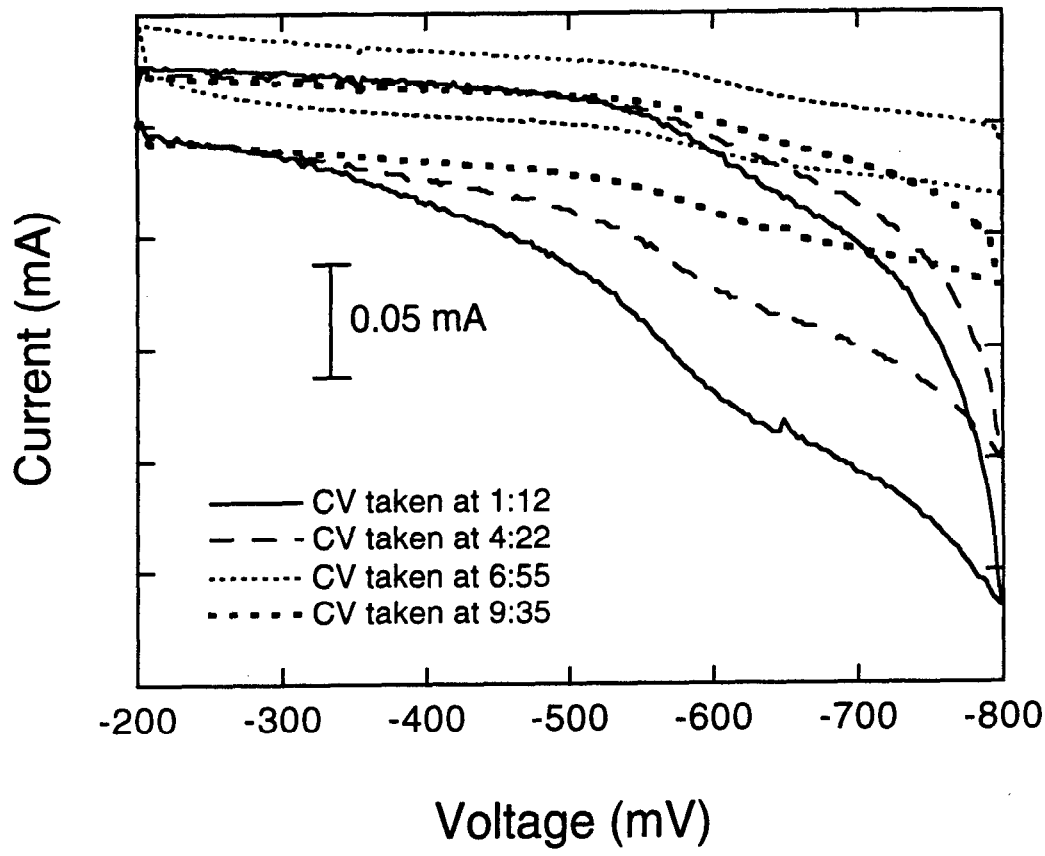

Figure 7.12. Cyclic Voltammograms from spectroelectrochemical experiment #3. Shown are CVs taken 1:12, 4:22, 6:55, and 9:35 after the experiment was begun.

One aspect of the experiment which contributed to the loss of electrochemical control was the length of time it took between the set-up of the experiment and the first coulometry experiment. This was particularly problematic at the S K-edge. In order to collect reliable data, the sample space must be fully purged with He. The presence of air attenuates the beam and the fluorescence signal. Because the sample space is relatively large for this experiment, it took up to 30+ minutes to completely purge the sample space. By the time a coulometry experiment could be performed, a significant loss of electrochemical response had already occurred. This problem was addressed by increasing the He flow. This decreased the purge time, but it may also have contributed to more rapid evaporation of the sample as described above. In the future, it would be helpful to design a smaller sample space which would require less purge volume.

Exp. #4 partially circumvented this problem by starting the strategic cycle at the Fe K-edge. At these energies, air in the beam path does not interfere with the data collection and so no waiting was necessary. The most successful coulometric experiment performed was during exp. #4 only 30 minutes into the experiment. Of course, once the apparatus was moved to the low energy set-up for S K-edge XAS, the delay described above was experienced before the sample could be reoxidized.

A second problem with these experiments was manifested as inconsistency in the XAS data. The above described electrochemical problems obviously led to unreliable XAS data. However, there were other problems which are less easily understood. The reference S K-edge spectrum of oxidized Fd collected in the teflon spacer cell (with no electrochemical control) was never reproduced in the spectroelectrochemical cell. Figure 7.13 shows the first oxidized scan at the S K-edge from exp. #5 compared with the oxidized sample collected in the teflon cell. The scan from exp. #5 was measured with no applied voltage (the voltammograph power off). These data are representative of all the electrochemical experiments. While the features are reproduced, the relative intensity ratios, particularly of the lowest energy feature, are totally different. The source of this problem is not known for certain, but there are two possible causes. First, it is possible that the contact with the electrochemical cell induces some change in the protein. However, the same samples (in the electrochemical cell) produced oxidized Fe K-edge spectra identical to the reference Fe K-edge spectrum measured in the teflon cell. Second, there were problems with the beam line used for the S K-edge XAS during the time when these experiments were conducted. The presence of a peak of unknown origin was dependent on the fill of the synchrotron ring and thus was most likely a scattering process dependent on the exact beam position. Regardless, the presence of this peak may

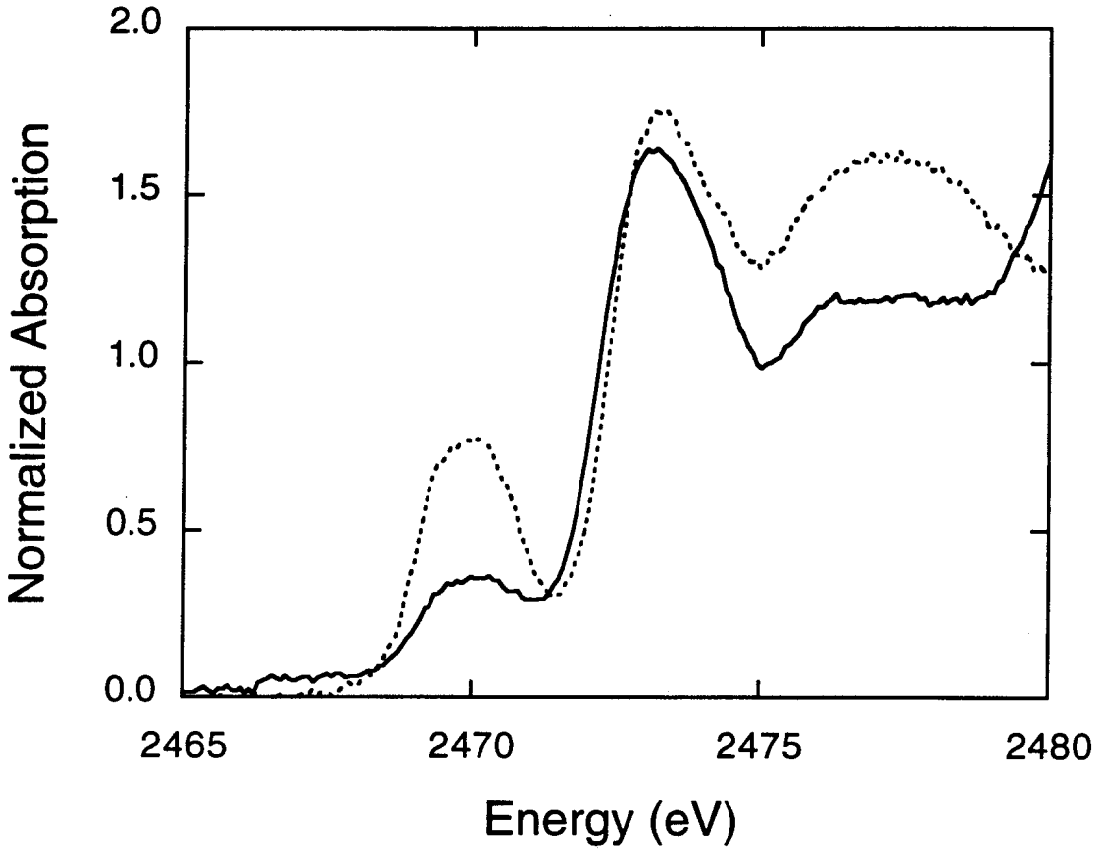

Figure 7.13. S K-edge X-ray absorption spectra of oxidized spinach ferredoxin in the electrochemical cell with no applied voltage (—) and in a teflon spacer sample cell (---). The spectrum taken in the electrochemical cell was the first exposure of the sample to the X-ray beam (taken in exp. #5).

interfere with the proper normalization of the data and result in spurious intensity ratios. The reference S K-edge oxidized sample was not affected by this problem.

The final problem associated with these experiments came from impurities in the sample. Figure 7.14 shows the S K-edge spectrum of an oxidized scan taken in exp. #2. A similar result was observed in exps #6-7. The unexplained feature at ~2477 eV in the data, which was present for all scans, is indicative of a high-valent form of sulfur in the sample. The Fe K-edge for this sample (taken with no applied voltage after coulometric reduction and reoxidation) is shown in Figure 7.15. As in the S K-edge case, the spectrum indicates the sample is very different. The pre-edge feature is a shoulder on the rising edge and there is a sharp maximum at ~7138 eV. Because the presence of the impurity in the sample was inconsistent, its source is unknown. The UV/Vis spectrum of this sample following recovery from the sample cell indicated that the sample remained reasonably pure. The A(422)/A(278) ratio was 0.47 before the experiment and 0.38 after XAS and both UV/Vis spectra show the same basic features. While this indicates a small amount of degradation of the sample, the electronic spectra indicate the site was largely intact. Thus, either the UV/Vis spectrum is not a very good indicator of sample integrity and/or the impurity which caused the unusual behavior was deposited on the electrode surface and was not recovered for UV/Vis analysis.

Exp. #2 was the only XAS experiment in which the unexplained peak at ~-0.3 V seen in several of the test CVs (see Section 7.2.4.2) was observed. This peak appeared only towards the end of the experiment and did not seem to effect the XAS data, indicating that it was unrelated to the unexplained XAS results (which were observed in exp. #3).

7.4.2.3. Spectroelectrochemical Experiment #4. Exp. #4 was the most successful of all the experimental attempts. Figure 7.16 shows the chronology of the experiment. Begun at the Fe K-edge, a single scan of the oxidized sample was taken (with no applied voltage), followed by a coulometric reduction within ~30 minutes of starting the experiment, which produced 76% of the calculated Q. Data was then collected with the voltammograph poised at -0.8 V. Figure 7.17 shows the CVs taken before and after the data set.

The sample was then moved to the S K-edge set-up and data was collected with the voltammograph poised at -0.8 V. A coulometric reoxidation was performed which now produced only 26% of the calculated Q. After this coulometric experiment, CVs no longer showed the characteristic redox features of Fd, indicating loss of electrochemical control. With the cell poised at -0.2 V, data was collected on the "oxidized" sample. Figure 7.18 shows the CVs associated with these data.

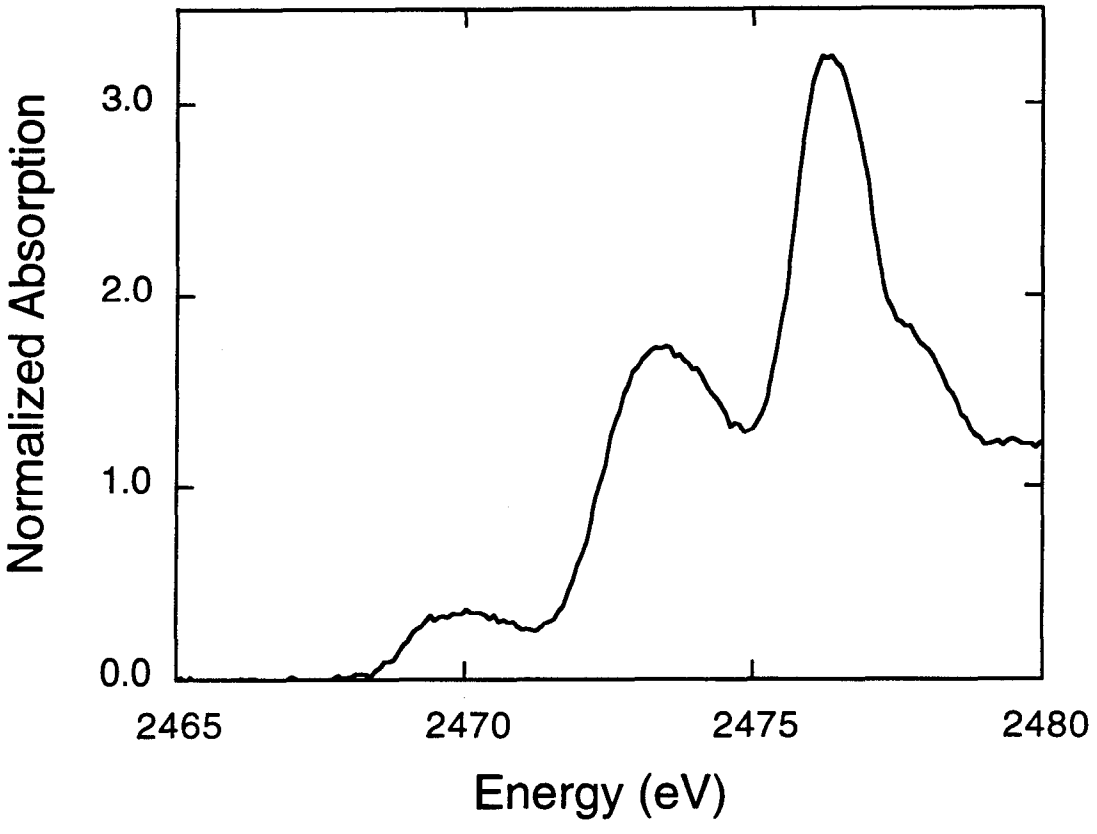

Figure 7.14. S K-edge X-ray absorption spectrum of oxidized spinach ferredoxin in the electrochemical cell from exp. #2. Applied voltage was -0.2 V. Sharp peak at ~2477 eV is impurity indicative of the presence of high-valent sulfur.

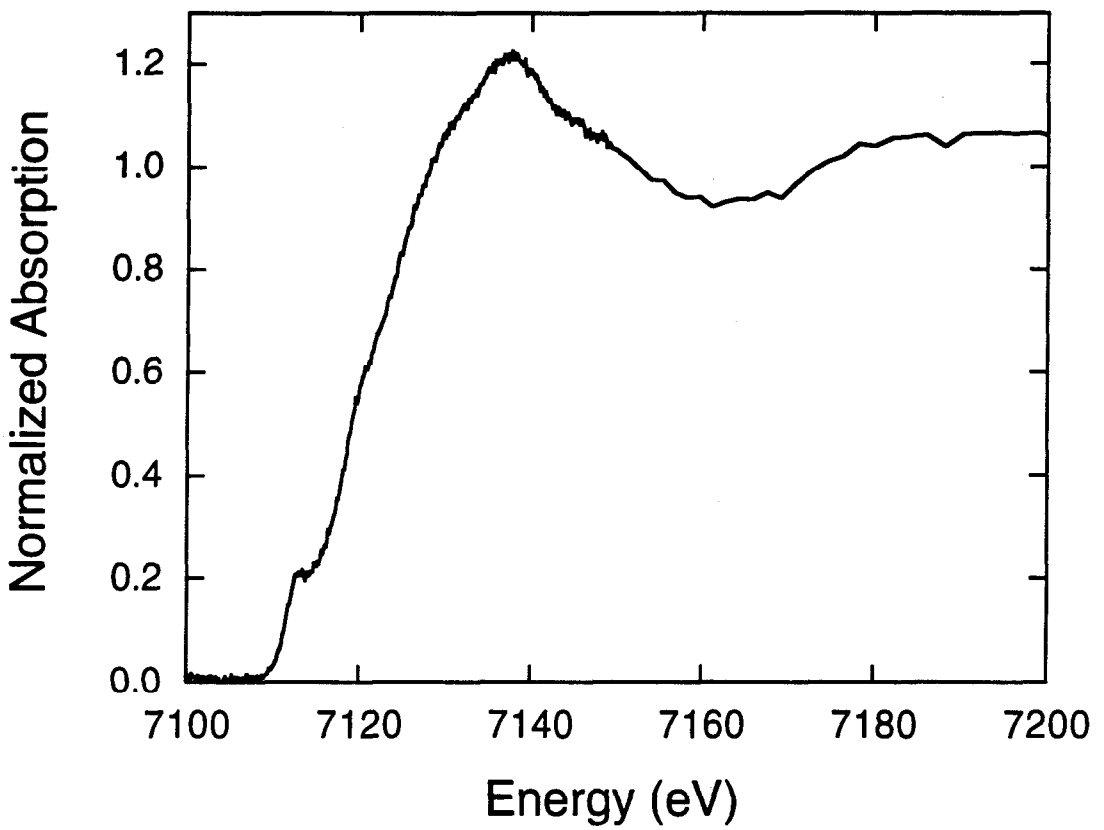

Figure 7.15. Fe K-edge X-ray absorption spectrum of spinach ferredoxin in the electrochemical cell from exp. #2. There was no applied voltage. Coulometric reduction and reoxidation had previously been performed on the sample.

Scheme for Spectroelectrochemical Experiment #4

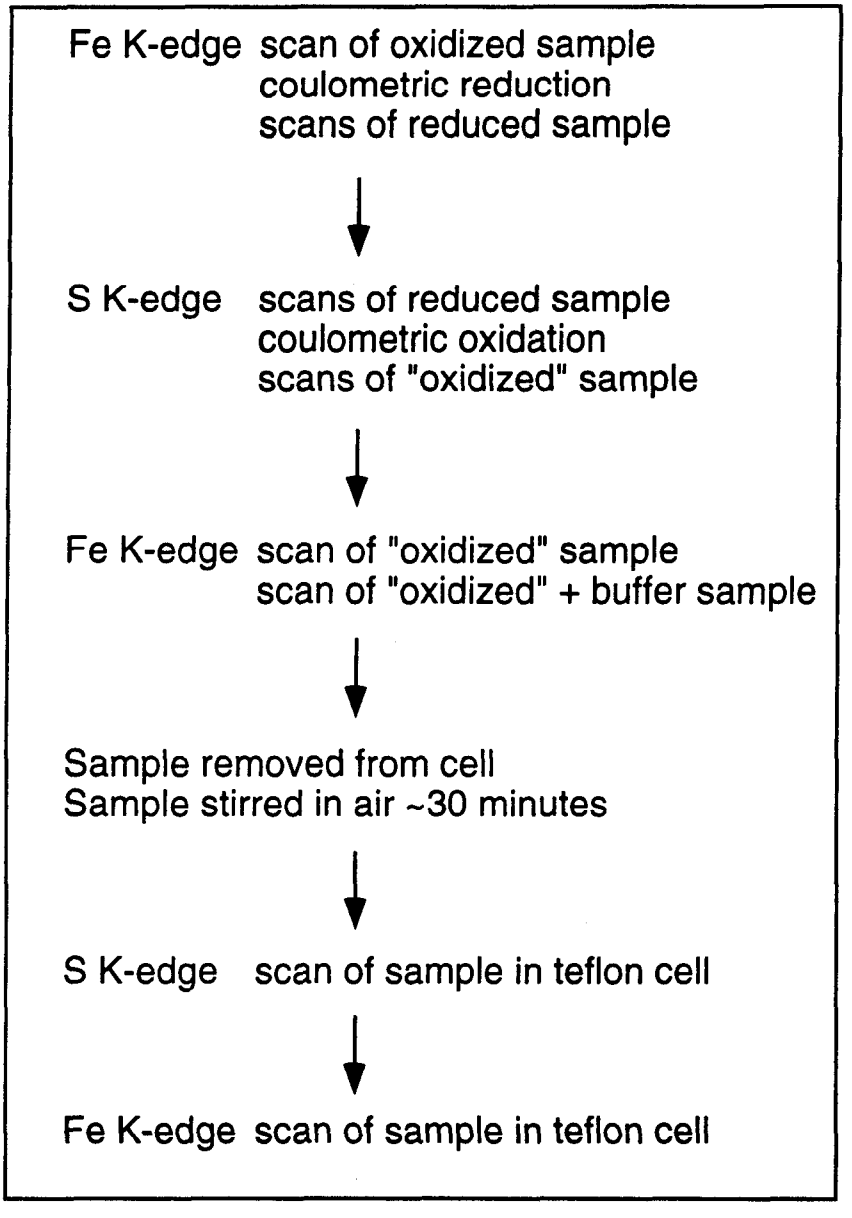

Figure 7.16. Experimental scheme used in spectroelectrochemical experiment #4 of spinach ferredoxin.

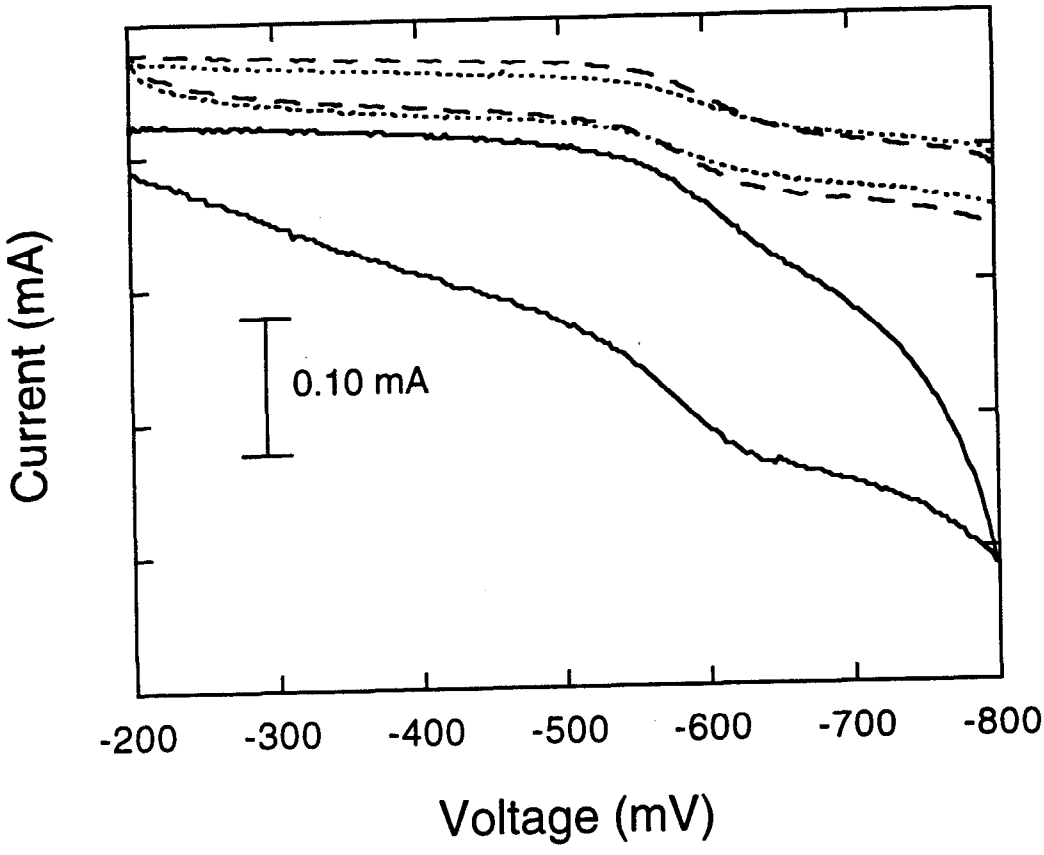

Figure 7.17. Cyclic voltammograms taken between Fe K-edge XAS measurements from spectroelectrochemical experiment #4. Shown are CVs after oxidized scan/before coulometric reduction (—), after coulometric reduction (- - -) and after scans taken while the voltammograph was poised at -0.8 V (---).

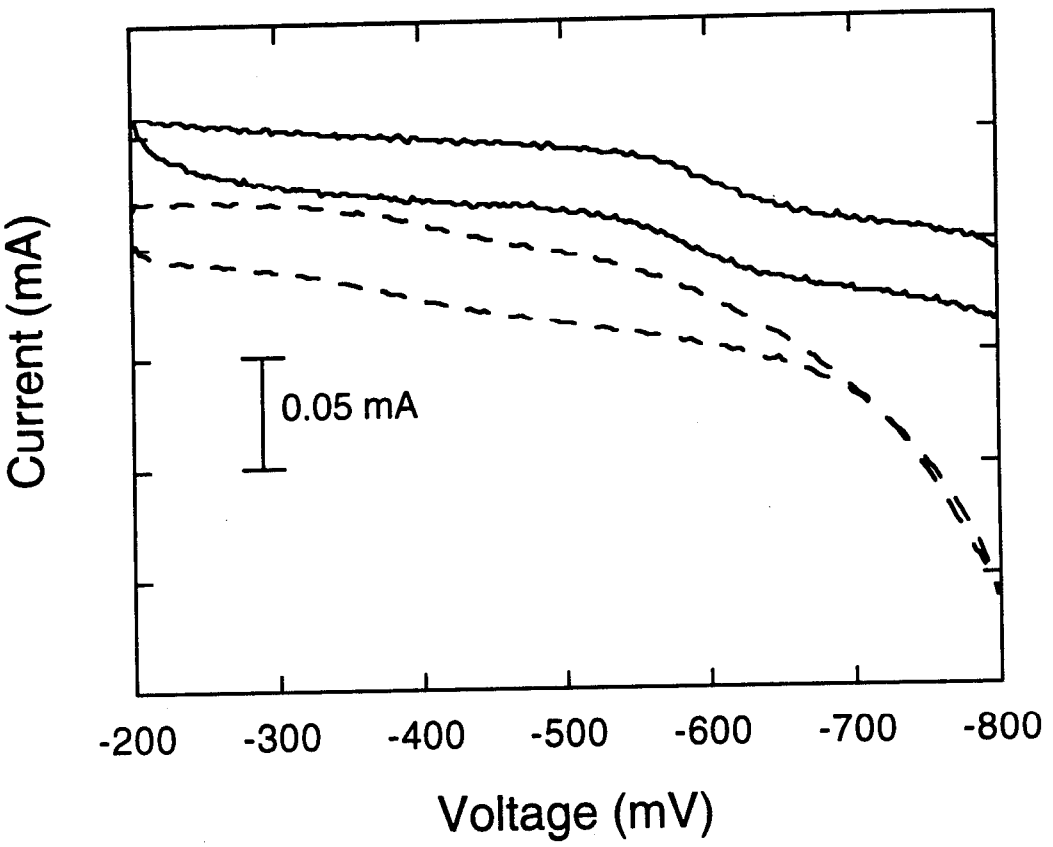

Figure 7.18. Cyclic voltammograms taken between S K-edge XAS measurements from spectroelectrochemical experiment #4. Shown are CVs after the sample was moved to the S K-edge set up (sample was previously reduced) (—) and after coulometric "reoxidation" (– – –). A CV taken immediately before the "reoxidation" was very similar to that taken before scanning.

The sample was then returned to the high-energy set up and the Fe K-edge of the "oxidized" sample was measured. (The voltammograph was poised at -0.2 V, but CVs remained featureless). At the point at which electrochemical control was lost, the cell had become partially dehydrated. After addition of 100 μl of anaerobic buffer, the cell was reconnected to the voltammograph; however, electrochemical control could not be reestablished. Following another Fe K-edge measurement, the sample was removed from the cell and stirred in a microcentrifuge tube in air (in a 4°C cold room) for ~30 minutes. The sample was then placed in a teflon cell and S K-edge and Fe K-edge measurements were performed.

Figure 7.19 shows the Fe K-edge spectra measured in exp. #4 compared to the reference oxidized data taken earlier in the teflon cell. The scan of the oxidized sample taken before electrochemistry was initiated is nearly identical to the reference oxidized data (Figure 7.19a). After coulometric reduction, a clear difference in the data is observed (Figure 7.19a). The pre-edge feature has decreased in intensity, the rising edge shoulder is less pronounced, and the rising edge comes to a clear maximum at ~7125 eV. The scans shown in Figure 7.19b, taken after "reoxidation" and addition of buffer are similar to the reduced scan in Figure 7.19a, indicating that the coulometric oxidation did not reoxidize the sample. However, after stirring in air, the characteristic features of the oxidized spectrum were nearly completely regenerated (Figure 7.19b).

Figure 7.20 shows the S K-edge data measured in exp. #4 compared to the reference oxidized data taken earlier in the teflon cell. As was described earlier (see Section 7.4.2.2.), none of the S K-edge spectra taken in the spectroelectrochemical cell reproduced the reference oxidized spectrum. This is clearly seen in these spectra. Nonetheless, clear differences are seen in the data in the rising edge region which are related to the electrochemically generated redox state of the sample. The data for the reduced Fd exhibits a sharp maximum at ~2474 eV, with a shoulder on the low energy side at ~2472 eV. The "oxidized" sample shows a slightly broader rising edge region. However, based on the Fe K-edge results, this sample is likely to be still reduced. After the sample was reoxidized by stirring in air, the rising edge features reverted back to those observed for the reference oxidized sample: a sharp maximum at ~2472 eV with a high energy shoulder.

The S K-edges display a larger variation from spectrum to spectrum than the Fe K-edges. This has three probable causes. First, the background/scatter problem described earlier induced by the beam line may make consistent background subtraction difficult. Second, the higher resolution at the S K-edge may make the spectra more sensitive to variations in the samples. And third, spectra at the S K-edge reflect

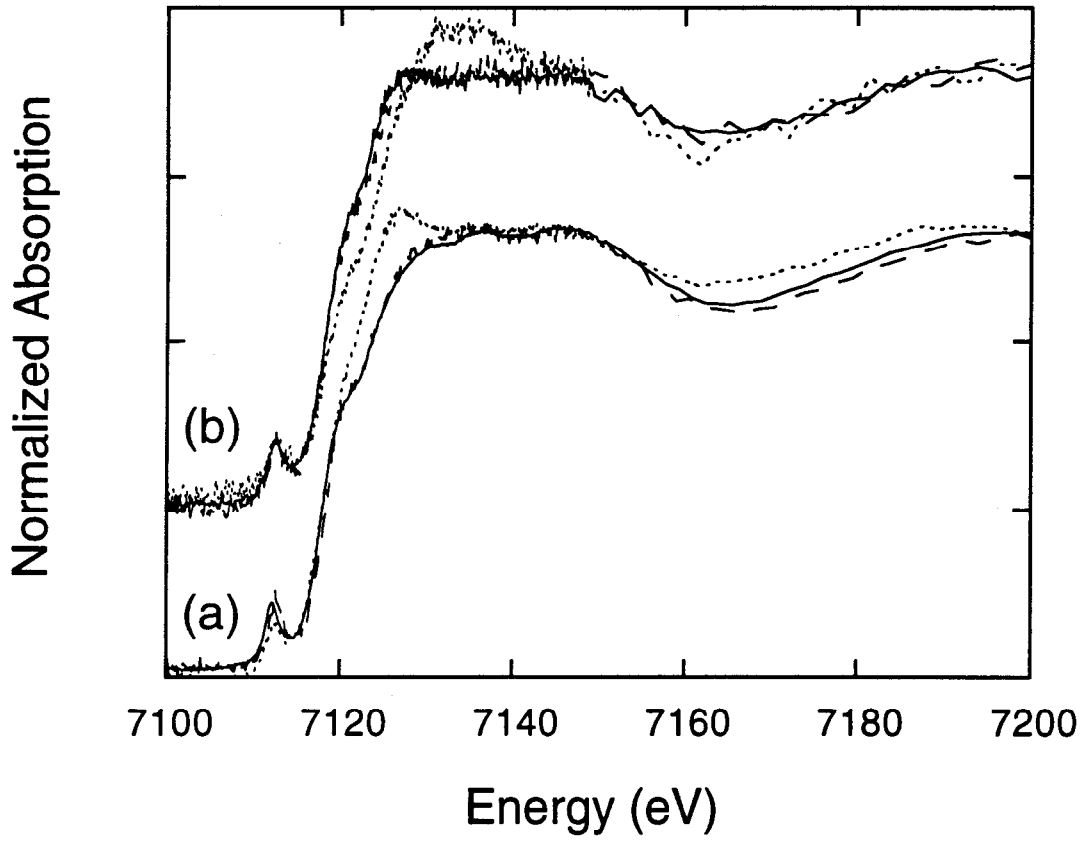

Figure 7.19. Fe K-edge X-ray absorption spectra of spinach ferredoxin taken during spectroelectrochemical experiment #4. Shown in (a) are data measured for the oxidized sample with no applied voltage (– – –) and data for which the voltammograph was poised at -0.8 V (•••••) compared to the spectrum measured for the oxidized sample in the teflon cell (—). Shown in (b) are data measured after a coulometric "reoxidation" of the sample (—); after addition of anearobic buffer to the sample space (– – –); and in the teflon cell, the sample having been stirred in air for ~30 minutes (•••••). Note that after the "reoxidation" electrochemical control was lost.

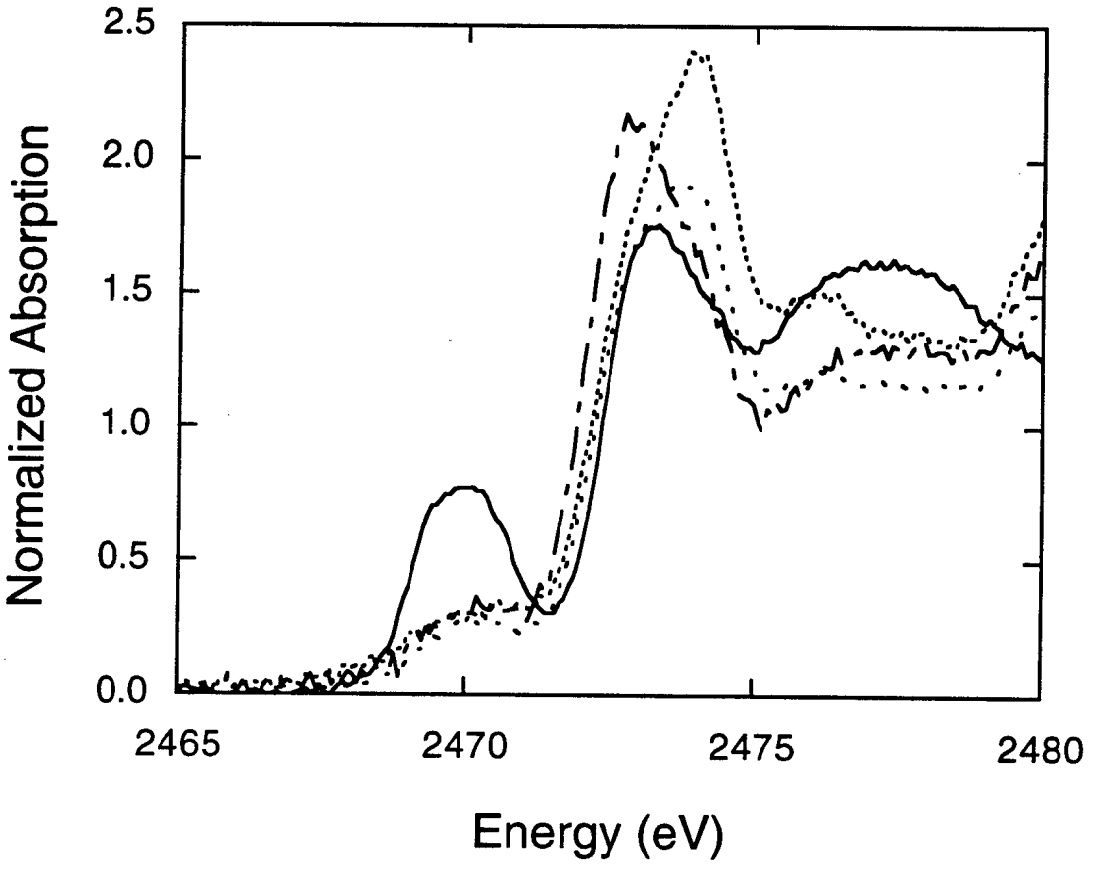

Figure 7.20. S K-edge X-ray absorption spectra of spinach ferredoxin taken during spectroelectrochemical experiment #4. Shown are data measured for the reduced sample (voltammograph poised at -0.8 V) (·····), data measured after coulometric "reoxidation" of the sample (• • • •), and data measured for sample in the teflon spacer cell, the sample having been stirred in air for ~30 minutes (— - — -). For comparison, the first scan of the oxidized sample collected earlier is shown (—).

fluorescence signal from only the sample closest to the surface. In contrast, Fe K-edge X-ray energies allow the beam to penetrate much further. Thus, the Fe K-edge spectra reflect fluorescence signal from the bulk of the sample. The S K-edge data, then, are much more sensitive to inhomogeneity within a given sample, especially at the surface.

7.5. Analysis

While it is premature to fully analyze the XAS data collected in these experiments, clear changes were observed in the data which appear to be dependent on the spectroelectrochemically generated redox state of the protein.

7.5.1. Fe K-edges

The one-electron reduction of the Fd active site converts the Fe(III)Fe(III) site to a Fe(III)Fe(II) localized mixed-valent site. The Fe K-edge spectra shown in Figure 7.19 reflect this change in oxidation state. The shift of the rising edge maximum to lower energy in the one-electron reduced site is indicative of the contribution of ferrous iron to the spectrum. The lower positive charge in Fe(II) results in a lower Fe 1s binding energy, causing transitions from this orbital to appear at lower energy. The mixed-valent site also exhibits a lower Fe 1s —> 3d pre-edge intensity. This is consistent with results observed for the Fe K-edge of ferric- and ferrous-tetrachlorides, for which the $Fe(III)Cl_4^-$ exhibits higher 1s —> 3d pre-edge intensity.[18]

7.5.2. S K-edges

As was discussed in Chapter 6 for oxidized 2Fe model complexes, S K-edge spectra of these sites reflect transitions from both sulfide and thiolate sulfurs. In the diferric models (Section 6.4.3, Figures 6.5 and 6.6), the pre-edge band was shown to contain partially-resolved transitions from both sulfide and thiolate, with the sulfide transitions being lower in energy. Each thiolate containing complex also exhibit a sharp thiolate-based transition at the onset of the rising edge.

7.5.2.1. Oxidized Fd. Figure 7.21 shows the S K-edge spectra of oxidized Fd and $[Fe_2S_2(SEt)_4]^{2-}$. The intensity ratios in the protein spectrum are somewhat different from the mode data, however, the energies are very similar. Based on the spectra, it is reasonable to assume similar assignments (2 sulfide and 2 Cys thiolate transitions) for the Fd S K-edge pre-edge band as for the model complexes. The oxidized Fd spectrum

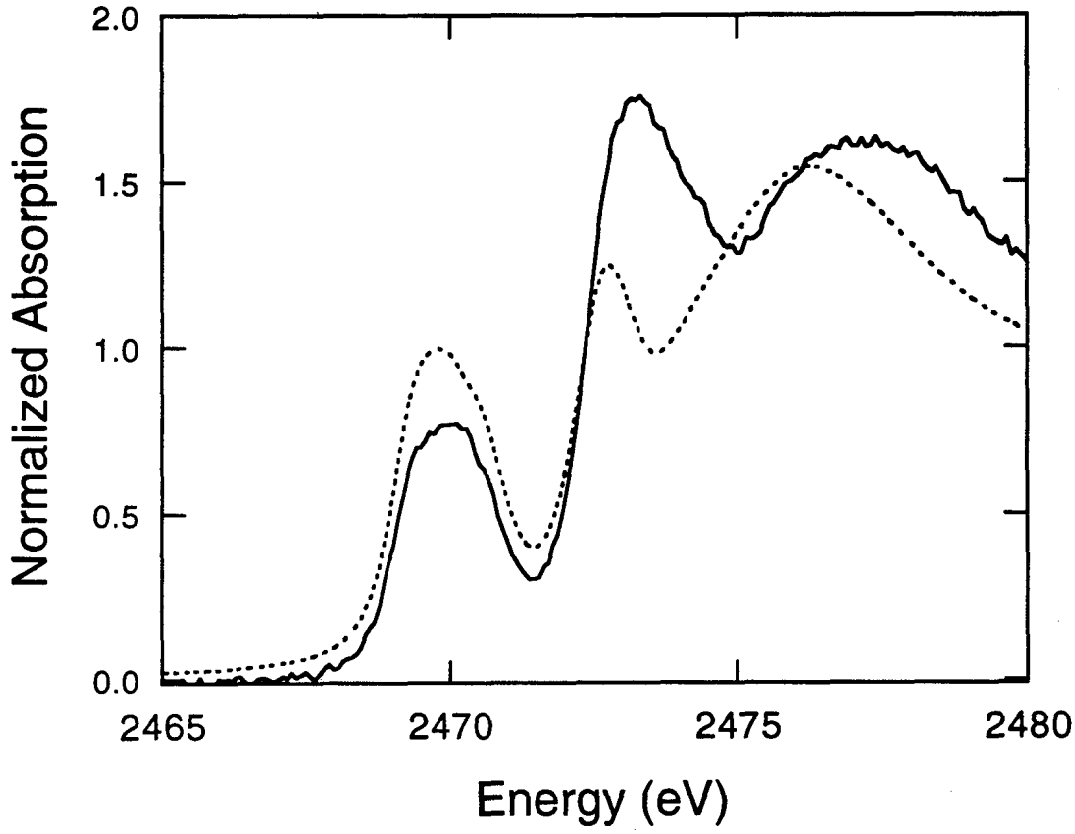

Figure 7.21. S K-edge X-ray absorption spectra of oxidized spinach ferredoxin in a teflon spacer sample cell (—) and the inorganic model complex $[Fe_2S_2(SEt)_4]^{2-}$ (·····).

exhibits a sharp maximum at the rising edge onset which has a shoulder/tail at higher energy, where the model complex spectrum exhibits a sharp well-resolved thiolate-based transition (~2472.7 eV). While, the rising edge feature in Fd clearly contains more than one transition, a Cys-based transition (analogous to the thiolate transition of the model) is possible in this energy region. Because the intensities of the oxidized Fd spectrum have been shown to vary with different experimental conditions (Figure 7.9), it is premature to discuss intensities in the oxidized Fd spectrum relative to those in the model complex spectrum.

7.5.2.2. Reduced *vs.* Oxidized Fd. The most dramatic difference between the S K-edge spectra of the oxidized and reduced (mixed-valent) Fd is the shift in the maximum intensity in the region ~2472-2474 eV. In the oxidized samples (Figure 7.13 and 7.20) there is a shoulder on the high energy side of the maximum in this region, while in the one-electron reduced spectrum (Figure 7.20) the intensity distribution has shifted to have a shoulder on the low energy side of the maximum. This would indicate at least two transitions give rise to intensity in this region and perhaps reflects the splitting of transitions associated with Cys thiolates, which are all bound to Fe(III) in the oxidized protein but which split into two sets (2Cys bound to Fe(II) and 2 Cys bound to Fe(III)) in the reduced form. Further, changes in the reduced spectrum may be related to the sulfide-based transition which was observed as a shoulder ~2474 eV on the rising edge in the model complex spectrum of $[Fe_2S_2Cl_4]^{2-}$ (Figure 6.6). This might be expected to change in energy or intensity when sulfide bridges Fe(II)Fe(III) rather than Fe(III)Fe(III).

Unfortunately, the pre-edge region of the spectrum, which is likely to reflect the most interesting changes due to variation in covalent interactions upon the addition of an electron to the site, is not observed with proper intensity for samples (oxidized or reduced) in the XAS e-chem cell (Figures 7.13 and 7.20). Clearly, before analysis of electronic structural changes from these spectra can be made, reliable XAS data must be measured in the e-chem cell.

7.6. Discussion

7.6.1. Electrochemistry

The results discussed in the previous section show that a number of unresolved problems need to be addressed before this electrochemical methodology can be used to generate and stabilize redox states of interest for aqueous protein solutions.

Most pressing is the need to generate long-lived, reproducible electrochemical responses. To do this, more tests must be performed to determine optimal experimental conditions. A cell has been designed by Dr. Patrick Frank which, like the test cell in Figure 7.2, will accommodate small sample volumes, but will allow the sample to be sealed to prevent the complication of evaporation. In addition to the suggestions for future modifications described in Section 7.4 (see Table 7.3), more tests on the electrochemistry of protein solutions at different concentrations would be useful to determine the effect of this experimental variable on the electrochemistry. The ability to use a more concentrated solution would decrease the XAS scanning time in these experiments; however, a more concentrated protein solution may passivate the electrode surface more rapidly.

The experiments described herein, however, suggest that electrochemical control of proteins in aqueous solution for XAS studies is feasible. In the future this approach will provide a valuable tool for the stabilization of biologically relevant redox states of metalloproteins for study by XAS.

7.6.2. Spectroelectrochemistry of Spinach Ferredoxin

We have presented preliminary spectroelectrochemical results for the oxidized and mixed-valent forms of Fd. The reduced Fd Fe K-edge spectrum clearly reflects the contribution of one Fe(II) ion and one Fe(III) ion. Since intensity in the S K-edge spectra in the region ~2472-2474 eV does not reflect pre-edge transitions, changes in the spectra in this region do not directly reflect changes in covalency in the redox active molecular orbitals of the site. However, variations in the spectra are certainly related to changes in the electronic structure of the site. In order to reliably interpret changes in intensity in this energy region, a better understanding of the nature of transitions in this energy region, which can be based on model complex studies, is necessary. While more reliable results must be obtained, these preliminary results demonstrate that changes in the electronic structure of the reduced 2Fe site relative to the oxidized site can be observed in X-ray absorption spectra.

7.7. Acknowledgments

The data reported herein were collected at the Stanford Synchrotron Radiation Laboratory which is supported by the U.S. Department of Energy, Office of Basic Energy Sciences, Divisions of Chemical Sciences and Material Sciences. The Stanford

Synchrotron Radiation Laboratory is also supported in part by the National Institutes of Health, Biomedical Research Technology Program, National Center for Research Resources (RR-01209) and by DOE's Office of Health and Environmental Research (OHER).

The author would also like to thank Professor Chris Chidsey for a helpful discussion about the choice of a mediator for this experiment. I also thank Michael Rocklin and Brian Cho who conducted research in Keith Hodgson's laboratory as undergraduates and from whom I inherited a great deal of spinach ferredoxin. Finally, the author thanks Dr. Patrick Frank for tireless hours spent discussing and conducting the test experiments and for sleepless hours spent in the measurement of the XAS data. Next time it is going to work!

7.8. References

(1) Evans, M. C. W. In *Iron-Sulfur Proteins*; Spiro, T. G., Ed.; John Wiley & Sons: New York, 1982; pp 249-284.

(2) Mascharak, P. K.; Papaefthymiou, G. C.; Frankel, R. B.; Holm, R. H. *J. Am. Chem. Soc.* **1981**, *103*, 6110-6116.

(3) Feldman, B. J.; Gheller, S. F.; Newton, W. E.; Frank, P.; Hedman, B.; Hodgson, K. O.; Schultz, F. A. to be submitted.

(4) Hedman, B.; Frank, P.; Hodgson, K. O.; Feldman, B. J.; Gheller, S. F.; Schultz, F. A.; Newton, W. E. In *X-ray Absorption Fine Structure*; Hasnain, S. S., Ed.; Ellis Horwood: Chichester, 1991; pp 168-170.

(5) Tagawa, K.; Arnon, D. I. *Biochim. Biophys. Acta* **1968**, *153*, 602-613.

(6) Landrum, H. L.; Salmon, R. T.; Hawkridge, F. M. *J. Am. Chem. Soc.* **1977**, *99*, 3154-3158.

(7) Harmer, M. A.; Hill, H. A. O. *J. Electroanal. Chem.* **1985**, *189*, 229-246.

(8) Armstrong, F. A.; Cox, P. A.; Hill, H. A. O.; Lowe, V. J.; Oliver, B. N. *J. Electroanal. Chem.* **1987**, *217*, 331-366.

(9) Armstrong, F. A.; Hill, H. A. O.; Walton, N. J. *Acc. Chem. Res.* **1988**, *21*, 407-413.

(10) Petering, D. H.; Palmer, G. *Arch. Biochem. Biophys.* **1970**, *141*, 456-464.

(11) Rocklin, M. **1990**, Undergraduate Honors Thesis, Stanford University.

(12) Ellefson, W. L.; Ulrich, E. A.; Krogmann, D. W. In *Methods in Enzymology*; San Pietro, A., Ed.; McGraw-Hill: New York, 1980; Vol. 69; pp 223-228.

(13) Borchert, M. T.; Wessels, J. S. C. *Biochim. Biophys. Acta* **1970**, *197*, 78-83.

(14) Wieghardt, K.; Schmidt, W.; Herrmann, W.; Küppers, H. *Inorg. Chem.* **1983**, *22*, 2953-2956.
(15) Wang, J. *Electrochimica Acta* **1981**, *26*, 1721-1726.
(16) Fujihira, M.; Osa, T. *Prog. Batteries Sol. Cells* **1979**, *2*, 244-248.
(17) Hedman, B.; Frank, P.; Gheller, S. F.; Roe, A. L.; Newton, W. E.; Hodgson, K. O. *J. Am. Chem. Soc.* **1988**, *110*, 3798-3804.
(18) Westre, T.E.; private communication.